



# Preparation and characterization of chitosan nanocomposite based on nanoscale silver and nanomontmorillonite

Fatemeh-Sadat Ebnerasool<sup>a</sup> and Negar Motakef-Kazemi<sup>b,\*</sup>

<sup>a</sup> Department of Food Sciences and Technology, Faculty of pharmacy, Tehran Medical Sciences, Islamic Azad University, Tehran, Iran.

<sup>b</sup> Department of Medical Nanotechnology, Faculty of Advanced Sciences and Technology, Tehran Medical Sciences, Islamic Azad University, Tehran, Iran.

## ARTICLE INFO:

Received 27 March 2019

Revised form 17 May 2019

Accepted 29 May 2019

Available online 18 Jun 2019

## Keywords:

Nanocomposite

Chitosan

Nanoscale silver

Nanomontmorillonite

Packaging

## ABSTRACT

The chitosan nanocomposites were rapidly prepared by simple solution method. This biopolymer matrix was modified by prepared nanoscale silver (Ag) using *in situ* synthesis from precursor and nanomontmorillonite (NMMT). Moreover, the samples were characterized by fourier transform infrared (FTIR) spectroscopy, thermogravimetric analysis (TGA), field emission scanning electron microscopy (FESEM), and energy dispersive x-ray spectroscopy (EDX). Moreover, the water vapor properties (WVP) of nanocomposites were investigated using gravimetric standard. In addition, the antibacterial activity of nanocomposite was measured by the well diffusion method on Muller–Hinton Agar against *Escherichia coli* (*E. coli*) by zone inhibition. Finally, based on the obtained results, the nanocomposite can have a good candidate for different applications and food packaging industry.

## 1. Introduction

Today, nanotechnology has expanded in various fields due to the potential of application benefits in the world [1]. Nanomaterials have size of 1-100 nm that showed unique properties because of small size and high surface area [2]. In recent years, population growth was resulted in the extension of packaging for food source protection [3]. Since, nanotechnology can be affected because of the wide application in production, processing, storage,

packaging, and transport of food products with environment protection and earth resources [4]. The main factor is included a lot of effort to produce functional materials, food processing, product development, methods, and tools design [5]. The application of nanocomposite is expanded because of its unique properties in food packaging [6,7]. The nanocomposites can control the permeability of polymer and increase shelf life to improve the efficiency of packaging materials [8]. In packaging industry, the use of biodegradable material can reduce the waste and results to consume the less material precursor [9].

The nanomaterials have been developed the

\* Corresponding Author: Negar Motakef-Kazemi

Email: [motakef@iaups.ac.ir](mailto:motakef@iaups.ac.ir)

DOI: <https://doi.org/10.24200/amecj>

research work in food products [10]. Recently, biodegradable nanocomposite has been used to investigate barrier materials and antimicrobials in packaging [11]. Moreover, nanocomposite based on biopolymer can be named such as starch [12,13], cellulose [14], and chitosan (CS) [15,16] for food packaging. Moreover, chitosan is derived from chitin, and its use has expanded as biomaterials [17]. The chitosan has several excellent properties such as biodegradability, non-toxicity, and antimicrobial properties which investigated in food packaging widely [18-20]. The polymer nanocomposite included the polymer as matrix phase and nanomaterial as filler phase to improvement of physical and mechanical properties [21]. In addition, the use of nanocomposites can enhance the applications of different properties for nanomaterials in food packaging technology [22]. Moreover, silver nanoparticles are well known as antimicrobial agents in curative and preventive health care with low toxicity for humans [23,24]. Clay filler has received significant attention because of suitable dispersion, thermal stability, and barrier properties in polymer nanocomposites [25]. In the present study, chitosan nanocomposite based on nanoscale silver and nanomontmorillonite has been prepared by a simple method using *in situ* synthesis of nanoscale silver for food packaging. The aim of this work is to study antibacterial activity against *Escherichia coli* and barrier for water vapor permeability of this nanocomposite.

## 2. Experimental procedure

### 2.1. Materials

All chemicals used were analytical grade. Chitosan was obtained from Sigma Aldrich with medium molecular weight. Glacial acetic acid, trisodium citrate and silver nitrate ( $\text{AgNO}_3$ ) were obtained from Merck. Ultra-pure water was used for the preparation of all reagents solutions. Moreover, the modified montmorillonite clay was obtained from Nano Pasargad Novin Company. The test strains, *Escherichia coli* ATCC 1399, were procured from Islamic Azad University.

### 2.2. Methods

#### 2.2.1. Preparation of nanoscale Ag

The nanoscale silver was prepared by reducing silver nitrate using trisodium citrate.  $\text{AgNO}_3$  solution (2 M) was added to the 1% acetic acid solution. Then trisodium citrate solution (4 M) was added to the resulting solution and stirred for 2 h. The nanoscale silver was centrifuged at 10,000 rpm for 10 min and dried at room temperature for 48 h [26].

#### 2.2.2. Preparation of chitosan–nanoscale Ag nanocomposite

Chitosan aqueous solution of 2 wt.% was prepared by dissolving chitosan powder (2 g) in 100 mL of 1% (v/v) acetic acid. Then  $\text{AgNO}_3$  solution (2 M) and trisodium citrate (4 M) were added to the chitosan solution and stirred for 2 h at room temperature. The preparation of chitosan–nanoscale Ag nanocomposite was done by *in situ* synthesis of nanoscale silver. The mixture solution was cast onto glass plates and dried at room temperature for 48 h [26-27].

#### 2.2.3. Preparation of chitosan–NMMT nanocomposite

Chitosan aqueous solution of 2 wt.% was prepared in acetic acid solution (1% v/v). The nanomontmorillonite was prepared by dispersing of montmorillonite clay into 10 mL of 1% acetic acid solution and vigorously stirring for 24 h. The nanomontmorillonite solution (1% and 3 wt.%) was added slowly to chitosan solution and stirred continuously for 2 h. Then the mixture was cast onto glass plates and dried at room temperature for 72 h [26-27].

#### 2.2.4. Preparation of chitosan–nanoscale Ag–NMMT nanocomposite

Chitosan aqueous solution of 2 wt.% was prepared by 1% (v/v) acetic acid. Then  $\text{AgNO}_3$  solution (2 M), trisodium citrate (4 M), and nanomontmorillonite solution (1% and 3% wt) were added into the chitosan solution and stirred for 2 h at room

temperature. Then the mixture was cast onto glass plates and dried at room temperature for 72 h [26].

### 2.3. Characterization of samples

The samples were characterized by Fourier transform infrared spectroscopy, thermogravimetric analysis, field emission scanning electron microscopy, and energy-dispersive x-ray spectroscopy. FTIR spectra were obtained using a FTIR spectrophotometer (Shimadzu Co.) in the range of 400–4000  $\text{cm}^{-1}$  at a resolution of 4  $\text{cm}^{-1}$  in a KBr matrix. The thermogravimetric analysis was measured by a TGA-SF1 (Mettler Co.) that carried out to 800 °C at the heating rate of 20 °C per min under nitrogen atmosphere. The morphologies of the samples were analyzed on a MIRA3 TeScan LMU (TeScan Co.) FESEM at 5 kV. Afterwards, the specimens were coated with a thin conductive gold layer before observation. The EDX analysis was measured by using ASK SEM-CL view VIS (Oxford instruments Co.) The antimicrobial activity was investigated for pure chitosan, montmorillonite, and chitosan-based nanocomposites by measurement of the minimum inhibition concentration (MIC) against *E. coli* as gram-negative bacteria. The cells of *E. coli* were cultivated on Mueller-Hinton Agar and incubated at 37°C for 1 day. The samples were systematically diluted from 0.02% (w/v) to 0.000625% (w/v) to determine of the MIC values.

The WVP of films was determined using gravimetric standard ASTM E96-05 [28]. Glass bottles were used to perform the test with a diameter of 20 mm and depth of 45 mm. The bottles were filled with 3 g of  $\text{CaCl}_2$  for maintaining a relative humidity (0% RH) and covered with the film specimen. The result bottles were placed in a container containing  $\text{K}_2\text{SO}_4$  super saturated solution (97% RH) at 25 °C. Then the bottles were weighed ten times at 3 h intervals. Afterwards, water vapor transmission rate (WVTR) was determined from slope of mass change of bottle versus time curve divided by area of glass bottle mouth ( $\text{m}^2$ ). Then the WVP of film was calculated using Eq. 1:

$$\text{WVP} = \text{WVTR} \times L / \Delta P \quad (1)$$

where WVTR is water vapor transmission rate

( $\text{g}/\text{m}^2\text{s}$ ) through film,  $L$  is the mean thickness of film (m), and  $\Delta P$  is partial water vapor pressure difference (Pa) across film [21].

## 3. Results and Discussion

### 3.1. FTIR

The FTIR spectra are shown for CS, nanoscale Ag, NMMT, CS-nanoscale Ag nanocomposite, CS-NMMT nanocomposite and CS-nanoscale Ag-NMMT nanocomposite in Fig. 1. The spectrum of chitosan (Fig. 1a) shows the band at 1647  $\text{cm}^{-1}$  that corresponds to the amide function due to acetylated amine, whereas the band at 1600  $\text{cm}^{-1}$  is corresponded to the free amine I function due to deacetylated amine. The broad band at 3400-3500  $\text{cm}^{-1}$  is assigned with the overlapping O-H stretching bands. The N-H bending, C-H bending, and C-O stretching are shown at 1600  $\text{cm}^{-1}$ , 1382  $\text{cm}^{-1}$  and 1087  $\text{cm}^{-1}$  respectively. The results corresponded to the results [27, 29]. The FTIR spectrum of NMMT (Fig. 1b) is shown the vibration bands at 3624  $\text{cm}^{-1}$  for O-H, at 3425  $\text{cm}^{-1}$  due to interlayered O-H, at 1641  $\text{cm}^{-1}$  for H-O-H bending, at 1035 and 914  $\text{cm}^{-1}$  for Si-O stretching, and at 528 and 468  $\text{cm}^{-1}$  for Si-O bending. These characteristic peaks have shifted to lower frequencies in nanocomposites which recommend some interaction between functional groups of chitosan and NMMT. The results are corresponded to the reported results [30, 31]. The FTIR spectra of CS-NMMT nanocomposite and CS-nanoscale Ag-NMMT nanocomposite (Fig. 1c and 1d) are shown the combination of the characteristic absorption bands due to nanoscale Ag, NMMT and amine groups of chitosan. The overlapping peak of O-H and N-H shows more broadening at 3103-3392  $\text{cm}^{-1}$  in pure chitosan. The bands of amine groups are shifted to 1616 and 1668  $\text{cm}^{-1}$  in the CS-NMMT and CS-NMMT -nanoscale Ag nanocomposites. This shift corresponds to deformation and vibration of chitosan amine groups. The characteristic bands of clay are all shifted to lower absorption wavenumber from 500 to 1035  $\text{cm}^{-1}$  as shown on the figure. These observations are confirmed the electrostatic interaction of chitosan's  $\text{NH}_2^+$  groups with the negatively charged silicate

layer of clay in both composites. The spectrum of CS-nanoscale Ag nanocomposites is investigated (Fig.1 e). The omission of existing shoulder in  $1548\text{ cm}^{-1}$  is related to NH bending vibration bond that shows interaction between chitosan and nanoscale Ag that corresponds to the results [27]. The FTIR spectra of nanoscale Ag (Fig.1f) are shown the peaks at  $1643\text{ cm}^{-1}$ ,  $1578\text{ cm}^{-1}$ ,  $1392\text{ cm}^{-1}$  and  $1278\text{ cm}^{-1}$  that corresponded to the results [31]. Based on FTIR results, the qualitative change is confirmed for nanocomposite formation.

### 3.2. TGA

The weight-loss curve was obtained by heating of samples and determined thermal stability analysis as the function of temperature. The TGA analysis is shown for CS-NMMT nanocomposite that two weight loss regions were observed (Fig. 2. a), about  $100^\circ\text{C}$  (related to loss of water), and about  $300^\circ\text{C}$  (related to degradation of chitosan), at the result the remained weight percent was related to NMMT. The TGA analysis is shown for CS-nanoscale Ag

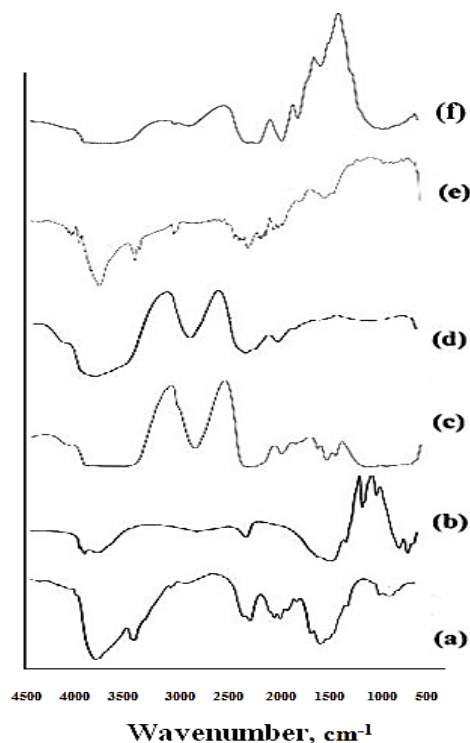


**Fig. 1.** Transmission FTIR spectra of (a) pure CS, (b) NMMT, (c) CS-NMMT nanocomposite, (d) CS-nanoscale Ag-NMMT nanocomposite, (e) CS-nanoscale Ag nanocomposite and (f) nanoscale Ag.

nanocomposite that two weight loss regions were observed (Fig. 2. b), about  $100^\circ\text{C}$  (related to loss of water), and about  $300^\circ\text{C}$  (related to degradation of chitosan), at the result the remained weight percent was related to silver. The TGA analysis is shown for CS-nanoscale Ag-NMMT nanocomposite that two weight loss regions were observed (Fig. 2. c), about  $100^\circ\text{C}$  (related to loss of water), and about  $300^\circ\text{C}$  (related to degradation of chitosan), at the result the remained weight percent was related to NMMT and silver. Based on TGA results, thermal stability of nanocomposite which are as follows: CS-NMMT > CS-nanoscale Ag- NMMT > CS-nanoscale Ag that the presence of NMMT and nanoscale Ag have been caused an increase and decrease in this property respectively. CS-nanoscale Ag- NMMT was average thermal stability because of the opposite effects of two fillers. The TGA results are comparable to those of previous researchers [32].

### 3.3. FESEM

The size and morphology structures of samples were studied using FESEM that shown nanoscale Ag, NMMT, CS-nanoscale Ag nanocomposite, CS-NMMT nanocomposite, CS-nanoscale Ag-NMMT nanocomposite in Figure 3. Moreover, the NMMT has shaped sheet-like layer silicates and that included a two-dimensional layer with thickness of about 1 nm and length and width of about 300 nm to several microns (Fig. 3a). The morphology of nanoscale Ag has been nanorod arrays with the mean diameter of about 40 nm and the length of

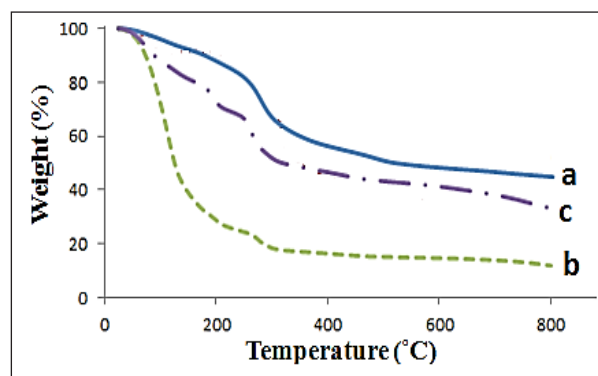


**Fig. 2.** The TGA of (a) CS-NMMT nanocomposite, (b) CS-nanoscale Ag nanocomposite, and (c) CS-nanoscale Ag-NMMT nanocomposite.

about 200 nm (Fig. 3b). The morphology of CS-nanoscale Ag has been nanorod arrays with the mean diameter of about 70 nm and the length of about 250 nm (Fig. 3c) that slightly increased in size due to the presence of chitosan. Moreover, the CS-NMMT nanocomposite is shown the palte-like structure with thickness of 30 nm and length and width of about 500 nm (Fig. 3d). The CS-nanoscale Ag-NMMT nanocomposite is shown nanoparticle morphology for nanoscale Ag with size of about 40 nm and palte-like structure for NMMT with diameter of 40 nm and length and width of 200 nm (Fig. 3e). These images are represented the uniform structure and complete distribution in the matrix of chitosan polymer. Also, the nanoscale silver morphology is observed nanoparticle instead of nanorod for chitosan nanocomposite in the presence of NMMT. In fact, NMMT is acted as capping agent and controlled crystal growth.

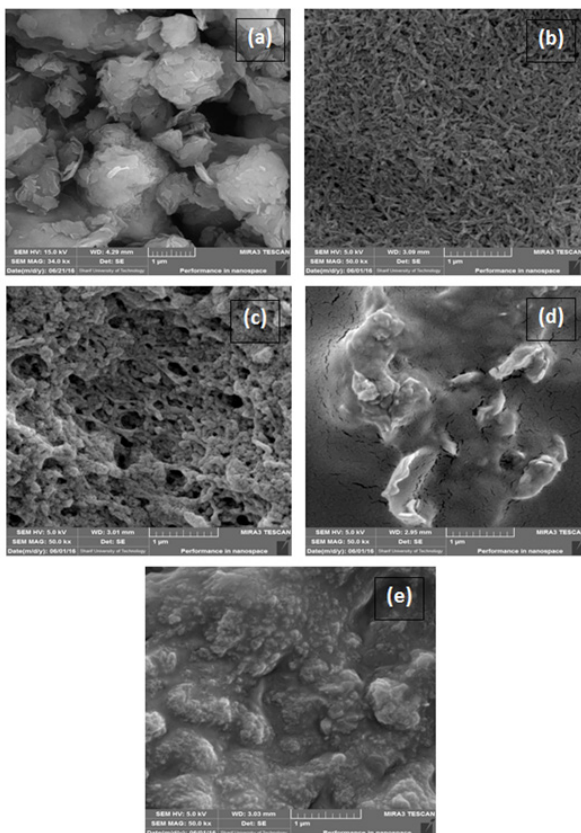


**Fig. 3.** The SEM of (a) NMMT, (b) nanoscale Ag, (c) CS-nanoscale Ag nanocomposite, (d) CS-NMMT nanocomposite and (e) CS-nanoscale Ag-NMMT nanocomposite.

### 3.4. EDX

The EDX analysis is shown for nanoscale Ag, Cs-nanoscale Ag nanocomposite, (c) CS-NMMT nanocomposite and CS-nanoscale Ag-NMMT nanocomposite in figure 4. The intense signal has been at 3 keV that confirmed the presence of nanoscale silver (Fig. 4a). The EDX analysis of CS-nanoscale Ag nanocomposite has been the signal of nanoscale silver at 3 keV and appeared the other signal of C, O, and N due to chitosan (Fig. 4b). Based on the result is confirmed the presence of CS and nanoscale silver. The EDX analysis of CS-NMMT has been the signal of clay for Al and Si and appeared the other signal of C, O, and N due to chitosan (Fig. 4c). The EDX analysis of CS-nanoscale Ag-NMMT nanocomposite has indicated the presence of silver, chitosan and clay in the nanocomposite (Fig. 4d).

### 3.5. WVP tests

WVP test is used to study water vapor barrier properties of packaging films and investigated the inhibition of the humidity exchange between food and environment. The WVP of samples was determined by the gravimetric method using WVP (Table 1). The chitosan film was showed the reduction in WVP permeability. The increase and decrease in WVP permeability were observed because of the addition of nanoscale Ag and NMMT respectively into chitosan nanocomposite films. The nanoscale Ag can form the hydrogen bond and resulted to the increase passage while NMMT with high aspect ratio can disperse uniformly in polymer matrix and lead to prevent permeability.

### 3.6. Antibacterial activity

The antibacterial activity of samples was tested against *E. coli* bacteria using the well diffusion method on Muller–Hinton Agar. All tests were done in triplicate. The antibacterial tests were summarized in Table 2 that observed the effect of chitosan and nanoscale Ag while NMMT has not exhibited any effect. The inhibition zone was the same for nanoscale Ag and chitosan–nanoscale Ag and the effect of nanoscale Ag has been

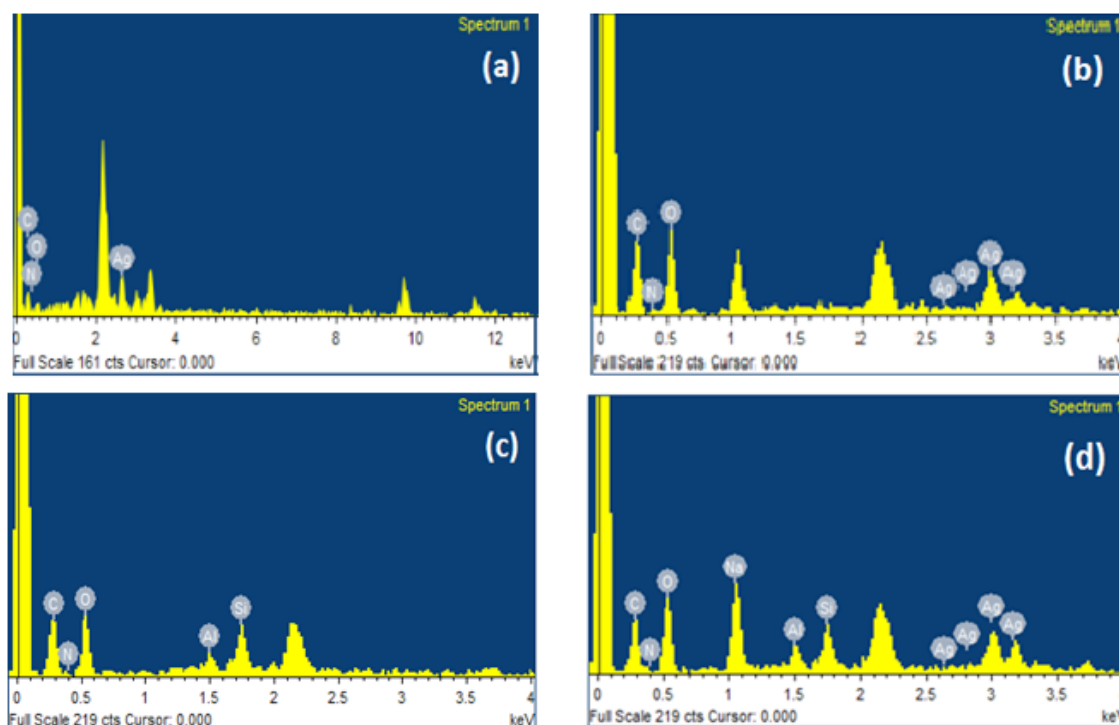


**Fig. 4.** EDX analysis of (a) nanoscale Ag, (b) CS-nanoscale Ag nanocomposite, (c) CS-NMMT nanocomposite and (d) CS-nanoscale Ag-NMMT nanocomposite.

**Table 1.** WVP test for samples.

Sample	Sample	WVP (g/(m s Pa))
1	CS solution 2% wt	$1.92 \times 10^{-10}$
2	CS-Silver nanocomposite	$4.31 \times 10^{-10}$
3	CS-MMT nanocomposite 3%	$1.63 \times 10^{-10}$
4	CS-MMT nanocomposite 5%	$1.17 \times 10^{-10}$
5	CS- Silver -MMT nanocomposite 3%	$4.78 \times 10^{-10}$
6	CS- Silver -MMT nanocomposite 5%	$3.25 \times 10^{-10}$

evident apparent in comparison with chitosan. The minimum inhibitory concentration was  $0.005 \text{ mol/L}^{-1}$  for chitosan–nanoscale Ag composite. Antibacterial activity results are comparable to those of previous researchers [33].

#### 4. Conclusions

The chitosan nanocomposites were successfully prepared from NMMT and *in situ* synthesis of nanoscale silver using the reduction of  $\text{AgNO}_3$  by trisodium citrate. Based on FESEM results, *in situ* synthesis of nanoscale Ag was formed silver nanoparticle in chitosan nanocomposite duo to the

presence of NMMT although the silver nanorod was observed by reduction of silver precursor. Moreover, the TGA analysis was shown the increase in thermal stability duo to the presence of NMMT. The FTIR and EDS of nanocomposites were confirmed the presence of chitosan and silver. Finally, the effective role of NMMT and nanoscale Ag were observed in the decrease of WVP permeability and increase in antibacterial activity against *E. coli* respectively. Furthermore, based on these results chitosan–nanoscale Ag–NMMT nanocomposite can have a good potential for packaging.

**Table 2.** Inhibition zone of samples.

Sample	Sample	Inhibition zone (mm)
1	CS solution 2% wt	9
2	CS-Silver nanocomposite	12
3	Silver nanoparticles	12
4	CS-MMT nanocomposite	9
5	CS- Silver -MMT nanocomposite	12

## 5. References

- [1] H. Chen, J. Weiss, F. Shahidi, Nanotechnology in nutraceuticals and functional foods, *Food Tech.*, 60 (2006) 30-36.
- [2] G. Christina, V. Dirk, I. Arnout, V. Blaaderen, A general method to coat colloidal particles with silica, *Langmuir*, 19 (17) (2003) 6693-6700.
- [3] W. Han, Y.J. Yu, N.T. Li, L.B. Wang, Application and safety assessment for nano-composite materials in food packaging, *Chin Sci Bull*, 56 (12) (2011) 1216-1225.
- [4] H. Bouwmeester, S. Dekkers, M.Y. Noordam, W.I. Hagens, A.S. Bulder, C.D. Heer, S.E.C.G.T. Voorde, S.W.P. Wijnhoven, H.J.P. Marvin, A.J.A.M. Sips, Review of health safety aspects of nanotechnologies in food production, *Regul. Toxicol. Pharmacol.*, 53 (2009) 52-62.
- [5] C.F. Chau, S.H. Wu, G.C. Yen, The development of regulations for food nanotechnology, *Trends Food Sci Technol*, 18 (2007) 269-280.
- [6] S.H. Peighambaroust, F. Beigmohammadi, S.J. Peighambaroust, Application of organoclay nanoparticle in low-density polyethylene films for packaging of UF cheese, *Package Technol. Sci.* 29 (2016) 355-363.
- [7] M. Auta, B.H. Hameed, Chitosan-clay composite as highly effective and low-cost adsorbent for batch and fixed-bed adsorption of methylene blue, *Chem. Eng. Sci.*, 237 (2014) 352-361.
- [8] G. Choudalakis, A.D. Gotsis, Permeability of polymer/clay nanocomposites: A review, *Eur. Polym. J.*, 45 (2009) 967-984.
- [9] T.V. Duncan, Applications of nanotechnology in food packaging and food safety: barrier materials, antimicrobials and sensors, *J. Colloid Interface Sci.*, 363 (2011) 1-24.
- [10] R.I. Quintero, F. Rodriguez, J. Bruna, A. Guarda, M.J. Galotto, Cellulose acetate butyrate nanocomposites with antimicrobial properties for food packaging, *Package Technol. Sci.*, 26 (5) (2013) 249-265.
- [11] R. Tankhiwale, S.K. Bajpai, Preparation, characterization and antibacterial applications of ZnO-nanoparticles coated polyethylene films for food packaging, *Colloids Surface B*, 90 (2012) 16-20.
- [12] S.S. Ray, K. Yamada, M. Okamoto, K. Ueda, Polylactide-layered silicate nanocomposite: a novel biodegradable material, *Nano Lett.* 2 (2002) 1093-1096.
- [13] M. Avella, J.J. DeVlieger, M. Emanuela-Errico, S. Fischer, P. Vacca, M. Grazia-Volpe, Biodegradable starch/clay nanocomposite films for food packaging applications, *Food. Chem.*, 93 (2005) 467-474.
- [14] V.P. Cyras, L.B. Manfredi, M.T. Ton-That, A. Vazquez, Physical and mechanical properties of thermoplastic starch/montmorillonite nanocomposite films, *Carbohydr Polym.*, 73 (2008) 55-63.
- [15] H.M. Azeredo, L.H. Mattoso, D. Wood, T.G. Williams, R.J. Avena-Bustillos, T.H. McHugh, Nanocomposite edible films from mango puree reinforced with cellulose nanofibers, *J. Food Sci.*, 74 (5) (2009) 31-35.
- [16] Y. Lu, L. Weng, L. Zhang, Morphology and properties of soy protein isolate thermoplastics reinforced with chitin whiskers, *Biomacromolecules*, 5 (2004) 1046-1051.
- [17] S.A. Siddiqi, U. Aahar, F. Manzoor, A. Jamal, M. Tariq, M. Saleem, A.A. Chaudhry, I.U. Regman, Fabrication of biocompatible nano-carbonated hydroxyapatite/polymer spongy scaffolds, *Dig. J. Nanomater. Bios.*, 13 (2) (2018) 439-450.
- [18] Z. Liu, M. Lv, F. Li, M. Zeng, Development, characterization, and antimicrobial activity of gelatin/chitosan/ZnO nanoparticle composite films, *J. Aquat. Food Prod. T.*, 25 (2016) 1056-1063.
- [19] Y. Xu, X. Ren, M.A. Hanna, Chitosan/clay nanocomposite film preparation and

- characterization, *J. Appl. Polym. Sci.*, 99 (2006) 1684-1691.
- [20] M.R.D. Moura, M.V. Lorevice, L.H.C. Mattoso, V. Zucolotto, Highly stable, edible cellulose films incorporating chitosan nanoparticles, *J. Food Sci.*, 76 (2) (2011) 25-29.
- [21] K. Lewandowska, A. Sionkowska, B. Kaczmarek, G. Furtos, Characterization of chitosan composites with various clays, *Int. J. Biol. Macromol.*, 65 (2014) 534-541.
- [22] P. Adibzadeh, N. Motakef-Kazemi, Preparation and characterization of curcumin-silver nanoparticle and evaluation of the effect of poly ethylene glycol and temperature, *J Nanoanal.*, 5(3) (2018) 156-162.
- [23] H. Jafari, M.K. Pirouzifard, M. Alizadeh-Khaledabad, H. Almasi, Effect of chitin nanofiber on the morphological and physical properties of chitosan/silver nanoparticle bionanocomposite films, *Int. J. Biol. Macromol.*, 92 (2016) 461-466.
- [24] P. Dallas, V.K. Sharma, R. Zboril, Silver polymeric nanocomposites as advanced antimicrobial agents: Classification, synthetic paths, applications, and perspectives, *Adv. Colloid Interface Sci.*, 166 (2011) 119-135.
- [25] E. Manias, A. Touny, L. Wu, K. Strawhecker, B. Lu, T.C. Chung, Polypropylene/Montmorillonite Nanocomposites. Review of the Synthetic Routes and Materials Properties, *Chem. Mater.*, 13 (10) (2001) 3516-3523.
- [26] M. Abdollahi, M. Rezaei, G. Farzi, A novel active bionanocomposite film incorporating rosemary essential oil and nanoclay into chitosan, *J. Food. Eng.*, 111 (2012) 343-350.
- [27] E.M.S. Azzam, S.M. Solyman, A.A. Abd-Elaal, Fabrication of chitosan/Ag-nanoparticles/clay nanocomposites for catalytic control on oxidative polymerization of aniline, *Colloids Surf. A: Physicochem, Eng. Aspects*, 510 (2016) 221-230.
- [28] Y.S. Han, S.H. Lee, K.H. Choi, I. Park, Preparation and characterization of chitosan-clay nanocomposites with antimicrobial activity, *J. Phys. Chem. Solids*, 71 (2010) 464-467.
- [29] S. Tripathi, G.K. Mehrotra, P.K. Dutta, Chitosan-silver oxide nanocomposite film: Preparation and antimicrobial activity, *Bull. Mater. Sci.*, 34 (2011) 129-135.
- [30] C. Paluszkievicz, E. Stodolak, M. Hasik, M. Blazewicz, FT-IR study of montmorillonite-chitosan nanocomposite materials, *Spectrochim Acta A.* 79 (2011) 784-788.
- [31] J. An, Z. Ji, D. Wang, Q. Luo, X. Li, Preparation and characterization of uniform-sized chitosan/silver microspheres with antibacterial activities, *Mater. Sci. Eng. C*, 36 (2014) 33-41.
- [30] C. Aguzzi, G. Sandri, C. Bonferoni, P. Cerezo, S. Rossi, F. Ferrari, C. Caramella, C. Viseras, Solid state characterisation of silver sulfadiazine loaded on montmorillonite/chitosan nanocomposite for wound healing, *Colloids Surface B*, 113 (2014) 152-157.
- [32] K. Shameli, M. Bin Ahmad, M. Zargar, W. Md Zin Wan Yunus, N. Azowa Ibrahim, P. Shabanzadeh, M. Ghaffari Moghaddam, Synthesis and characterization of silver/montmorillonite/chitosan bionanocomposites by chemical reduction method and their antibacterial activity, *Int. J. Nanomedicine*, 6 (2011) 271-284.
- [33] N. Feizi Langaroudi, N. Motakef Kazemi, Preparation and characterization of O/W nanoemulsion with Mint essential oil and Parsley aqueous extract and the presence effect of chitosan, *Nanomed. Res. J.*, 4 (2019) 48-55.



# Microplastics, an emerging concern: A review of analytical techniques for detecting and quantifying microplastics

Verla Andrew Wirnkor<sup>a</sup>, Enyoh Christian Ebere<sup>a,\*</sup> and Verla Evelyn Ngozi<sup>b</sup>

<sup>a</sup> Group Research in Analytical Chemistry, Environment and Climate change (GRACE&CC), Department of Chemistry, Faculty of Science, Imo State University, Owerri, Imo State, Nigeria

<sup>b</sup> Department of Environmental Technology, School of Environmental Technology Federal University of Technology, Owerri, Imo State, Nigeria.

## ARTICLE INFO:

Received 13 Apr 2019

Revised form 30 Apr 2019

Accepted 12 May 2019

Available online 17 Jun 2019

## Keywords:

Anthropogenic

Fragmentation

Health implications

Hyphenated methods

Matrices

Seafood

## ABSTRACT

Microplastics are ubiquitous tiny plastic particles (< 5 mm) nonbiodegradable and have large surface area in the environment or the body of living things due to anthropogenic activities or fragmentation of plastic debris. Though they have been found in sea food and human body, their health implications are still speculative. Moreover, a major reason for dearth of information on this topical issue is the lack of standard operating protocol for detecting and quantifying microplastics as a result of their presence in more complex environmental matrices. In the present review some methodologies for analyzing microplastics reported in the period 2000 to 2018 have been documented with the aim of assessing which methods is most suitable and in what matrix. The following methods have been studied: CHN analyzers, pyrolysis-gas chromatography/mass spectroscopy (PyrGC/MS), optical microscopy, fourier transform infrared microspectroscopy (Micro-FTIR), raman microspectroscopy (RMS) and scanning electron microscopy with energy dispersive x-ray spectroscopy (SEM-EDS), effective for particles <500 μm. However, the quality of result obtained strongly relies on good sampling and sample purification. Specifically, Micro-Raman spectroscopy is best for particles of <1 μm while degradation process of plastics is best monitored with SEM-EDS. Generally, studies have been conducted with often a combination of two methods: one separating and the other quantifying which can be problematic moreso in living tissue where there is no harm reported as at the time of this study. Ultimately based on this study, microplastics have become a cause for concern and advance studies are required to unravel the potential risk of their presence in our food and environment.

## 1. Introduction

Plastics are organic polymers, synthesized from the polymerisation of monomers extracted from oil or gas. Since its first modern development in 1907 called “Bakelite”, its global production rose from 0.3 billion tons in 2010 [1] to 348 million metric tons in 2017 [2]. Approximately 10 % end up in the marine environment [3] and only a fraction of about 3 % was recycled in 2016. The plastics while in the environment break down to form debris. Many studies have reported that majority (60-80

%) of debris in marine environment are made up of plastics [4-6], which are further broken down to tiny particles through weathering processes. The tiny particles are defined as “microplastics” together with primary plastic particles manufactured at microsize dimensions [5,7].

Microplastics can simply be defined as small plastic particles in the environment. Term “microplastics” was recently coined, although the occurrence of small plastic particles on beaches and in coastal waters was first reported in the 1970s [8]. The U.S. National Oceanic and Atmospheric Administration (NOAA) classified microplastics as less than 5 mm in diameter

Corresponding Author: Enyoh Christian Ebere

Email: [Cenyoh@gmail.com](mailto:Cenyoh@gmail.com)

DOI: <https://doi.org/10.24200/amecj>

[5]. However, different authors have given different classifications of microplastics with numerous size-ranges. Graham and Thompson [9] classified microplastics with diameters of <10 mm, diameter of <5 mm was given by Barnes et al. [5] and Betts [10], 2–6 mm by Derraik [3], <2 mm and <1 mm [11-13]. Their sources vary including cosmetics, clothing, and industrial processes via urban wastewater treatment etc. Microplastics are classified as primary microplastics and secondary microplastics. The primary microplastics are produced from anthropogenic means while secondary microplastics are derived from breakdown of larger plastic debris into microscopic plastic fragments [14].

Microplastics can be ubiquitous and remain in the environment at high levels for many years because of their difficulty in breaking down. In the last decade, many researchers have developed interest and conducted studies on microplastics due to their massive buildup in the environment [12,13,15-17].

Currently, their mobility and entire cycle in the environment is not yet known. They are more particularly in aquatic and marine ecosystems. Due to their persistence in the environment, they find their way and accumulate in the bodies and tissues of many organisms. When in the host organism they could easily undergo chemical exchange due to their large surface area. This may possibly pose some health issues to the host organisms. In addition, they serve as vector to pollutants whose health implications are already established; which include heavy metals (HMs) and persistent organic pollutants (POPs) (i.e. polyaromatic hydrocarbons, PAHs, organochlorine pesticides, OCPs and polychlorinated biphenyls, PCBs). Many research reports have shown that PCBs are capable of attaching to the surface of plastics [18-21] and become bioavailable when ingested by animals [22,23]. For heavy metals, studies by Holmes [24] and Rochman [25] reported their adsorption to plastics surface when suspended in the marine environment. Ashton and coworkers [26], also reported adsorption of heavy metals such as iron (Fe), manganese (Mn), aluminium

(Al), lead (Pb), copper (Cu), silver (Ag), zinc (Zn) in seawater on virgin (new) polyethylene pellets. In the same study, heavy metals, such as Cu, Zn, Fe, were found in higher concentration on plastic production pellets than local sediments in coastline of South West, England [26]. According to Holmes et al. [24, 27], the extent of adsorption of metals on plastics in marine environment is probably due to the weathering, adhesion to foreign material (viz organic matter) over time, surface area and availability of anionic active sites.

Many scientist worldwide have reported on the uptake of microplastics by various marine organisms such as fish, sandhoppers, sea turtle, crustacean and mussel [7,11,28-30]. Due to this, their digestive system may be blocked, thereby leading to potentially serious injuries [31]. Furthermore, microplastics have been found in table salts used for cooking, potable water and human excreta [32]. However, the health implications of microplastics are still scantily studied with no evidence of impacts on human. This is an emerging area of concern. The very scarce available evidence is currently under review by World Health Organization (WHO). Their objectives are to identify gaps in evidence and create an agenda for research, in order to provide detailed information concerning risk pose to human by microplastics [33].

Researchers argued that the scantily research on microplastics have majorly centered on lack of standard operation protocols (SOP) or methodology for sampling, detecting and quantifying them in the environment [34-38]. Although, different methods have been developed and used by different researchers due to their presence in more complex environmental matrices [35,36,39,40]. A review by Klein et al. [41] summarized possible procedure provided by different researchers for analyzing microplastics in environmental matrix. The review describes the entire study process from sample collection to reporting of results (presented in Figure 1). One key aspect of some of the analytical methods is the extraction of microplastics from dissolving biomass using one or more fairly aggressive chemicals such as potassium hydroxide

(KOH), hydrogen peroxide ( $H_2O_2$ ), perchloric acid ( $HClO_4$ ) and nitric acid ( $HNO_3$ ) which can be destructive to the plastic particles and thus not accurately identifying and quantifying their presence in a sample. These aggressive chemicals are best suited for extracting heavy metals from samples of soil [42-44], water [45,46] and sediment [47].

Microplastics quantification is simply based on differentiating or separating these particles from other matter whether inorganic (e.g. sediment) or organic (e.g. plant material). Density based methods have been applied by many researchers in order to separate lighter compartments of the sample from sediment in a marine environment [35,36,39,48]. Using the density based method, Song et al. [49], explained that interference from other organic particles poses a major problem when identifying microplastics as synthetic polymers. Other methods involve the use of enzymatic digestion and

lipophilic dye Nile Red (9-diethylamino-5H-benzo [ $\alpha$ ]phenoxazine-5-one) quantitative differential staining for small microplastics (1 mm to 20  $\mu m$ ) in a samples [40, 50-52].

Here, we review common analytical techniques by which plastic types are identified, which can also be used in microplastic detection in the environment. These techniques are commonly used in analytical and environmental studies. They have been reported to be sensitive and accurate for indentifying and detecting microplastics in the environment.

## 2. Sources of data

Materials such as statistical bulletins, journals articles and conference/workshop/seminar papers were used for sourcing information. Web of Science and Google Scholar were two major scientific databases used to search for related articles and at least one of the following keywords needed to sample appear in

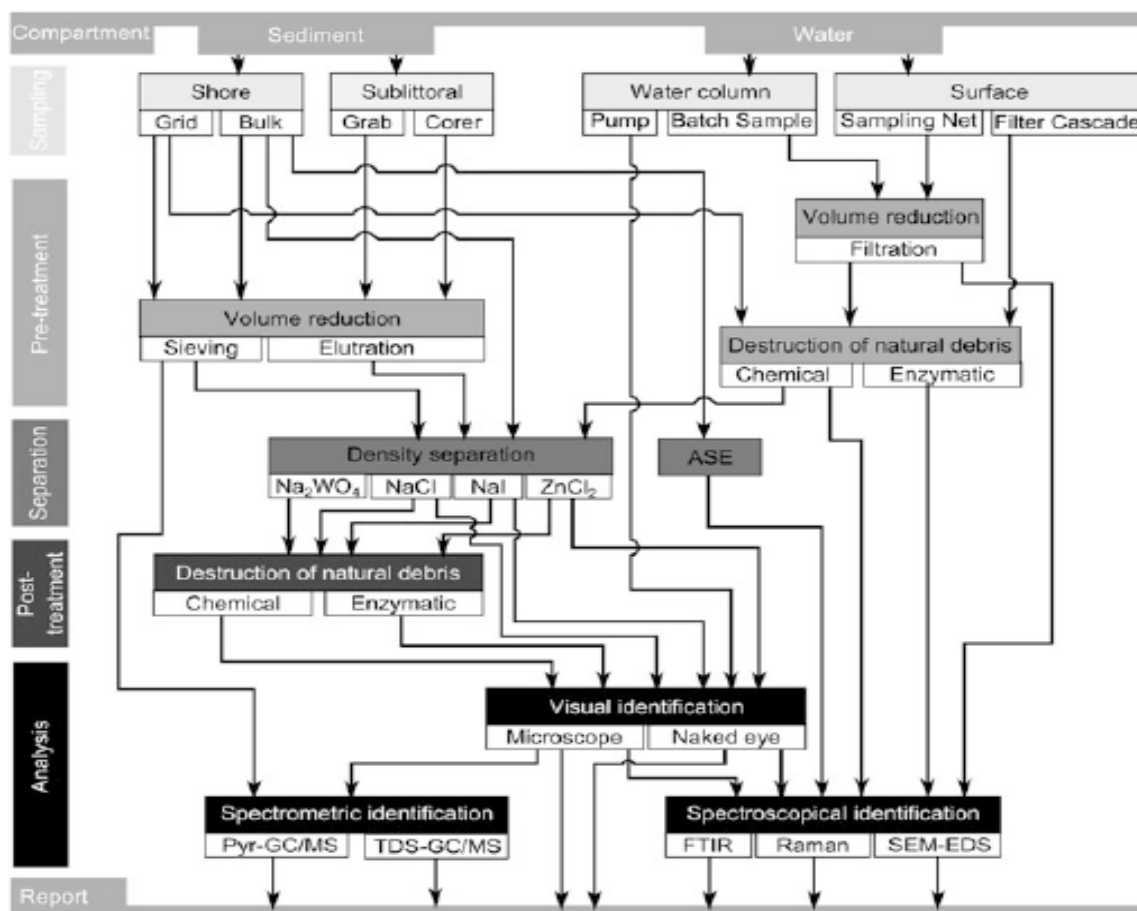


Fig. 1. Strategies provided by researchers for microplastics analysis from sampling to reporting results [41].

article's title or abstract: "Microplastics", "Plastics", "Marine", "Spectrophotometer", "Microscopy" and "Spectroscopy" (conducted in May, August and December 2018). One or more of the aforementioned keywords must be present in an article for the article to be included in the present review. All searches were restricted to peer-reviewed articles written in English that were published after 2000 to ensure review focus on recent literature on microplastics. Additionally, selected article prior to 2000 were included (e.g [53] and [54]) due to importance in the initial set of empirical studies.

### 3. Experimental procedures and methods

#### 3.1. CHN analyzers

CHN Analyzer is a scientific instrument which can determine the concentrations of elements in a given sample using combustion technique. The analyzer is useful in the development and production of plastics. It identifies plastic materials and quantifies nitrogen, carbon, hydrogen, sulfur and oxygen contents in plastics. No sample digestion or toxic chemicals is required for Using it ,thus making it a reliable system [55].

Liliana and Guido [56] characterized plastics (pellets, powders and films) by the Thermo Scientific FLASH 2000 Elemental Analyzer. This instrument operates with dynamic flash combustion of the sample. A graphical flow diagram of the instrument is presented in Figure 2. The first thing

was to introduce samples into the combustion reactor with oxygen using tin containers. The gases produced after combustion was transported by a helium flow to a layer containing copper, and then passed through a GC column, which separate these gases. The gases will be finally measured by a thermal conductivity detector (TCD). The measured gases revealed acrylonitrile (monomer), a main component of many types of compounds (polyacrylonitriles) such as plastics. The configuration can be achieved using either sulphur (CHNS) or oxygen (CHNO) respectively [56].

In an environment sample, the CHN analyzer will detects microplastics by the ability to identify materials with higher percentage of carbon, hydrogen and nitrogen content. The sizes of the samples are very small (a few milligrams), but may differ depending on system. Some samples matrix being heterogenous in nature and thus larger mass is preferred for their analysis using CHN analyzer. This method was modified by Morét-Ferguson and coworkers [57], using density separation with subsequent C:H:N analysis to identify the polymer origin of visually sorted microplastics. They concluded that the approach narrows the search for the potential polymer, thus enabling identification of microplastic particles by type, which requires no rigorous chemical analysis. However, the major drawbacks of this technique are (1) the relatively

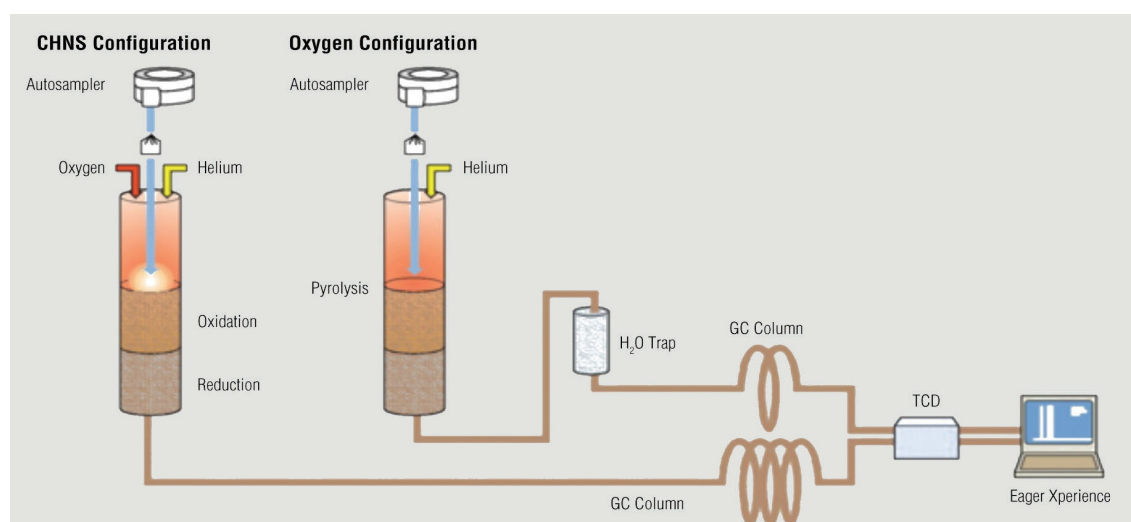


**Fig. 2.** CHNS/O configuration [56].

high time effort, which impede a high sample throughput and (2) not applicable to smaller particles [38].

### 3.2. Pyrolysis-gas chromatography/mass spectrometry (PyrGC/MS)

Pyrolysis–gas chromatography–mass spectrometry (PyrGC/MS) is a chemical analytical technique in which the sample are decomposed into smaller molecule through heating which are separated by gas chromatography and detected using mass spectrometry [48,58]. It is classified under mass spectrometry. The analytes for PyrGC/MS includes polymer, biomolecules and paint. A simple schematic representation of PyrGC/MS process is presented in Figure 3.

The sample is placed in pyrolyzers and rapidly heated to 600–1000 °C (or > 1000 °C, depending on the application). The heating techniques that can be employed include: isothermal furnace, inductive heating and resistive heating. Large molecules are decomposed into volatile fragments through the combustion [59,60]. The fragments will be separated by gas chromatography (GC), which will provide characteristic combustion products. These products will then be identified by mass spectroscopy (MS) and structural information elucidated by comparing them with reference of known pyrograms samples [37,61]. This method has been used by researchers to identify unknown plastic samples of different

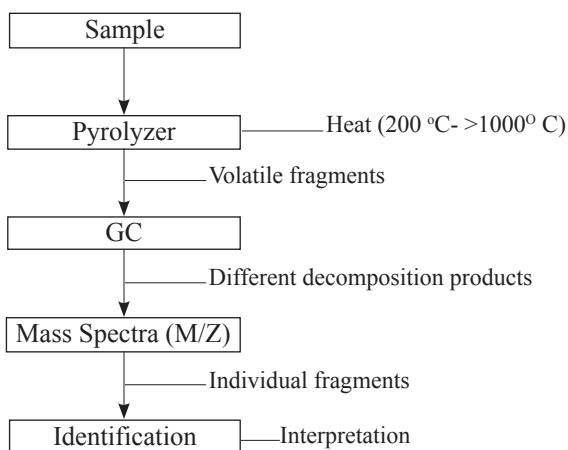


**Fig. 3.** A simple schematic representation of PyrGC/MS process.

polymer types and organic plastic additives (OPAs) [61,62]. A typical Pyrolysis–GC/MS chromatogram of a plastic sample is presented in Figure 4.

The major drawback is the manual place of sample particle into the pyrolyzer. This limits the size of particle that can be analyzed because only particles of a certain minimum size can be manipulated manually [38]. For this reason, samples are analyzed in sequence (one particle per run) and thus not suitable for routine monitoring programs where samples are analyzed in continuous manner. However, at 2015 promising pyrolysis-GC/MS approaches for the qualitative/quantitative analysis of microplastics on whole environmental sample filters was being developed. This will address the drawbacks of analyzing a particle per run.

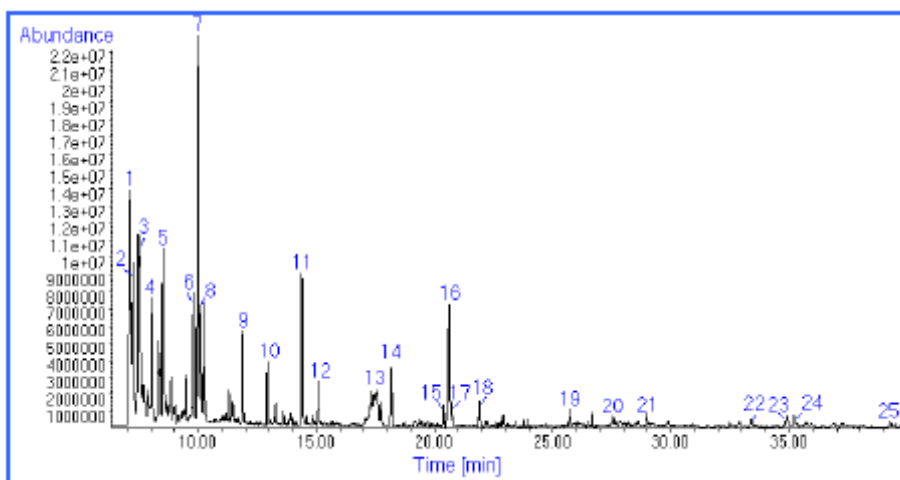


**Fig. 4.** A typical Pyrolysis–GC/MS chromatogram of a plastic sample pyrolyzed at 600 °C, identified as flexible poly vinyl chloride (PVC) [62].

### **3.3. Optical Microscopy**

Optical microscopy is the use of optical microscope (light microscope) to magnify images of small subjects using visible light and a system of lenses. The image from an optical microscope can be captured by normal, photosensitive cameras to generate a micrograph. This method is based on visual identification under a microscope. Visual sorting works well in separating large microplastics as well as separating potential microplastics from other organic or inorganic material in the sample residues [34,57] whereas dissection microscope is used in sorting smaller microplastic particles [63].

The use of this method has been reported in literature [40,52,64]. Wagner et al [40] used two reflected-light stereozoom microscopes (Leica S8APO and S6D) with digital CCD cameras (Leica DFC 420 and 320) for initial documentation, gut dissection, and pre-screening of any observed particles that visually resembled microplastics in fish samples. The optical microscopy was conducted at 6.3x- 80x with a minimum resolution of approximately 10  $\mu\text{m}$  [52]. Wang et al [67] also used optical microscope for analyses of microplastics in ocean trawl and fish guts.

This method can be aided by staining using dyes such as Nile Red [52,64]. Samples will be treated first with the dye solution (often 1 mL) for 48 hours under a fume cupboard until all moisture evaporated to form a dyed membrane. Subsequently, the dyed membrane filters were photographed using a camera under Ultra-violet (UV) light. Example of a useful camera is the Pentax K-30 with resolution 2420x2343 used by Matthias and coworkers [64] in their study.

The dye solution can be prepared using different extraction solvent such as acetone, chloroform and n-hexane. Chloroform with recovery rates of 83.3 % was reported to be most suitable solvent for the group of high-density and low-density polyethylene (HDPE, LDPE), polypropylene (PP) and PVC [64,65]. However, the findings of Shim et al [66] implicated n-hexane to be most effective for PE and PP, whereas PET and PA were not detectable. The variation in solvent efficiency in detecting the

different microplastic type could be due to different surface and density properties of the microplastic materials. Also, a typical visually identified stained microplastics under an optical microscope is shown in Figure 5.

It is asserted by Wang et al [67] that optical microscopy enables morphological classification of particles or fibers types, quantification of particle size ranges and fiber lengths presents in a sample. However, it is suggested by Hidalgo-Ruz et al. [34] that for particles < 500  $\mu\text{m}$ , ordinary visual sorting with the naked eye or hand lens should not be applied. This may cause misidentification of particles with high probability. To sort visually, there are factors that should be considered generally, which they include source, type, shape, degradation stage, and color of the particles [34,57], which is extremely time-consuming. Martin and Gunner [38] explained that, "even an experienced person cannot discriminate all potential microplastic particles unambiguously from sand grains, chitin fragments, diatom frustule fragments etc." Thus the error rate of this method reported ranges from 20 % [68] to 70 % [34], which increases as particle size decreases. Therefore, a size limit of 1 mm was recommended for visual sorting [34,57].

### **3.4. Fourier Transform InfraRed Microspectroscopy (Micro-FTIR)**

Fourier transform infrared (FTIR) microspectroscopy is a technique which produces molecular microscopic images from samples. The instrument allows observation of spectra measured from regions as small as 5 microns across because it uses an infrared microscope. The spectra correspond to specific chemical bonds between atoms which makes it possible to identify the exact composition of the particle [69]. In Micro-FTIR, two feasible measuring modes are used viz reflectance and transmittance [70]. The former (i.e. reflectance mode) handles difficult spectra obtained from measurements of irregularly-shaped microplastics that may not be interpretable due to refractive error [71]. The later mode (i.e. transmittance mode) handles the total absorption patterns and

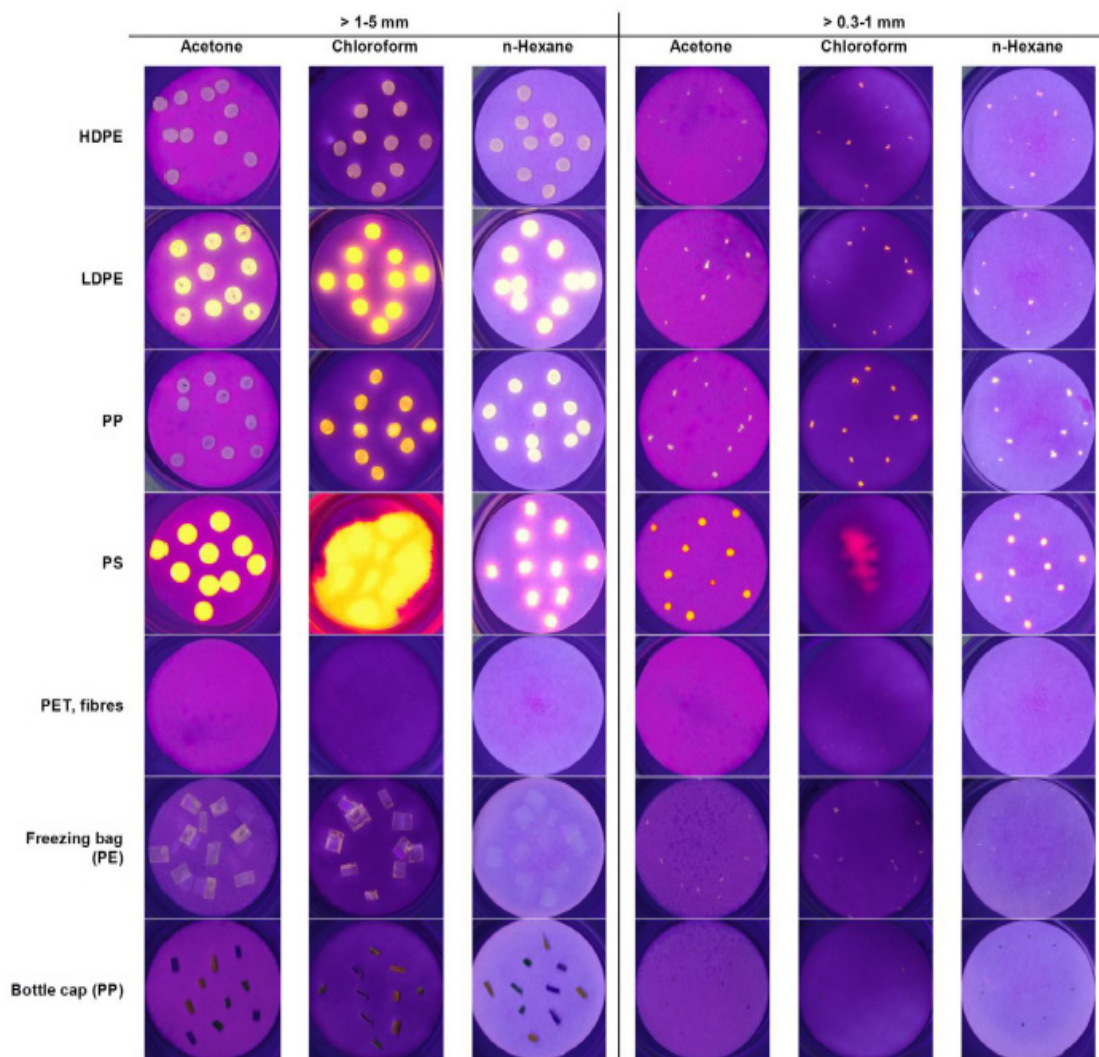


**Fig. 5.** A typical visually identified stained microplastics under an optical microscope [64].

uses IR transparent filters (e.g. aluminium oxide). Furthermore, it can only be limited by a certain thickness of the microplastics sample [38]. In addition, the use of micro-ATR (Attenuated Total Reflectance) in combination with microscopy enables the direct measurement on the sample filter without the need for manual handling of particles, when IR spectra are collected at the surface of a particle [40,70-72].

The micro-FTIR method has been used on biological samples such as articular cartilage [73] and to track microplastics in the environment with Attenuated Total Reflectance (ATR) [40,73,72] and Focal Plane Array-Based Reflectance [38,70,74]. Wagner [40] and Bradley et al [72] both used

the Thermo Scientific Nicolet Continuum FTIR Microscope with 10x optical objective, 15x IR objective, and a Nexus 470 spectrometer with attenuated total reflectance (ATR) (diamond and Ge-ATR). In the study, majority of the particles were analyzed either on glass slides or directly on filter. All acquired FTIR spectra were compared to quantitative matches from commercial FTIR libraries. In addition, in Figure 6, FTIR spectra of a microplastic fiber on filter from a river water sample are shown.

Kerstin and Federik [69] screened microplastic particles in and down-stream a wastewater treatment plant with a Bruker FTIR Tensor in attenuated total reflectance (ATR) mode equipped with a diamond

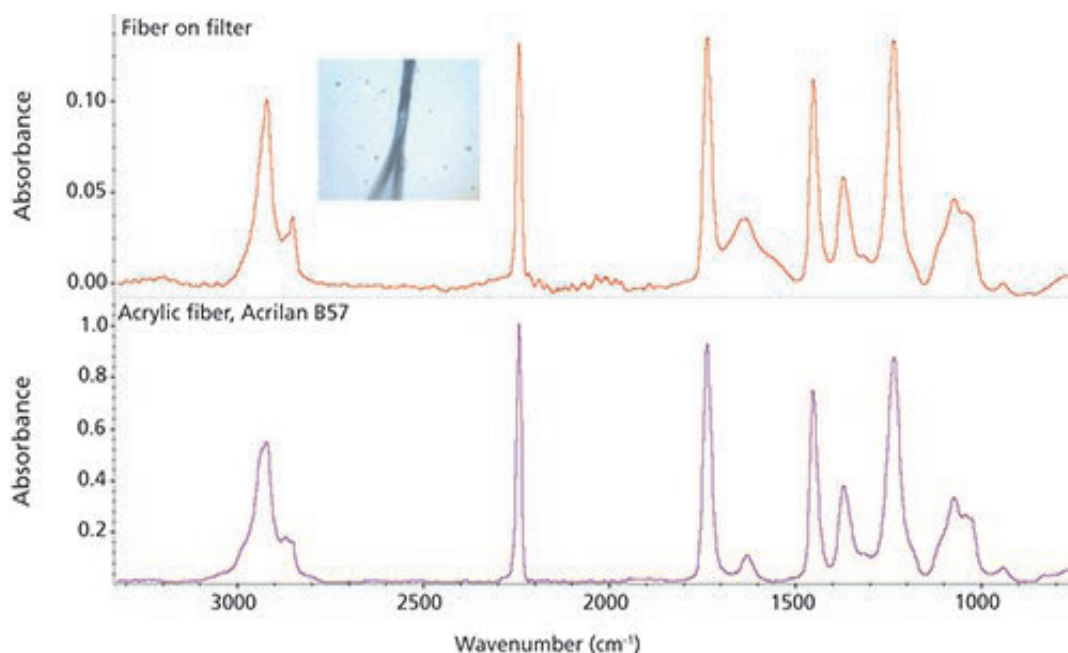


**Fig. 6.** FTIR spectra of a microplastic fiber on filter from a river water sample. The top spectrum is from Nicolet iN5 microscope fitted with Ge-ATR; the lower spectrum is a library search result [72].

crystal. Different plastic fragments ( $\geq 300 \mu\text{m}$ ) were reportedly found in wastewater treatment plant. Alexander et al. [74] used the FPA based reflectance micro-FT-IR imaging to identify and quantify microplastics in wastewater. The authors concluded that the tool is good for identifying and quantifying microplastics in wastewater and also to determine the abundance of microplastics in other organic-rich environments, such as peat soils [74]. This FPA based micro-FTIR spectroscopy is a very promising technique for verifying polymer origin of microplastic particles. Martin and Gunner [38] recommended for use in monitoring programs on microplastics.

Micro-FTIR enables identification of repetitive fingerprint-like molecular composition of plastic polymers for a clear assignment of a sample to a certain polymer origin. It offers the possibility of accurate identification of plastic polymer particles according to their characteristic IR spectra [15-17,48,71,75], simultaneously record several thousand spectra within an area with a single measurement and thus the generation of chemical images (Fig. 7) [38]. In figure 7, the analysis was done by FPA based micro-FTIR spectroscopy. The intensity of the chosen spectral bands is reflected

by the color scale according to peak area (bluish color scale intensity of the peak  $1,931\text{--}1,832 \text{ cm}^{-1}$ ; reddish color scale intensity of the peak  $2981\text{--}2780 \text{ cm}^{-1}$ ). This enabled clear identification of a quartz particles in light blue (a) at band of  $1931\text{--}1832 \text{ cm}^{-1}$  and a polyethylene particle in orange (b) at band of  $2981\text{--}2780 \text{ cm}^{-1}$  in a sample.

The simplicity of this method is in both sampling and analyzing. Samples are simply

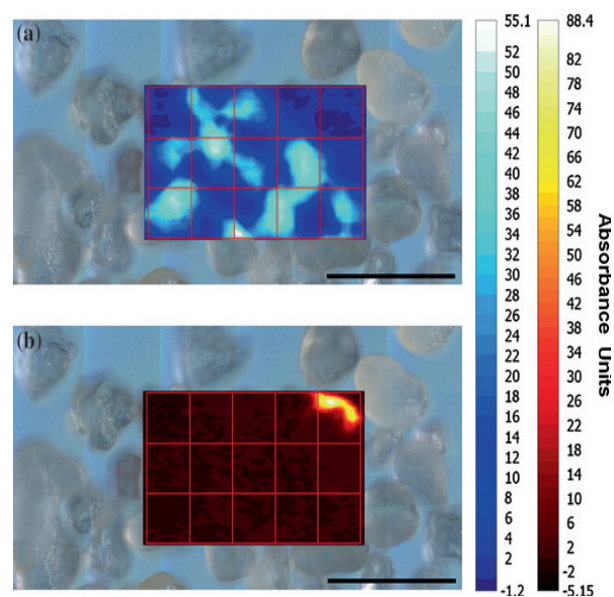


**Fig. 7.** Chemical image of an integration of typical spectral bands [38].

filtered and analyzed directly on the dried filter without further sample preparation. This enables the rapid assessment of microplastic encroachment and can assist in the development of remediation techniques [72]. However, it is extremely time-consuming when targeting the whole sample filter surface at a high spatial resolution because it uses only a single detector element, which happens to be limitation of this technique [15,71].

### 3.5. Raman micro-spectroscopy (RMS)

Raman spectroscopy is a “surface technique”, thus large, visually sorted microplastic particles can be analyzed and the technique can also be coupled with microscopy. Raman micro-spectroscopy is straightforward and uses a scattering technique. The simple principle of this technique is measuring the wavelength and intensity of inelastically scattered light from molecules caused by a monochromatic light. The Raman scattered light occurs at wavelengths that are shifted from incident light by the energies of molecular vibrations giving out spectra (Fig. 8). A very small volume ( $< 1 \mu\text{m}$  in diameter) of the sample can generate the Raman spectra which allow the identification of species

present in that volume [76].

The instrument consists of a standard optical microscope, an excitation laser, a notch filter, a monochromator, and a sensitive detector (such as a charge-coupled device (CCD), or photomultiplier tube (PMT)). The notch filter is used to block elastically scattered light which would otherwise overwhelm the weak signal from the Raman or inelastically scattered photons ( $\sim 1/10^6$  scattered photons). The Raman scattered light may be dispersed according to wavelength and detected by a CCD as shown in Figure 8. Angel et al [53] stated that when a UV laser source is used for Raman microspectroscopy (RMS), then ultraviolet microscopes and UV aided optics must be used. Earlier studies by Taylor et al [78] and Adrian et al [79] have expressed the suitability of RMS for the microscopic examination of minerals, materials such as polymers and ceramics, cells, proteins and forensic trace evidence.

RMS have been used by a lot of researchers for detecting microplastics with high reliability in marine environment [7,16,28,36,80] and for testing simulated microplastics polluted water [81]. Wagner et al [40] performed the analyses

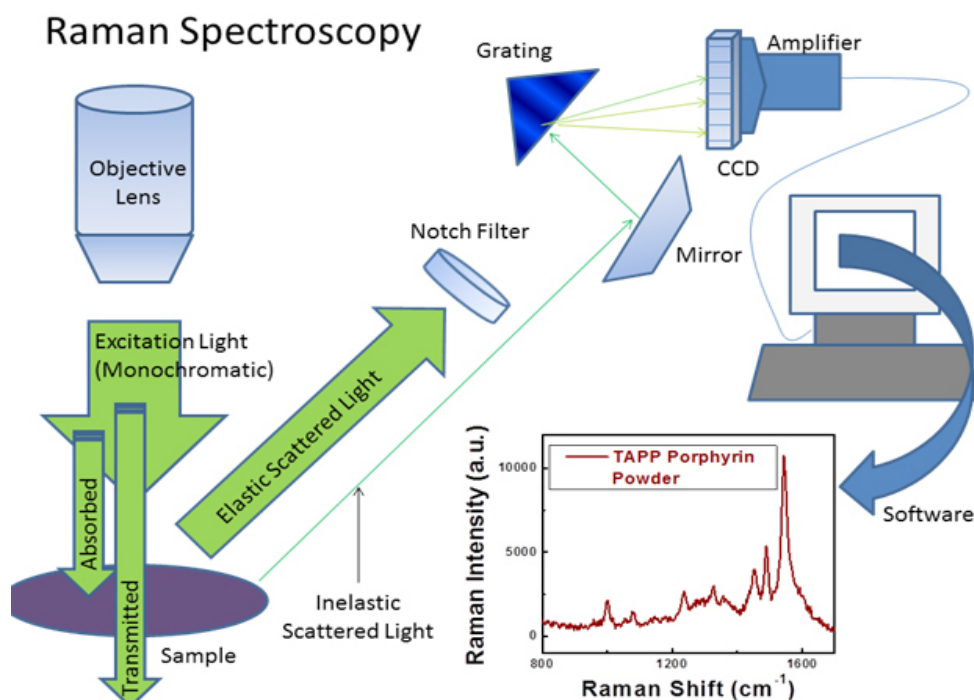


**Fig. 8.** Schematic for process involved in collecting Raman spectra. A Raman spectrum for tetra(4-aminophenyl) porphyrin (TAPP) powder is shown [77].

on ocean trawl and fish using both Renishaw inVia and Bruker Senterra dispersive Raman microscopes with 785 nm and 532 nm lasers. In the study, analytical laser optimization was achieved using several different objectives (5x, 20x, 50x and 100x). The author matched the Raman spectra obtained with spectral matching performed using GRAMS software, which was equipped with commercially available Raman spectral libraries. Rocchia et al [81] simulated microplastics polluted water. A few milligrams of three different reference materials (irregularly shaped polyethylene particles sieved at 74 microns, polystyrene-divinylbenzene PS-DVB microspheres sieved between 37-74 microns and polyethylene-titanium dioxide PE-TiO<sub>2</sub> microspheres with a size range of 27-45 micron) were used to simulate microplastic debris with different particle sizes in 0.5 L of water. The Raman spectra data were collected using the DXR2xi Raman imaging microscope and the accompanying Thermo Scientific OMNICxi Raman imaging software. The obtained spectra are presented in Figure 9. The author concluded that Raman microscopy allows the analysis of particles

below 1-micron size and the correct identification of plastic materials as well as inorganic materials such as titanium dioxide or other additives.

The Raman techniques have one major advantage over FTIR, which is its ability to identify particles up to 500 nm in size [80]. By comparison with reference spectra or standard library spectra (e.g. from GRAMS software), specific plastic polymers can be identified within minutes. Accordingly, RMS allows broad range of detection and quantification of very small plastic particles of sizes < 1 μm [7,35] and when combined with Raman spectral imaging, spatial chemical images can be produced based on the Raman spectra of a sample. This was recently demonstrated by researchers [81]. Cole et al [7] demonstrated that polymer particles within biological tissues with subcellular precision can be located with Raman technique when coupled with confocal laser-scanning microscopy. One limitation of this technique is drawn from its inability to measure laser excited fluorescent samples (e.g. residues of biological origin from samples) as they block the generation of interpretable Raman spectra [38]. Generally, lower laser wave lengths

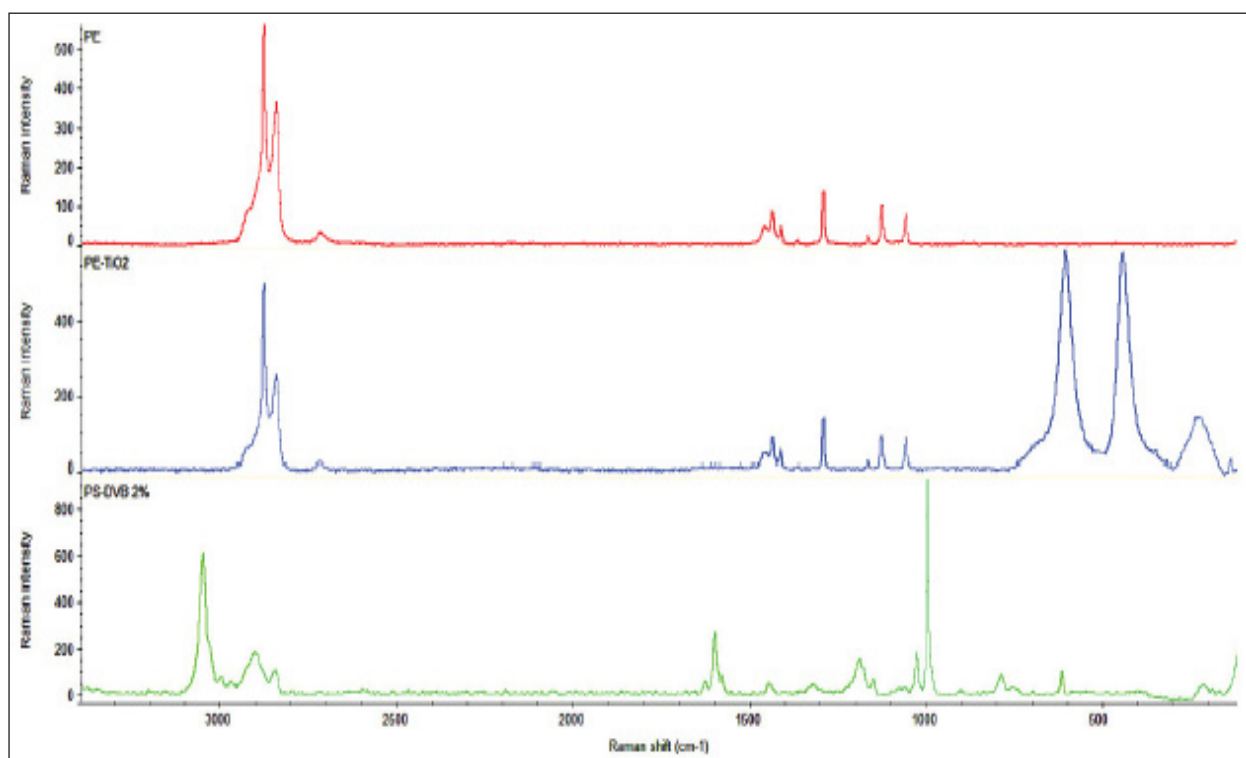


**Fig. 9.** Raman spectra of PE - polyethylene; PE-TiO<sub>2</sub> polyethylene-titanium dioxide and PS-DVB – polystyrene-divinylbenzene microplastic standards [81].

transmit high energy result and signal intensity but also in a high fluorescence. Therefore, higher laser wavelengths greater than 1000 nm will minimize fluorescence but the lower energy of the laser results in a lower signal of the polymer sample. More study is required to find the optimum wave length of the laser light which will address this problem of fluorescence and low intensity for assessments of microplastics in environmental samples. In line, [38] recommended that fluorescence should be prevented through a sample pre-purification step prior to measurements for a clear identification of the polymer type of microplastic particles

Raman spectroscopy and FTIR are complementary techniques. Molecular vibrations, which are Raman inactive are IR active and vice versa and can thus provide complementary information on microplastic samples [38].

### ***3.6. Scanning electron microscopy with energy-dispersive x-ray spectroscopy (SEM/EDS)***

Scanning Electron Microscopy (SEM) magnifies a specific sample region using a high energy focused beam of electrons. The analyzed region evaluated with SEM can also be assayed for specific elements using Energy Dispersion Spectroscopy (EDS). SEM generates micrographs while EDS provides concentration of chemical composition of the sample. Thus the combined technique is referred to as SEM/EDS or SEM/EDX Analysis. The SEM/EDS method enables the detection of microplastics and its degradation process in a sample due to its micro-scale and nano-scale features with magnification up to 500,000x [15,36]. The method determines particle sizes and elemental composition of microplastics in your test sample. It can only be performed only on solid samples [82].

A key factor in SEM is the interaction volume, which depends on the accelerating voltage of the electron beam and other factors including specimen nature, composition and sample preparation. The higher the accelerating voltage applied, the larger the interaction volume. This in turn determines the emission depth of the different signals used. The emission of secondary electrons (topography)

and backscattered electrons (atomic number) are used to generate micrographs in SEM. Thereby providing information on topography, morphology, composition and crystallographic nature of microplastics in an environmental sample [83]. This method has been used to detect microplastics particles in sample [15,36]. Vianello [15] analysed sediments collected from Lagoon of Venice in Italy using SEM to characterize the surface morphology of the microplastic particles. Result showed irregular shapes and similar surface textures for several microplastics in contrast with comparable amorphous and regular surfaces of other plastic microfibers. Furthermore, the method revealed possible occurrence of degradation processes by showing images of weakened surfaces caused by adhering particles [15]. Imhof et al. [36] identified degraded microplastics in sediments of subalpine lake beach using SEM imaging. Many of the PP microplastics showed cracks, pits, grooves, disintegration, and adherent and attached diatoms. A typical SEM image of microplastic particles is presented in Figure 10.

Whilst SEM is effective for identification, EDS helps in quantification. In addition, SEM/EDS analyses have been conducted on ocean trawl and fish gut for microplastics by [40] and [67]. Potential microplastics using particle morphology and elemental chemistry profiles have been tested by Wagner et al [40]. The analytical instrument used has been FEI XL30 Environmental SEM and a Thermo Fisher Scientific Noran System 7 EDS System. Moreover, samples has been imaged at 50x – 10,000x using an atomic number sensitive, backscattered electron (BSE) detector with a resolution of approximately 0.1  $\mu\text{m}$  [67] reported that SEM/EDS is effective in identifying chlorinated plastics such as polyvinyl chloride (PVC) due to their unique elemental signatures. Typical SEM-EDS results for microplastics in an environmental sample are shown in Figure 11.

The technique (SEM/EDS) has been used in identification of plastic additives of inorganic origin contained in microplastic particles, characterization and toxic chemicals extracted from microplastics

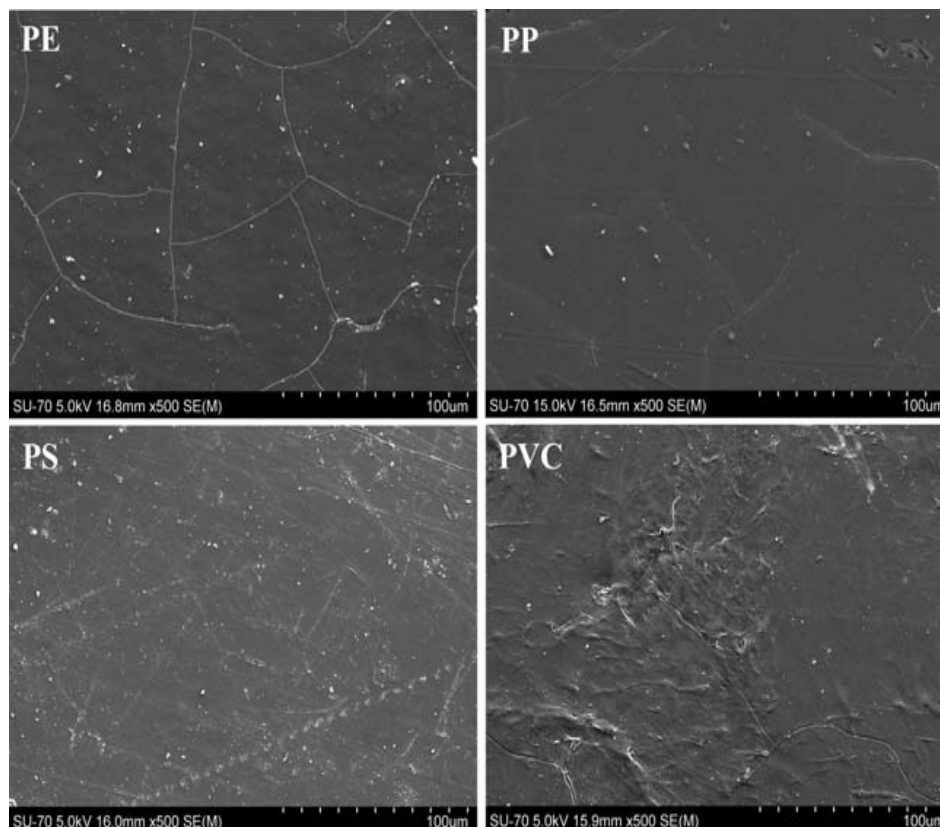


**Fig. 10.** Scanning electron microscopy images showing the surface of several thermoplastics: polyethylene (PE), polypropylene (PP), polystyrene (PS) and polyvinyl chloride (PVC) [83].

in samples from the North Pacific Gyre by Mendoza and Jones [84]. SEM-EDS have become an indispensable tool for analysis microplastic particles present in a sample. This method enables scientists to monitor how plastics degrade to form microplastic particles, emergent pollutants expressively threatening biota life [61,83].

The limitation of quantitative SEM-EDS is that, this technique should only be carried out in flat polished samples or very thin films with irrelevant topography. Prior to spectra acquisition for quantification purpose, it is imperative that several well-assigned spectra with sufficient X-ray counts have been previously collected (serving as a reference). Then, the spectra need to be processed with matrix corrections with oxygen calculated by stoichiometry and the appropriate ZAF (the atomic number-Z, absorption-A and fluorescence-F correction) procedure. Again, EDS software applies the ZAF correction and carries out subsequent integration of the peaks to give the final semiquantification of the elements present in

the specimen. Nevertheless, the user should be as critical as possible when accepting each step of the quantification process provided by the software [85].

#### **4. Conclusions**

This study reviewed spectroscopic techniques for quantifying and identification of microplastics in an environmental sample. Generally, for microplastics particles  $<500\ \mu\text{m}$ , spectroscopic techniques is important for their identification while the quality of result obtained strongly rely on good sampling and effective sample purification. During purification aggressive agents (e.g. strong acidic or alkaline solutions) should be avoided to conserve the whole plastic spectrum and because aggressive solutions negatively affect certain plastic polymer. Also, ordinary visual inspection of samples alone is insufficient but when in tandem with optical microscope it becomes effective, especially, in the case of particles  $<500\ \mu\text{m}$ . In

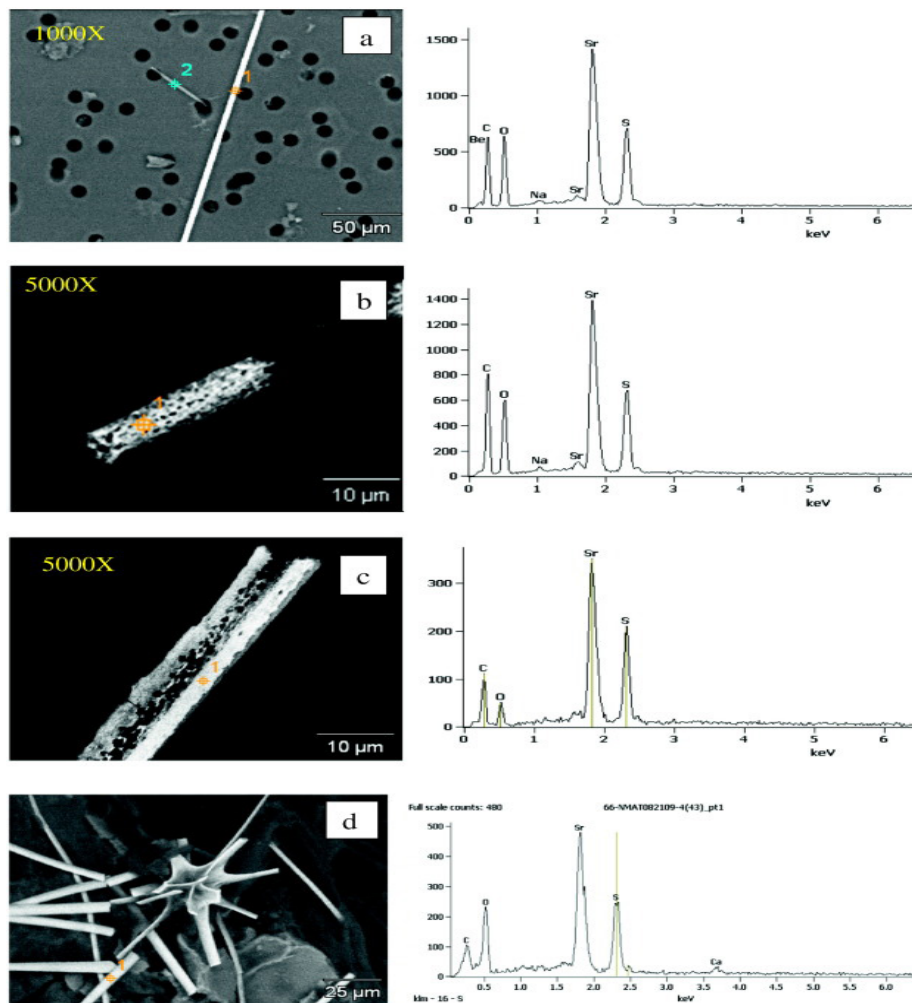


Fig. 11. Typical SEM-EDS results for microplastics in an environmental sample [67].

addition, CHN analyzer, pyrolysis-GC/MS and SEM-EDS have been used effectively for sample identification and quantification. The former which is based on combustion techniques works better for larger particle while SEM-EDS techniques is a better update to optical microscopy by providing information on the degradation process of plastic particles. A spectroscopic verification of microplastic particles by micro-FTIR or micro-Raman spectroscopy is essential and has also been used successfully for analyzing the particles of microplastics. Micro-Raman spectroscopy is very effective for microplastic particles of  $<1$   $\mu\text{m}$ . Furthermore, spectroscopic techniques create an added value as they also provide information on the polymer composition. However, some of the discussed methods have its drawbacks in their use which include cost effectiveness, time

consuming and difficulty to use (especially if you are inexperienced) like pyrolysis-GC/MS where samples have to be placed manually.

Finally, microplastics have been studied with non destructive methods often a combination of two methods: one separating and the other quantifying. It could be observed that since microplastics undergo very few reactions, their identification and quantification can be problematic more so in living tissue where there is no harm reported as at the time of this study. However, microplastics have become a cause for concern and advance studies are required to unravel the potential risk of their presence in our food and environment.

## 5. Conflicts of interest

The authors declare no conflicts of interest

## 6. Acknowledgement

This research did not receive any specific funding

### *Nomenclatures (Abbreviations)*

NOAA: National Oceanic and Atmospheric Administration;

POPs: Persistent organic pollutants;

PAHs: Polyaromatic hydrocarbons;

OCPs: Organochlorine pesticides;

PCBs: polychlorinated biphenyls;

WHO: World Health Organization;

SOP: standard operation protocols;

FTIR: Fourier Transform infrared spectroscopy;

SEM-EDS: scanning electron microscopy energy-dispersive X-ray spectroscopy (SEM-EDS);

PyrGC/MS: pyrolysis- chromatography/mass spectrometry;

TD-GC/MS: thermal desorption-gas chromatography/mass spectrometry;

GC: gas chromatography;

MS: mass spectroscopy;

TCD: thermal conductivity detector;

OPAs: organic plastic additives;

HDPE, LDPE: high-density and low-density polyethylene;

ATR: Attenuated Total Reflectance (ATR);

FPA: Focal Plane Array-Based Reflectance;

RMS: Raman micro-spectroscopy;

CCD: charge-coupled device;

PMT: photomultiplier tube;

UV: Ultraviolet;

PE: polyethylene;

PE-TiO<sub>2</sub>: polyethylen-titanium dioxide;

PS-DVB: polystyrene-divinylbenzene;

SEM: Scanning Electron Microscopy;

EDS: Energy Dispersion Spectroscopy;

PP: polypropylene;

PS: polystyrene;

PVC: polyvinyl chloride;

ZAF: atomic number-Z, absorption-A and fluorescence-F.

## 7. References

- [1] R.U. Halden, Plastics and public health, *Annu. Rev. Pub. Health*, 31 (2010) 179-194.
- [2] Statista, Production of plastics worldwide from 1950 to 2017 in million metric tons, 2018. <https://www.statista.com/statistics/282732/global-production-of-plastics-since-1950/>
- [3] R.C. Thompson, Plastic debris in the marine environment: consequences and solution, marine nature conservation in Europe, federal agency for nature conservation, Stralsund, 2006.
- [4] J.G. Derraik, The pollution of the marine environment by plastic debris: a review, *Mar. Poll. Bull.*, 44 (2002) 842–852.
- [5] C.J. Moore, G. L. Lattin, A.F. Zellers, Density of plastic particles found in zooplankton trawls from coastal waters of California to the north pacific central gyre, The plastic debris river to sea conference, Redondo Beach, California, 2005.
- [6] D. Barnes, F. Galgani, R. Thompson, M. Barlaz, Accumulation and fragmentation of plastic debris in global environments. *Philos. Trans. Royal Soc. B*, 364 (2009) 985-998.
- [7] M. Cole, P. Lindeque, C. Halsband, T. S. Galloway, Microplastics as contaminants in the marine environment: a review. *Mar. Poll. Bull.*, 62 (2011) 2588–2597.
- [8] Greenfacts, Marine Litter: What are micro-plastics and how do they enter the marine environment? (2018). <https://www.greenfacts.org/en/marine-litter/1-2/3-micro-plastics.htm> [Accessed 09 May 2018].
- [9] E.R. Graham, J.T. Thompson, Deposit- and suspension-feeding sea cucumbers (Echinodermata) ingest plastic fragments. *J. Exp. Mar. Bio. Eco.* 368 (2009) 22–29.
- [10] K. Betts, Why small plastic particles may pose a big problem in the oceans, *Env. Sci. Tech.*, 42(2008) 8995-8999.
- [11] M.A. Browne, A. Dissanayake, T.S. Galloway, D.M. Lowe, R.C. Thompson, Ingested microscopic plastic translocates to the circulatory system of the mussel, *Mytilus edulis* (L), *Env. Sci. Tech.*, 42 (2008) 5026–5031
- [12] M.A. Browne, P. Crump, S.J. Niven, E. Teuten, A. Tonkin, T. Galloway, Accumulation of microplastic on shorelines worldwide: Sources and sinks, *Env. Sci. Tech.*, 45 (2011) 9175–9179.

- [13] M. Claessens, S. De Meester, L. Van Landuyt, K. De Clerck, C. R. Janssen, Occurrence and distribution of microplastics in marine sediments along the Belgian coast. *Mar. Poll. Bull.*, 62 (2011) 2199–2204.
- [14] J. Hammer, M.H. Kraak, J.R. Parsons, Plastics in the marine environment: the dark side of a modern gift". *Reviews of environmental contamination and toxicology*, 220 (2012) 1–44.
- [15] A. Vianell, A. Boldrin, P. Guerriero, V. Moschino, R. Rella, A. Sturaro, Microplastic particles in sediments of Lagoon of Venice, Italy: First observations on occurrence, spatial patterns and identification. *Estuarine, Coastal and Shelf Sci.*, 130 (2013) 54–61.
- [16] L. Van Cauwenberghe, A. Vanreusel, J. Mees, C.R. Janssen, Microplastic pollution in deep-sea sediments. *Env. Poll.*, 182 (2013) 495–499.
- [17] K.L. Ng, J.P. Obbard, Prevalence of microplastics in Singapore's coastal marine environment, *Mar. Poll. Bull.*, 52 (2006) 761–767.
- [18] T. Bowmer, P. Kershaw, Bioaccumulating and Toxic Substances in the Oceans, In: *Proceedings of the GESAMP International Workshop on Microplastic Particles as a Vector in Transporting Persistent*, (2010).
- [19] S. Endo, R. Takizawa, K. Okuda, H. Takada, K. Chiba, H. Kanehiro, H. Ogi, R. Yamashita, T. Date, Concentration of polychlorinated biphenyls (PCBs) in beached resin pellets: variability among individual particles and regional differences, *Mar. Poll. Bull.*, 50 (2005) 1103–1114.
- [20] Y. Mato, T. Isobe, H. Takada, H. Kanehiro, C. Ohtake, T. Kaminuma Plastic resin pellets as a transport medium for toxic chemicals in the marine environment, *Env. Sci. Tech.*, 35 (2001) 318–324.
- [21] L. M. Rios, C. Moore, P.R. Jones, Persistent organic pollutants carried by synthetic polymers in the ocean environment, *Mar. Poll. Bull.*, 54 (2007) 1230–1237.
- [22] A.A. Koelmans, E. Besseling, E.M. Foekema, Leaching of plastic additives to marine organisms, *Env. Poll.*, 187 (2014) 49–54.
- [23] C. M. Rochman, E. Hoh, T. Kurobe, S.J. Teh, Ingested plastic transfers hazardous chemicals to fish and induces hepatic stress, *Scientific Reports*, 3 (2013) 3263.
- [24] L.A. Holmes, A. Turner, R.C. Thompson, Adsorption of trace metals to plastic resin pellets in the marine environment, *Env. Poll.*, 160 (2012) 42–48.
- [25] C.M. Rochman, B.T. Hentschel, S.J. Teh, Long-term sorption of metals is similar among plastic types: implications for plastic debris in aquatic environments, *PLoS One*, 9 (2014) 85433.
- [26] K. Ashton, L. Holmes, A. Turner, Association of metals with plastic production pellets in the marine environment, *Mar. Poll. Bull.*, 60 (2010) 2050–2055.
- [27] L.A. Holmes, A. Turner, R.C. Thompson, Interactions between trace metals and plastic production pellets under estuarine conditions, *Marine Chemistry*, 23 (2014) 1–8.
- [28] F. Murray, P.R. Cowie, Plastic contamination in the decapod crustacean *Nephrops norvegicus*, *Mar. Pollu. Bull.*, 62 (2011) 1207–1217.
- [29] A. Ugolini, G. Ungherese, M. Ciofini, A. Lapucci, M. Camaiti, Microplastic debris in sandhoppers. *Estuarine, Coastal and Shelf Sci.*, 129 (2013) 19–22.
- [30] E.M. Foekema, C. De Gruijter, M.T. Mergia, J.A. van Franeker, A.J. Murk, A.A. Koelmans, Plastic in North Sea fish, *Env. Sci. Tech.*, 47 (2013) 8818–8824.
- [31] S.L. Wright, R.C. Thompson, T.S. Galloway, The physical impacts of microplastics on marine organisms: A review, *Env. Poll.*, 178 (2013) 483–492.
- [32] S.L. Wright, F.J. Kelly, H. Ren, Plastic and Human Health: A Micro Issue, *Environ. Sci. Technol.*, 51(2017) 6634–6647.
- [33] G. Readfearn, The Guardian WHO launches health review after micro-plastics found in 90% of bottled water, *Water Res.*, 2 (2018) 1–47.
- [34] V. Hidalgo-Ruz, L. Gutow, R.C. Thompson, M. Thiel, Micro-plastics in the marine environment: a review of the methods used for identification and quantification, *Env. Sci. Tech.*, 46 (2012) 3060–3075.
- [35] M. Claessens, L. Van Cauwenberghe, M.B. Vandegehuchte, C.R. Janssen, New techniques for the detection of microplastics in sediments and field collected organisms, *Mar. Poll. Bull.*, 70 (2013) 227–233.
- [36] H.K. Imhof, J. Schmid, R. Niessner, N.P. Ivleva, C. Laforsch, A novel, highly efficient method for the

- separation and quantification of plastic particles in sediments of aquatic environments, *Limnology and Oceanography: Meth.*, 10 (2012) 524–537.
- [37] M.T. Nuelle, J. H. Dekiff, D. Remy, E. Fries, A new analytical approach for monitoring micro-plastics in marine sediments, *Env. Poll.*, 184 (2014) 161–169.
- [38] G.J.L. Martin, G. Gunnar, Methodology Used for the Detection and Identification of Microplastics—A Critical Appraisal. M. Bergmann (eds.), *Mar. Anthropol. Lit. Chap.*, 8 (2015) 201-227.
- [39] M. Kedzierski, V. Le Tilly, P. Bourseau, H. Bellegou, G. César, O. Sire, Microplastics elutriation from sandy sediments: A granulometric approach, *Mar. Poll. Bull.*, 107 (2016) 315-323.
- [40] J. Wagner, Z. Wang, S. Ghosal, C. M. Rochman, M. Gassel and S. Wall, Novel Method for the Extraction and Identification of Microplastics in ocean trawl and fish gut matrices, *Anal. Meth.*, 9 (2016) 1479-1490.
- [41] S. Klein, I.K. Dimzon, T.P. Knepper, Analysis, Occurrence, and Degradation of Microplastics in the Aqueous Environment. M. Wagner, S. Lambert (eds.), *Freshwater Microplastics, Hdb. Env. Chem.*, 58 (2018) 51-62.
- [42] E. N. Verla, M.J. Horsfall, A.I. Spiff, Physico chemical Characterization of Playgrounds Soils of public Schools in Owerri Metropolis, Imo State, Nigeria. *Int. J. Inn. App. Studies*, 13 (2015) 472-480.
- [43] E.N. Verla, A.W. Verla, C.E. Enyoh, Pollution Assessment Models Of Soils In Portharcourt City, Rivers State, Nigeria. *Wor N. Nat. Sci.*, 12 (2017) 1-23.
- [44] C.E. Enyoh, E.A. Ihionu, A.W. Verla, P. N. Ebosie, Physicochemical Parameter Of Palm Oil And Soil From Ihube Community, Okigwe, Imo State Nigeria, *Int. Letters Nat. Sci.*, 62 (2017) 35-43.
- [45] C.E. Enyoh, A.W. Verla, N.J. Egejuru, pH variations and chemometric assessment of borehole water in Orji, Owerri Imo State, Nigeria. *J. Env. Anal. Chem.*, 5 (2018) 1-9.
- [46] A. W. Verla, E. N. Verla, C. E. Amaobi, C. E., Enyoh Water Pollution Scenario at River Uramurukwa Flowing Through Owerri Metropolis, Imo State, Nigeria. *Int. J. App. Sci. Res.*, 3 (2018) 40-46.
- [47] L. Jing, Risk Assessment of Heavy Metals in Surface Sediments from the Yanghe River, China. *Int. J. Environ. Res. Public Health*, 11 (2014) 12441-12453.
- [48] R.C. Thompson, Y. Olsen, R.P. Mitchell, A. Davis, S.J. Rowland, A.W. John, Lost at sea: where is all the plastic?, *Sci.*, 304 (2004) 838–838.
- [49] Y.K. Song, S.H. Hong, M. Jang, G.M. Han, M. Rani, J. Lee, A comparison of microscopic and spectroscopic identification methods for analysis of microplastics in environmental samples. *Mar. Poll. Bull.*, 93 (2015) 202-209.
- [50] J.P.W. Desforges, M. Galbraith, N. Dangerfield, P.S. Ross, Widespread distribution of microplastics in subsurface seawater in the NE Pacific Ocean, *Mar. Poll. Bull.*, 79 (2013) 94–99.
- [51] G. Erni-Cassola, M.I. Gibson, R.C. Thompson, J.A. Christie-Oleza, Lost, but Found with Nile Red: A Novel Method for Detecting and Quantifying Small Microplastics (1 mm to 20  $\mu\text{m}$ ) in Environmental Samples, *Env. Sci. Tech.*, 5 (2017) 13641-13648.
- [52] T. Maes, J. Rebecca, W. Nikolaus, H. Karsten, G.M. Andrew, A rapid-screening approach to detect and quantify microplastics based on fluorescent tagging with Nile Red. *Scientific Reports*, 7 (2017) 44501.
- [53] S.M. Angel, T.J. Kulp, T.M. Vess, Remote-Raman Spectroscopy at Intermediate Ranges Using Low-Power cw Lasers, *Appl. Spectrosc.*, 46 (1992) 1085–1091.
- [54] R. Goodacre, D.B. Kell, Pyrolysis mass spectrometry and its applications in biotechnology, *Curr. Op. Biotech*, 7 (1996) 20–28.
- [55] G. Guido, Characterization of Polymers and Plastics Using an Elemental Analyzer, (2016).
- [56] K. Liliana, G. Guido, Characterization of Polymers and Plastics (pellets, powders and films) by the Thermo Scientific FLASH 2000 Elemental Analyzer, Application note, 42230 (2016) 1-5.
- [57] S. Morét-Ferguson, K.L. Law, G. Proskurowski, E.K. Murphy, E.E. Peacock, C.M. Reddy, The size, mass, and composition of plastic debris in the Western North Atlantic Ocean, *Mar. Poll. Bull.*, 60 (2010) 1873–1878.
- [58] P.M. Peacock, C.N. McEwen, Mass Spectrometry of Synthetic Polymers, *Anal. Chem.*, 78 (2006) 3957–3964.
- [59] R. K. Erwin, K. Mitsuhiro, G. Margit, J. Hans-Gerd, Hyphenation of aqueous liquid chromatography to pyrolysis-gas chromatography and mass spectrometry for the comprehensive

- characterization of water-soluble polymers, *J. Chrom. A*, 1186 (2008) 222–227.
- [60] P. Eckerle, M. Pursch, H.J. Cortes, K. Sun, B. Winniford, J. Luong, Determination of short-chain branching content in polyethylene by pyrolysis comprehensive multidimensional gas chromatography using low thermal mass column technology, *J. Sep. Sci.*, 1 (2008) 3416–3422.
- [61] E. Fries, J.H. Dekiff, J. Willmeyer, M.T. Nuelle, Ebert M., D. Remy, Identification of polymer types and additives in marine microplastic particles using pyrolysis-GC/MS and scanning electron microscopy, *Environ. Sci. Process Impacts*, 15 (2013) 1949–1956.
- [62] P. Kusch, Pyrolysis-Gas Chromatography/Mass Spectrometry of Polymeric Materials. *Advanced Gas Chromatography-Progress in Agricultural, Biomedical and Industrial Applications*, Dr. Mustafa Ali Mohd (Ed.), *In. Tech.*, 6 (2012) 21–24.
- [63] A.J. Underwood, M.G. Chapman, M.A. Browne, Some problems and practicalities in design and interpretation of samples of microplastic waste, *Anal. Methods*, 9 (2017) 1332–1345.
- [64] T. Matthias, H. Elena, K.F. Elke, Nile Red Staining as a Subsidiary Method for Microplastic Quantification: A Comparison of Three Solvents and Factors Influencing Application Reliability, *DRP J. Earth Sci. Env. Studies*, 2 (2017) 1–8.
- [65] R. Geyer, J.R. Jambeck, K.L. Law, Production, use, and fate of all plastics ever made, *Law Sci. Adv.* 3 (2017).
- [66] W. J. Shim, Y.K. Song, S.H. Hong, M. Jang, Identification and quantification of microplastics using Nile Red staining, *Mar. Poll. Bull.*, 104 (2016) 109–117.
- [67] Z.M. Wang, J. Wagner, S. Ghosal, G. Bedi, S. Wall, SEM/EDS and optical microscopy analyses of microplastics in ocean trawl and fish guts. *Sci. Total. Environ.*, 603–604 (2017) 616–626.
- [68] M. Eriksen, S. Mason, S. Wilson, C. Box, A. Zellers, W. Edwards, Microplastic pollution in the surface waters of the Laurentian Great Lakes, *Mar. Poll. Bull.* 77 (2013) 177–182.
- [69] M. Kerstin, N. Fredrik Screening Of Microplastic Particles In And Down-Stream A Wastewater Treatment Plant. IVL Swedish Environmental Research Institute, Stockholm, (2014) 1–22.
- [70] I. W. Levin, R. Bhargava Fourier transform infrared vibrational spectroscopic imaging: Integrating microscopy and molecular recognition, *Annual Rev. Phys. Chem.*, 56 (2005) 429–474.
- [71] J. P. Harrison, J.J. Ojeda, M.E. Romero-Gonzalez, The applicability of reflectance micro-Fourier-transform infrared spectroscopy for the detection of synthetic microplastics in marine sediments, *Sci. Total. Environ.*, 416 (2012) 455–463.
- [72] M. Bradley, S. Suja, L. Steven, W. Stephan, Tracking Microplastics in the Environment via FT-IR Microscopy, *Spectroscopy*, 32 (2017) 17–23.
- [73] S. Saarakkala, L. Rieppo, J. Rieppo, J. S. Jurvelin, Fourier Transform Infrared (FTIR) Microspectroscopy of Immature, Mature and Degenerated Articular Cartilage. *Microscopy: Science, Technology, Applications and Education*, A. Méndez-Vilas and J. Díaz (Eds.), Formatex (2010).
- [74] S. T. Alexander, S. Melanie, P.H. Jesse, J.O. Jesús, Identification and quantification of microplastics in wastewater using focal plane array-based reflectance micro-FTIR imaging, *Anal. Chem.*, 87 (2015) 6032–6040.
- [75] M. M. Reddy, M. Deighton, R.K. Gupta, S.N. Bhattacharya, R. Parthasarathy, Biodegradation of oxo-biodegradable polyethylene. *J Appl. Polym. Sci.*, 111 (3) (2009) 1426–1432.
- [76] S. Schlücker, Design and synthesis of Raman reporter molecules for tissue imaging by immunoSERS microscopy, *J. Biophotonics*, 4 (2011) 453–463.
- [77] D.N. Sathyanarayana, *Vibrational spectroscopy: theory and applications*, book, 2015.
- [78] P.D. Taylor, O. Vinn, A. Kudryavtsev, J.W. Schopf, Raman spectroscopic study of the mineral composition of cirratulid tubes (Annelida, Polychaeta), *J. Struc. Bio.*, 171 (2010) 402–405.
- [79] G. Adrian, C.P. flavius, S. Virginie, S. Chris, N. Ioan, Applications of Raman micro-spectroscopy to stem cell technology: label-free molecular discrimination and monitoring cell differentiation, *EPJ Tech. Instrument*, 2 (2015) 6–9.
- [80] A. Kappler, F. Windrich, M.G.J. Loder, M. Malanin, Identification of microplastics by FTIR and Raman microscopy: a novel silicon filter substrate opens the important spectral range below 1300  $\text{cm}^{-1}$  for FTIR transmission measurement, *Anal. Bional. Chem.*, 407 (2015) 6791–6801.

- [81] M. Rocchia, I. Ruff, A. Vianello, Microplastic identification and characterization by Raman imaging spectroscopy, Thermo, Fisher Scientific Inc., 8 (2017) 1-5.
- [82] M. Tirrel, Fundamentals of polymer solutions, Talor and francis, 2018.
- [83] M. Scimeca, S. Bischetti, H. Kaur Lamsira, R. Bonfiglio, E. Bonanno, Energy dispersive X-ray (EDX) microanalysis: A powerful tool in biomedical research and diagnosis, Eur. J. Histochem. 62 (2018) 2841
- [84] L.M.R. Mendoza, P.R. Jones, Characterisation of microplastics and toxic chemicals extracted from microplastic samples from the North Pacific Gyre, Env. Chem., 12 (2015) 611-617.
- [85] A.J. Garratt-Reed, D.C. Bell, Energy Dispersive X-Ray Analysis in the Electron Microscope, BIOS Scientific Publishers Limited, Oxford, 2003.



## Investigation of graphene/CNT hybrid structural effect on absorption of $Mn^{2+}$ by activated carbon

Ahmad Ghozatloo<sup>a\*</sup>, and Mojtaba Shariaty-Niassar<sup>b</sup>

<sup>a</sup> Research Institute of Petroleum Industry (RIPI), West Blvd. Azadi Sport Complex, Tehran, Iran

<sup>b</sup> Transport phenomena and Nanotechnology Laboratory (TPNT), Department of Chemical Engineering, School of Eng., University of Tehran, Tehran, Iran

### ARTICLE INFO:

Received 12 Apr 2019

Revised form 28 Apr 2019

Accepted 13 May 2019

Available online 15 Jun 2019

### Keywords:

Adsorption

Manganese

Activated Carbon

Graphene

CNT

Hybrid

### ABSTRACT

In this paper, an effort is made to improve the adsorption amount by adding graphene/CNT hybrid in the structure of activated carbon (AC) for removing manganese ions from aqueous solutions. The bonding G/CNT hybrid with activated carbon creates a structure which is an excellent absorbent for removing some heavy metal ions. Therefore, a comparison between the performance increasing ion adsorption and AC results as the blank adsorbent was made. Moreover, the influence of time, pH solution, initial concentration of  $Mn^{2+}$ , and temperature investigated as experimental conditions. Finally, the maximum adsorption was 89.38% and 96.18% for AC and AC/G/CNT composite respectively at 30 min, initial concentration of  $30 \text{ mgL}^{-1}$ ,  $\text{pH}=4.5$  in  $15 \text{ }^\circ\text{C}$  for both adsorbents. Finally, the results showed that under the same conditions, the presence of G/CNT hybrid in the structure of AC increased the amount of adsorption by 7.5%.

### 1. Introduction

Heavy metal ions and organics are two major classes of water pollutants. Heavy metal (a range of toxic metals) ions as poisonous compounds are one of the main problems that pollute the waters and plants. Discharging of pollutant water in plants will be absorbed in soil and will not degrade and accumulate in living organisms, causing various poisoning problems in animals and indirection for humans. Therefore, elimination of these heavy metal ions from waste water is necessary and interest [1].

Moreover, the major techniques have been used to reduce or decrease the heavy metal ions from wastewaters such as flotation, solvent extraction, silica, adsorption processes, ion exchange, reverse osmosis, lime chemical precipitation and coagulation [2]. Among these, adsorption is an industrial and good method for removing heavy metals from aqueous solutions [3]. Copper (Cu), mercury, cadmium, manganese ( $Mn^{2+}$ ), nickel, chromium and lead are known to be greatly toxic effect on waters [4]. The ion of  $Mn^{2+}$  can be found in the effluents of petrochemical plants is one of dangers source of pollution. In addition, pore structure of some substances which have active

\*Corresponding Author. Ahmad Ghozatloo

E-mail: [ghozatlooa@ripi.ir](mailto:ghozatlooa@ripi.ir)

DOI: <https://doi.org/10.24200/amecj>

surface such as chitosan, anthracite, lignite, and specially activated carbon (AC) are common and suitable for adsorption of  $Mn^{2+}$  and widely used for high adsorption capacity [5]. The objective of this paper was to improve performance of AC by G/CNT structures. Because the multi-layer configuration of graphene/CNT (G/CNT) hybrid structure is to have good adsorption performance, so recently, graphene hybrid structure has been applied as the adsorbent for absorption of some pollutants from waste water, because of its excellent capacitance. To improve interface and chemistry surface behavior, wide researches have been conducted on the structure of G/CNT hybrid structures [6]. In this paper, the effects of temperature, time, pH, and initial  $Mn^{2+}$  concentration were investigated to remove the cations of  $Mn^{2+}$  from water by AC/G/CNT composite as adsorbent and comparison with AC.

## 2. Material and Methods

The chemicals used for this paper were all Merck grade and used without further purification. Analytical grade of AC Powder was obtained from activated charcoal with the purity of > 99.9%. The solutions were prepared in deionized water. The Synthetic aqueous solutions of  $Mn^{2+}$  were prepared by dissolving enough amount of  $Mn(NO_3)_2$  in pure water. In order to prepare the aqueous solutions with various concentrations, first a stock solution was prepared with a concentration of 1000 mg/L of  $Mn^{2+}$ . For this purpose, 0.65 g of  $Mn(NO_3)_2$  was introduced in 1000 mL volumetric flask, added adequate water, and stirred the solution. Then

the purposed solutions were prepared with lower concentrations by dilution.

### 2.1. Preparation of activated carbon

First, 200 g of powdered glucose are placed in a tubular quartz reactor into the furnace under nitrogen atmosphere for 30 min. It is then gently warmed up to a temperature of 350 °C and remains for 2 hr. The glucose is carbonized under these conditions and is colored as a black powder. The powder placed in a furnace and heated at 400 °C for 1 hr under neutral atmosphere. Next the powder was extracted from the reactor and poured into 1 molar HCl at 90 °C for 30 min. The remaining mixture is filtered and washed with distilled water several times. Afterwards, the filter cake was dried in oven 65 °C for 11 hr. Dried powder is a activated carbon that is susceptible to participation in the carbon nanostructures.

### 2.2. Synthesis of AC/G/CNT composite

To synthesis of Graphene/CNT hybrid (G/CNT hybrid) a two-step method of chemical vapor deposition (CVD) was used. Its mechanism includes copper sheets by FeMo nanoparticles (as a catalyst) in the space of interlayer of copper sheets to formation of CNT/Graphene nanostructure as illustrated in figure 1.

According to figure 1 in the section (a), metal NPs nucleated on the surface of copper sheets as activated catalyst for growth of CNT. Section (b) is as first step of G/CNT hybrid synthesis which CNT fully grown on copper sheets by FeMo in 600 °C as low temperature process CVD catalyst

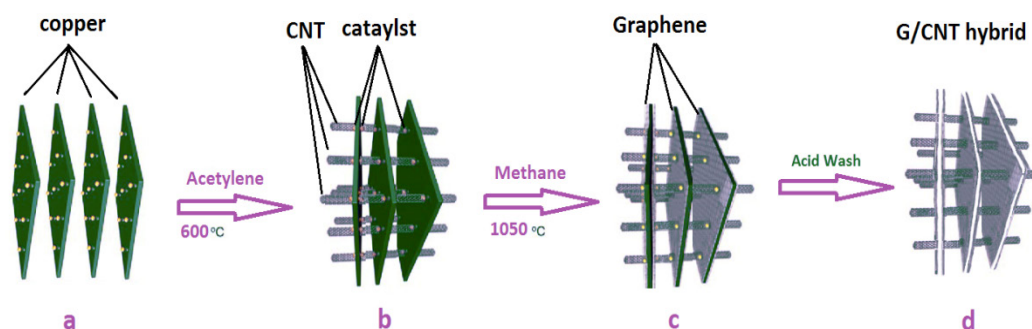


Fig. 1. Schematic illustration synthesis of G/CNT hybrid.

**Table 1.** The levels of independent variables process.

Independent Variables	-1 level	0 level	+1 level
Mn <sup>2+</sup> conc. (mgL <sup>-1</sup> )	30	80	130
Temperature (°C)	15	25	35
Time (min)	15	30	45
pH	3.5	4.5	5.5

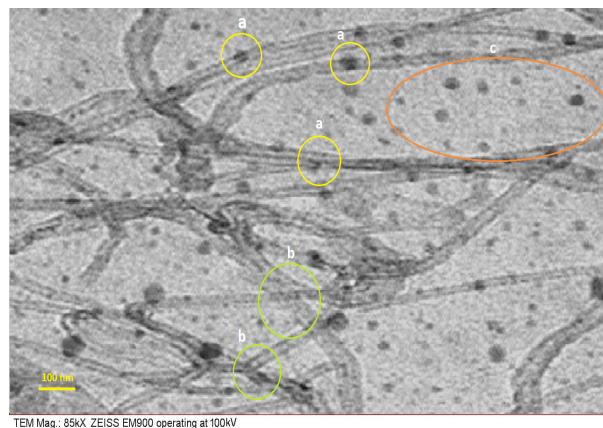
and section (c) is as second step of G/CNT hybrid synthesis which uniform Graphene nanosheets deposited on copper for G/CNT hybrid formation as higher temperature process. Finally, in section (d), acid washing was done to remove FeMo, copper sheets and other pollutants from G/CNT hybrid structure to obtain the high carbon purity [7]. 0.3 g of G/CNT powder prepared in 200 ml of distilled water and exposed to ultrasounds at 100 W for 2 hr. Then the amount of 20 g of AC powder is slowly added to the ultrasonic mixture for 3 hr. The mixture is then placed in the 50 °C for a day and then the water evaporates. The remaining solid layer was entering in tube quartz, under nitrogen atmosphere and slowly heated to 350 °C and remains for 2 hr. The residual product in reactor us AC/G/CNT composite. TEM image of the AC/G/CNT composite structure was shown in Fig. (2).

### 2.3. Independent variables & experiment design

For economic removal of Mn<sup>2+</sup> from the wastewater, it is necessary to find the optimum conditions of adsorption. Moreover, adsorption experimental parameters such as Mn<sup>2+</sup> ions concentration (30-

130 mgL<sup>-1</sup>), temperature (15-35°C), time (15-45 min), and pH (3.5-5.5) were studied in a batch mode. All experiments were conducted in 500 mL Erlenmeyer flasks. The levels of variables are shown in Table 1.

According to Table 1, for design of experiments because of various variables (each at 3 varied levels), Taguchi method was used. The software of Design Expert 8.3 was used to decrease the number of experiments to 9 based on Taguchi, and the results were shown in Table 2 include of detail of conditions.

**Fig. 2.** TEM image of AC/G/CNT composite (a) AC/GCNT (b) G/CNT (c) AC/G.**Table 2.** Condition of designed experiments by Taguchi method.

No.	Independent Variables <sup>a</sup>				AC/G/CNT			AC
	Mn <sup>2+</sup> (mg/L <sup>-1</sup> )	Temp. (°C)	Time (min)	pH	C <sub>0</sub> (mg/L)	C <sub>e</sub> (mg/L <sup>-1</sup> )	Reduction (%)	Reduction (%)
1	0	-1	-1	0	80	4.26	94.68	88.02
2	0	0	0	+1	80	5.29	93.38	86.45
3	0	+1	+1	-1	80	7.07	91.16	84.81
4	-1	-1	+1	+1	30	1.15	96.18	89.38
5	-1	0	-1	-1	30	2.05	93.17	86.64
6	-1	+1	0	0	30	2.17	92.76	86.26
7	+1	-1	0	-1	130	13.20	89.85	84.49
8	+1	0	+1	0	130	13.85	89.35	83.15
9	+1	+1	-1	+1	130	17.90	86.23	80.31

<sup>a</sup> Batch Adsorption process

The surfaces of adsorbents are cleaned from pollutants, fats, and activates by alkali washing [8]. For this purpose, treatment of AC and AC/G/CNT hybrid as adsorbents were done before using by alkali washing. Therefore, adsorbents separately were poured into 5 wt.% of HCl, stirred for 25 min, and washed with hot distilled water. Then the adsorbents washed with 1 wt.% of NaOH solution to eliminate the residual HCl [9]. The samples were filtered and washed with pure water until the pH of the filtrating solution was neutral. Next adsorbents were dried in oven (OVEN, XU 112, France) at 90 °C for 6 hr. Ground and sifted to obtain fine powder. Finally, the adsorbents kept in desiccators for subsequent uses.

The required amount of adsorbents was introduced in a stirred tank reactor containing 250 mL of the prepared solution of  $Mn^{2+}$  ions. The flasks were mechanically agitating for the desired time, wished temperature in fixed 650 rpm. Solution of hydrochloric acid/sodium hydroxide 0.1 M was also prepared for pH adjustments. According to Table 2, after each condition, the adsorbent was separated from the solution and filtered (0.45 $\mu$ m cellulose acetate paper). All experiments were performed in duplicate. After filtration,  $Mn^{2+}$  ions remaining in the solution were determined with a Perkin-Elmer 3100 atomic absorption spectrophotometer. The amount of adsorbed  $Mn^{2+}$  ions was calculated using the  $q_e = (C_0 - C_e) \times v/m$  equation. where  $q_e$  is the quantity of adsorbed  $Mn^{2+}$  ions at equilibrium (mg/g),  $C_0$  and  $C_e$  respectively are the initial and equilibrium concentrations of  $Mn^{2+}$  ions (mg/L),

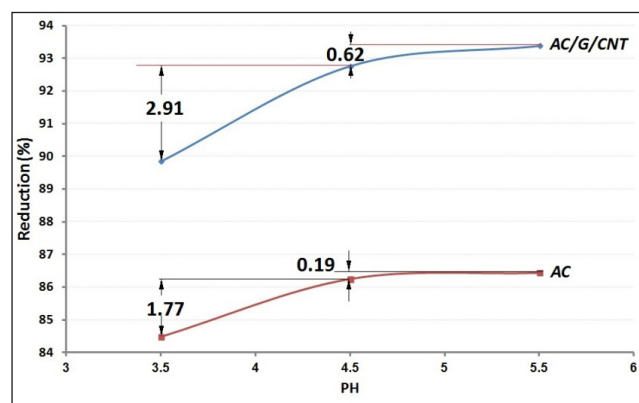


Fig. 3. Effect of pH on adsorption.

$V$  is the volume of metal solution (L), and  $m$  is the weight of adsorbent used (g). Moreover, the removal percentage of  $Mn^{2+}$  ions was calculated using the  $R(\%) = (C_0 - C_e)/C_0 \times 100$  equations.

### 3. Results and Discussion

#### 3.1. Effect of pH

According to surface chemistry, the amount of Adsorption depends on the surface behavior of adsorbent, such as porosity and situation and distribution of active sites for bonding with metal ions. These indexes generally depend on the pH of the solution [10]. At this study the pH solution was varied at 3.5, 4.5 and 5.5. During adsorption process, pH of solution adjustment at fix purposed value and measure with a pH meter using a combination glass electrode. Figure 3 indicates the effect of pH solution on the removal of  $Mn^{2+}$  ions onto AC and AC/G/CNT composite from aqueous solutions at 30 min.

The  $Mn^{2+}$  removal was 86.45% and 93.38% at pH 3.5 by AC and AC/G/CNT respectively, it was 86.26% and 92.76% for adsorbent at pH which is equal to 4.5 and decreased 84.49% and 89.85% for pH=5.5. It is seen that removal of  $Mn^{2+}$  was strongly dependent on pH conditions at AC/G/CNT than AC as an adsorbent. In addition, the percentage removal of  $Mn^{2+}$  first sharply increased by increasing of the pH until 4.5 and half flat in higher pH of solution more than 4.5. Good adsorption at middle range of pH (4.5) indicates that low pH leads to an increase in  $H^+$  ions on the Adsorbents surface, resulting in significantly strong electrostatic attraction between positively charged surface of Adsorbents and  $Mn^{2+}$  ions. At higher pH values, from 4.5, the precipitation of  $Mn^{2+}$  ions is occurred and both ion exchange and aqueous metal hydroxide formation are then occurred. So the best value of solution pH is equal to 4.5.

#### 3.2. Effect of Time

Contact time is a significant factor affecting removal of initial  $Mn^{2+}$  ions in the solution. Effect of time on the adsorption was shown in Table 2. The Results reveal that increasing contact time caused

increasing the adsorption of  $Mn^{2+}$  ions or different initial concentrations. So, if the time increases from 15 to 30 min, the amount of absorption increases with more slopes, while with increasing time from 30 to 45 min, the absorption rate increases with less intensity. The  $Mn^{2+}$  removal is higher at the first 30 min. This is due to larger surface area of the Adsorbents at the beginning for the adsorption of Manganese. It has been matched with other results [11]. For example, at fix  $Mn^{2+}$  concentration 80 mg/l, with the increasing time from 15 to 30 min, the absorption rate was 3.6% while with the increasing time from 30 to 45 min, this value was changed by only 2%. Therefore, based on economic considerations and the rate of absorption changes, the best time for the absorption process is 30 min.

### 3.3. Effect of temperature and $Mn^{2+}$ Concentration

Thermodynamically behavior of large amount adsorption process is exothermic and so temperature has a negative effect on removing metal ions and other pollutants [12]. According to this, the mechanism of  $Mn^{2+}$  ions adsorption by AC and AC/G/CNT was a function of temperature and has been considered this research. Figure 4 shows the effect of temperature on  $Mn^{2+}$  removing for both adsorbents of AC and AC/G/CNT.

The results of figure 4 were shown at initial concentration of 30 mg  $Mn^{2+}$  removing decreased

from 89.3% to 84.1% by AC and 96.18% to 91.16% by AC/G/CNT with increasing of temperature from 15 to 35 °C. This change for high concentration of  $Mn^{2+}$  is more evident at higher temperatures. But the best initial concentration of  $Mn^{2+}$  is 80 mg/L<sup>-1</sup>. At higher concentrations of this, between the adsorption of metal ions and the surface of adsorbent, a competition phenomenon was occurred based on steric hindrance and as a result, the amount of absorption decreases. The simultaneous effect of three variables include initial  $Mn^{2+}$  concentration in the range of 30, 80, and 130 mg/L for temperatures of 15, 25, and 35 °C and contact time of 15, 30, and 45 min were done at fixed pH of 4.5, and the results are shown in Figure 5.

Based on Figure 5, it is observed that the effect of Temperature on amount of absorption is more than time because by increasing temperature, this decreases with a constant trend. However, when time increases, the amount of adsorption decreases, and then it is flat that due to the saturation of the adsorbent surface. It is also observed that the best absorption conditions occur at lower temperatures for medium concentrations of  $Mn^{2+}$  at 30 min. At lower Manganese concentration, the percentage removal of  $Mn^{2+}$  ions is high and by increasing temperature the slop of adsorption decreases, this means is the ratio of  $Mn^{2+}$  ions removing more decrease in high temperature. Therefore,

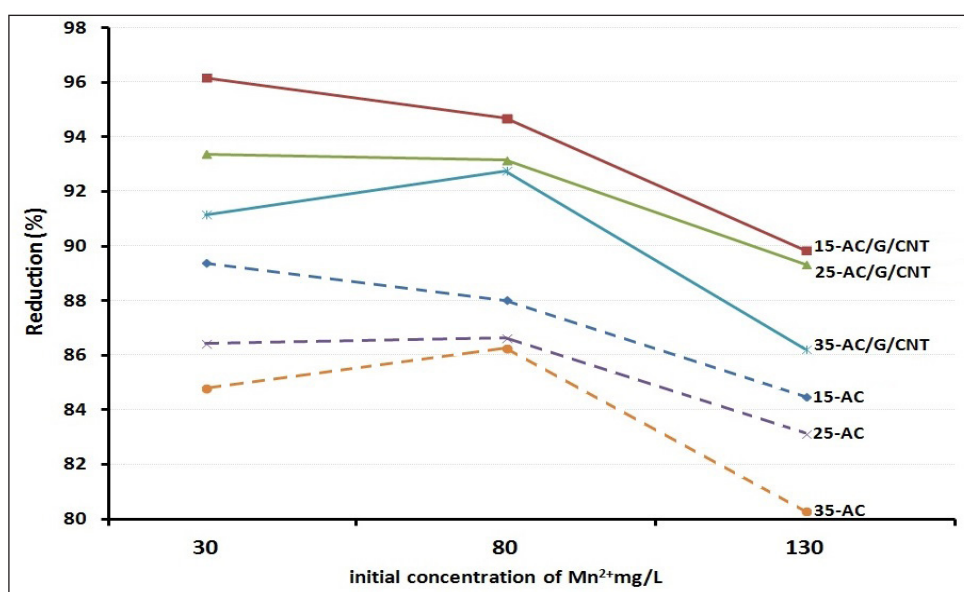


Fig. 4. Temperature effect on  $Mn^{2+}$  removing for both adsorbents.

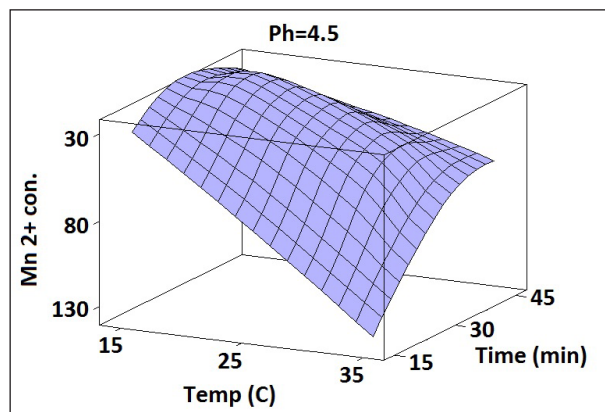


Fig. 5. simultaneous effect of three variables on  $Mn^{2+}$  removing.

the technique of diluting wastewater and cooling during the removing process can be used to absorb more metal  $Mn^{2+}$  ions.

#### 4. Conclusions

Generally, at fix conditions, the presence of G/CNT hybrid in the structure of AC 7.5% increases the amount of adsorption. Moreover, the most important reason being to improve surface properties and create more porosity in the AC structure. In addition, the inherent property of CNT in absorption of  $Mn^{2+}$  ions based on ionic bonding under a wide range of graphene sheets has enhanced the absorption performance of AC. The best absorption conditions occurred at a  $15^{\circ}C$  and a concentration of  $30\text{ mg }Mn^{2+}$  at pH of about 4.5. Increasing pH of the solution caused to the partial hydrolysis of  $Mn^{2+}$ , bringing the arrangement of complexes. The result of this present shown adsorption of  $Mn^{2+}$  was exothermic mechanism and the rate of removing was decrease by increasing temperature. This difference is a result of the enhanced escaping tendency of metal ions moving and species in higher temperatures. In addition, a solubility increase in  $Mn^{2+}$  ions in water at higher temperatures caused decreasing sorption on surface of adsorbents. Ultimately, because AC is a basic, available and inexpensive sorbent, the results of this study will be useful for the removal of  $Mn^{2+}$  from industrial effluents.

#### 5- References

- [1] H. Bessbousse, T. Rhlalou, J.F. Verche re, L. Lebrun, Removal of heavy metal ions from aqueous solutions by filtration with a novel complexing membrane containing poly(ethyleneimine) in a poly(vinyl alcohol) matrix, *J. Membr. Sci.*, 307 (2008) 249-259.
- [2] C. Namasivaysm, K. Kadirvelu, Uptake of mercury (II) from wastewater by activated carbon from an unwanted agricultural solid waste by-product: coirpith. *Carbon*, 37 (1999) 79-84.
- [3] C. Brasquet, P. Le Cloirec, Effects of activated carbon cloths surface on organics adsorption in aqueous solutions-utilization of statistical methods for mechanisms approaches. *Langmuir*, 15 (1999) 5906-12.
- [4] I. Mobasherpour, E. Salahi, M. Pazouki, Removal of divalent cadmium cations by means of synthetic nano crystallite hydroxyapatite. *Desalination*, 266 (2011) 142-148.
- [5] P.A. Brown, S.A. Gill, S.J. Allen, Metal removal from wastewater using peat. *Water Res.*, 34 (2000) 3907-16.
- [6] V. Varshney, S.S. Patnaik, A.K. Roy, Modeling of thermal transport in pillared-graphene architectures. *ACS nano.*, 4 (2010) 1153-1161.
- [7] K. Xia, H. Zhan, G. Yuantong, Graphene and Carbon Nanotube Hybrid Structure: A Review, *Procedia IUTAM*, 21 (2017) 94-101.
- [8] W. Feng-Chin, T. Ru-Ling, J. Ruey-Shin, Preparation of highly microporous carbons from fir wood by KOH activation for adsorption of dyes and phenols from water, *Sep. Purif. Technol.*, 47 (2005) 10-19.
- [9] Z. Hu, M.P. Srinivasan, Preparation of high-surface-area activated carbons from coconut shell, *Micropor. Mesopor. Mater.*, 27 (1999) 11-18.
- [10] K.K. Wong, C.K. Lee, K. Low, M.J. Haron, Removal of Cu and Pb by tartaric acid modified rice husk from aqueous solutions. *Chemospher.*, 50 (2003) 23-28.
- [11] M. Ajmal, R.A. Rao, S. Anwar, J. Ahmad, R. Alunad, Adsorption studies on rice husk: removal and recovery of Cd (II) from wastewater. *Bioresour. Technol.*, 86 (2003) 147-149.
- [12] S. Netpradit, P. Thiravetyan, S. Towprayoon, Application of waste metal hydroxide sludge for adsorption of azo reactive dyes, *Water Res.*, 37 (2003) 763-772.



## Determination of H<sub>2</sub>S in crude oil via a rapid, reliable and sensitive method

Amir Vahid<sup>a,\*</sup>

<sup>a</sup> Research Institute of Petroleum Industry (RIPI), West Entrance Blvd., Olympic Village, P.O. Box: 14857-33111, Tehran, Iran

### ARTICLE INFO:

Received 27 March 2019

Revised form 24 Apr 2019

Accepted 22 May 2019

Available online 20 Jun 2019

### Keywords:

Crude Oil

Determination

Experimental Design

Field test

Hydrogen Sulfide

### ABSTRACT

Determination of hydrogen sulfide (H<sub>2</sub>S) in crude oil is very important due to the environmental impacts, industrial problems, and legal international limitation of transportation. In the present work, H<sub>2</sub>S of crude oil is determined by liquid-liquid extraction followed by potentiometric titration. Moreover, three factors including dilution ratio of crude oil with toluene, extraction time of H<sub>2</sub>S into the caustic phase and API of crude oil were investigated via factorial design. The ANOVA results have revealed that the dilution ratio, crude type, and extraction time have the highest effect of the recovery of H<sub>2</sub>S from crude oil. In addition, the linear dynamic range of the method was from 1 up to 2000 ppm which can be manipulated for lower or higher concentration by further optimization of the above-mentioned parameters. Finally, this method is rapid, reliable, operator-independent, which these characteristics make it a useful technique for the field test of crude oil and overcome extreme uncertainty of H<sub>2</sub>S measurement.

### 1. Introduction

H<sub>2</sub>S is one of the most hazardous compounds which is colorless gas and can dissolved in aqueous and organic solvents. In addition, it is a poisonous and corrosive compound. In addition, it causes environmental damages [1-3]. H<sub>2</sub>S can be present in petroleum and petroleum products including asphalt, residual fuel oil, mid-distillates and their blend, natural gas and LPG [4-6]. H<sub>2</sub>S is evolved

and produced in production of fossil fuels in oil and gas industry. There is very tight international regulations in the transportation of crude oil and hydrocarbons [7]. Due to this regulations, determination of H<sub>2</sub>S at low level and also high level is very critical from industrial and environmental point of view [8, 9]. There are many methods for the determination of H<sub>2</sub>S in crude oil and its derivatives. The method of measurements is given in Table 1. As can be seen, there is no a valid and standard method for the determination of H<sub>2</sub>S in crude oil

\* Corresponding author: Amir Vahid

Email: [avahid753@gmail.com](mailto:avahid753@gmail.com)

DOI: <https://doi.org/10.24200/amecj>

specially in the presence of mercaptan, chlorine and some basic additives and scavengers [10-17]. Furthermore, there is demand for a method which comprises requirements of a good method. These requirements including easy operation in field or laboratory, low health and safety problem, operator independent, low cost, repeatable, reproducible and providing very low detection limit as well as wide linear dynamic range. Among the methods of H<sub>2</sub>S determination, each of them has its own limitation [18-20]. The health and safety hazards related to H<sub>2</sub>S are summarized in Table 2 [21]. Furthermore, among the properties of the crude oil reported for the sale and refinery designing, H<sub>2</sub>S may be the most unstable parameter, even in comparison with Reid vapor pressure and specific gravity. So far, to the best of our knowledge, there is not an appropriate analytical method for determination of H<sub>2</sub>S in crude oil for use in both oil field and laboratory test. In the present work, a rapid method was developed and investigated using factorial

experimental design for the determination of H<sub>2</sub>S of crude oil which can be used in laboratory or field test and led to the repeatable and accurate results.

## 2. Materials and Methods

All chemicals were purchased from Merck and used as received. In a typical determination, 50 mL of crude oil and predetermined amount of toluene as Diluting ratio were poured into a decanting funnel and shaken for a about 5 minutes. Then 25 mL of 5 w/w% aqueous caustic solution was used as extracting agent and was shaken for a predetermined time. The mixture was aged for 10 minutes to separate oil and aqueous solution. Afterwards, 10 mL of aqueous solution was decanted on a paper filter, and the filtrate was collected in a titration beaker. After addition of 2 mL on concentrated solution of ammonia, the filtrate was titrated with 0.05 N of silver nitrate solution. The first equivalent point at about -600 mV is related to the H<sub>2</sub>S. Titration was carried out

**Table 1.** Standard methods of H<sub>2</sub>S determination and their properties (Nadkarni 2000).

Method	Disadvantage	Scope of work	Dynamic range
ASTM D5623	Narrow dynamic range, High cost, Limited sample boiling range	GC of Liquid distillates with FBP < 230 °C	0.1 - 100 ppm
UOP 212	Limited sample boiling range, High cost	Potentiometric titration, ethane to such gasoline	1 to several thousand ppmw of H <sub>2</sub> S
ASTM D5705	Only applicable to vapor phase, Poor repeatability	H <sub>2</sub> S in the vapor phase (equilibrium) of a residual fuel oil for field test using gas detection tubes and Can test	5 ppm v/v to 4000 ppm v/v
UOP 163	Not applicable to crude oil, Complex data interpretation	H <sub>2</sub> S in Liquid hydrocarbons by potentiometric titration	1 up to 100 ppmw.
ASTM D7621 IP 570 ISO 8217	Not applicable to crude oil, mercaptan interference	H <sub>2</sub> S in Fuel Oils by Rapid Liquid Phase Extraction	1 up to 50 ppmw
UOP 41 ASTM D4952 Doctor Test	Only for qualitative analysis, Using of poisonous metal	qualitative test of H <sub>2</sub> S in gasoline, jet fuel, kerosine and similar petroleum products and solvents	
ASTM 6021	skilled operator and complex calculations, High cost	H <sub>2</sub> S in Residual Fuels by Multiple Headspace Extraction and Sulfur Specific Detection	0.01 to 100 ppmw
IP 399	Complex procedure and pure materials needed. Oxidation and absorption may occur.	H <sub>2</sub> S in Residual Fuels by spectrophotometric determination.	0.50 to 32 ppmw

**Table 2.** Exposure limit and its related hazards.

Concentration mg/kg	Health & Hazard Effect
< 0.02	Odor Detection Limit
10	8 Hours Exposure Limit
15	15 Min. STEL
100	Common Ship Headspace Spec.
300	Considered Immediately Hazardous
713	LC50 Concentration
1000	Common Tank, Ship Headspace Concentration

using a Metrohm titrando 880 according to the UOP 209.

For the optimization of the condition of determination, a factorial design was applied for the investigation of three main effects, including time required for extraction, diluting ratio and crude type according to its API. 12 experimental runs were designed and carried out. Calculation and modeling of results were done using Design Expert 7.

Recovery is defined as the ratio of the concentration of the H<sub>2</sub>S obtained in the designed test to H<sub>2</sub>S obtained at 2 hours and 60 C with diluting ratio of 5.

### 3. Results and Discussion

The condition of statistically designed runs and

their corresponding results are given in Table 3.

Analysis of variance of obtained results is calculated and give in Table 4. The obtained Equation for model is given as Eq. 1 in terms of coded factors.

$$\text{Recovery} = +91.75 - (1.25 * A[1]) + (0.50 * A[2]) + (4.75 * B) + (1.75 * C) + (0.42 * BC) \text{ (Eqn. 1)}$$

As seen in Figure 1, and according to the Equation 1 and ANOVA (Table 4), it can be said that Time has very little effect on the recovery of H<sub>2</sub>S. It is a very good property for an analytical method to carry out in short time.

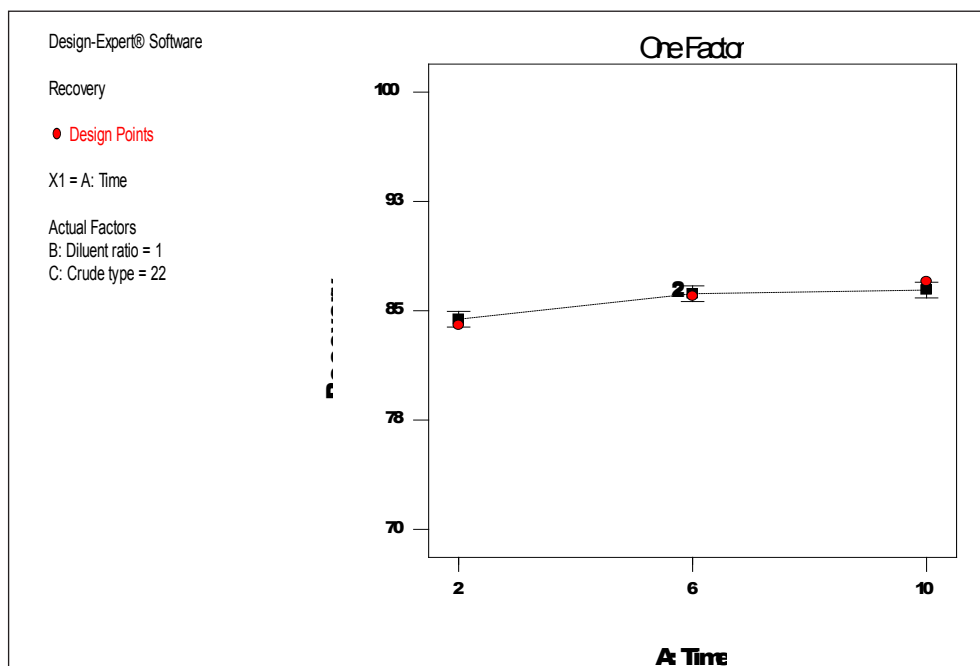
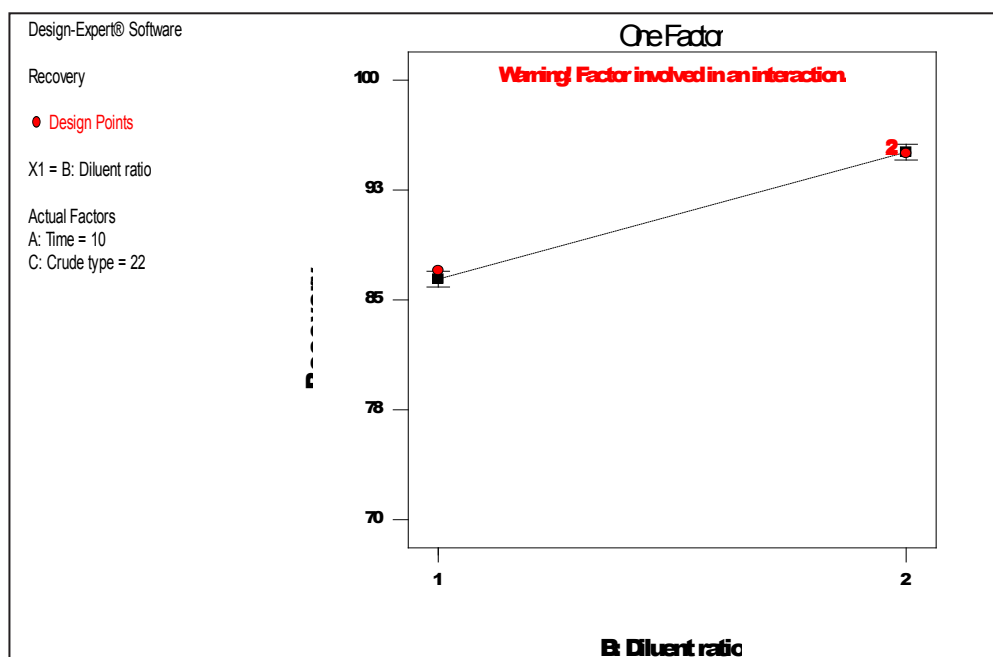
Figure 2 displays the effect of Diluting ratio which is the most effective factor among all. Moreover, it is generally known that crude oil has very broad range of properties in term of density and viscosity. H<sub>2</sub>S is trapped in the complex matrix

**Table 3.** Designed test runs for H<sub>2</sub>S determination.

Std. run order	A: Time (min)	B: Diluting ratio	C: Crude type (API)	Recovery %
1	2	1	22	84
2	6	1	22	86
3	10	1	22	87
4	2	2	22	93
5	6	2	22	95
6	10	2	22	95
7	2	1	36	87
8	6	1	36	89
9	10	1	36	89
10	2	2	36	98
11	6	2	36	99
12	10	2	36	99

**Table 4.** ANOVA of obtained results of H<sub>2</sub>S analysis.

Source	Sum of Squares	df	Mean Square	F Value	P-value Prob > F
Model	319.1	5	63.8	328.2	< 0.0001
A-Time	9.5	2	4.8	24.4	0.0013
B-Diluting ratio	270.8	1	270.8	1392.4	< 0.0001
C-Crude type	36.8	1	36.8	189.0	< 0.0001
BC	2.1	1	2.1	10.7	0.0170
Residual	1.2	6	0.2	-	-
Corr. Total	320.3	11	-	-	-

**Fig. 1.** Effect of factor A: Time on recovery.**Fig. 2.** Effect of factor B: Diluting ratio on recovery.

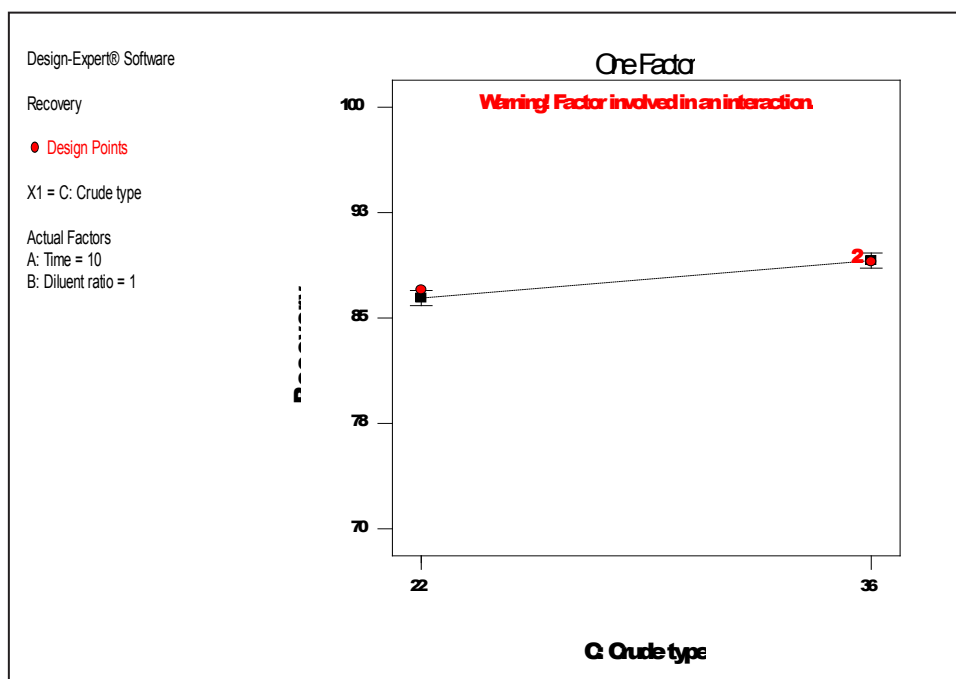


Fig. 3. Effect of factor C:Crude type on recovery.

of crude oil. Thus, the presence of toluene is essential for the dilution of the crude oil and breaks its complex matrix and semi ordered array of large molecules (wax, resin, and asphaltene) to easily evolve the trapped H<sub>2</sub>S.

As the crude oil becomes heavier as well as viscose, the evolve of H<sub>2</sub>S becomes more difficult and led to the reduction of recovery. So higher Diluting ratio is necessary in case of heavy crude oil. This means that Diluting ratio is the most important factor, as could be deduced from its F value in Table 4.

Figure 3 shows the effect of crude type on the recovery of H<sub>2</sub>S. As the API of crude oil increases, the crude oil become lighter and recovery is higher due to the better contact of oil phase and caustic phase an so need to low Diluting ratio and vice versa.

Figure 4 illustrates the interaction of the crude type and diluting ratio in a 3D curve. In case of heavier crude oil, i.e. at lower API, the effect of diluting ratio is very large while at higher API, this

effect is lower.

It can overall said that higher diluting ratio and lower extraction time are in favor of recovery despite the fact that higher time, 10 minutes, is steel low for a typical analytical method. For the determination of other merits of this analytical method, additional test was done. In addition, one of the most important properties of a robust analytical methods is Linear Dynamic Range. Four crude oils containing H<sub>2</sub>S concentration ranged from 0.2 to 1902 ppmw were examined. Moreover, obtained results showed that any concentration of H<sub>2</sub>S can be determined by manipulation of amount of aliquot of crude oil used for test. For the Crude oil contains 1902 ppmw, only 2 grams of crude oil is adequate while for sample containing 0.2 ppmw of H<sub>2</sub>S, 100 grams of crude oil is needed. RSD for the 148 ppmw H<sub>2</sub>S, in four determinations, was obtained 98%.

Another advantage of this methods is its compatibility for field determination because H<sub>2</sub>S is very volatile and unstable. It is generally known

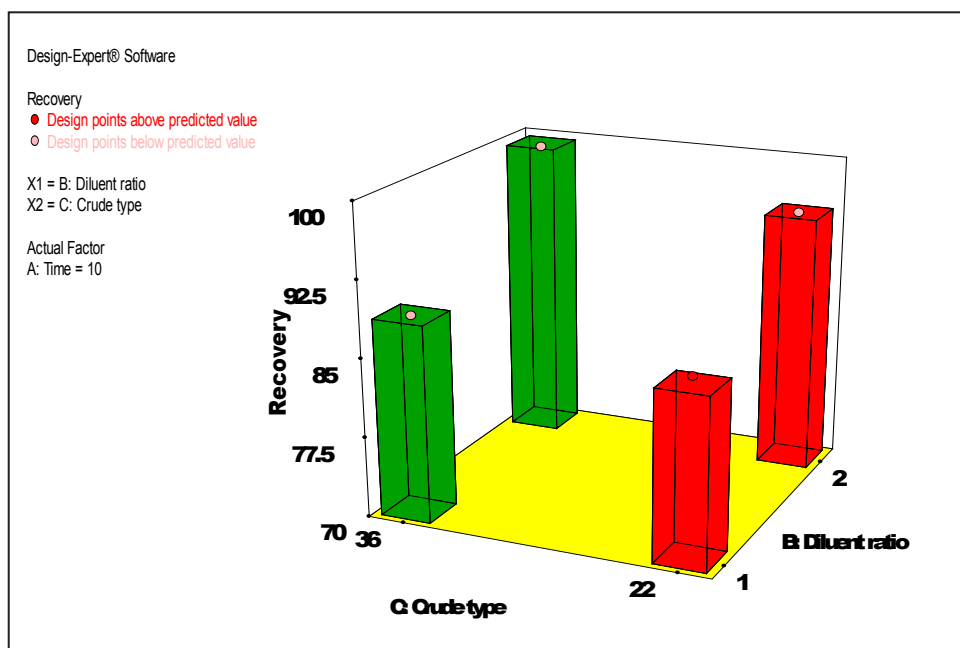


Fig. 4. 2D representation of interaction of Crude type and Diluting ratio.

that long delay between sampling and determination led to the loss of  $H_2S$  and causes lower result.

Furthermore, for field test, operator can pour the fresh crude sample into the decanter containing toluene and caustic solution. After that, vigorous stirring of this mixture led to the absorption of  $H_2S$  into the caustic phase and prevent loss of the analyte before titration or transport to laboratory.

It is noteworthy to say that for further improvement of quantification limit and RSD of method, once can increase the absolute amount of crude oil and extraction time. Furthermore, decreasing the amount of caustic solution, which results in higher concentration factor, and using centrifuge instead of decanter for separation of caustic phase prior to titration can improve quantification limit and RSD.

It is well known for those who work in petroleum laboratories that  $H_2S$  is very unstable and as the time between sampling and analysis increases, the error of the obtained results drastically increases. In this method, once can pour known quantity of caustic solution in to the pre-weighed sample container

and then rinse the crude oil from sampling point in to the container to absorb  $H_2S$  into the caustic solution during transfer to the laboratory.

#### 4. Conclusions

In this work, a method comprising the merits of very good analytical method is reported. The method is rapid because the time needed for extraction is lower than 10 minutes and a traditional potentiometric titration. Quantification limit of the method is low enough. Linear Dynamic Range of the method is very broad and this range can be tuned by changing the amount of crude oil. In addition, RSD of the method is up to 98% which is very good for a volatile and unstable compound, i.e.  $H_2S$  in a complex matrix of crude oil. The equipment needed for this method is very simple, accessible and cheap. Finally, the procedure of determination, including extraction and titration, is very traditional and don't need high level of expertise and skill. Furthermore, the method is capable of performing for field test which is very important from industrial point of view. Also, main

factors of the method can be tuned easily according to the properties of the crude oil to manipulate lower and upper limit of quantification.

## 5. Acknowledgment

This work was financially supported by Research Institute of Petroleum Industry under the grant number of 1647601.

## 6. References

- [1] R.J. Dieffenstein, W.C. Hulbert, S.H. Roth, Toxicology of Hydrogen Sulfide, *Annu. Rev. Pharmacol. Toxicol.*, 32 (1992) 109-134.
- [2] H. Kimura, Metabolic turnover of hydrogen sulfide, *Front Physiol.*, 3 (2012) 1-3
- [3] H.S. Kalal, A.A.M. Beigi, M. Farazmand, Determination of trace elemental sulfur and hydrogen sulfide in petroleum and its distillates by preliminary extraction with voltammetric detection, *Analyst*, 125 (2000) 903-908.
- [4] L. Zhang, P. De Schryver, B. De Gussemé, Chemical and biological technologies for hydrogen sulfide emission control in sewer systems: A review, *Water Res.*, 42 (2008) 1-12.
- [5] M. Abdouss, N. Hazrati, A.A. Miran Beigi, Effect of the structure of the support and the aminosilane type on the adsorption of H<sub>2</sub>S from model gas, *RSC Adv.*, 4 (2014) 6337-6345.
- [6] N. Hazrati, M. Abdouss, A. Vahid, Removal of H<sub>2</sub>S from crude oil via stripping followed by adsorption using ZnO/MCM-41 and optimization of parameters, *Int. J. Environ. Sci. Technol.*, 11 (2014) 997-1006.
- [7] X. Zhao, J.B. Gao, W.D. Zhang, B. Wang, Study on the risk of a crude oil shipping channel in China, *ICCTP*, 6 (2011) 3877- 3886.
- [8] J. Blomberg, P. Schoenmakers, U.A.T. Brinkman, Gas chromatographic methods for oil analysis, *J. Chromatogr. A*, 972 (2002) 137-173.
- [9] N.E. Heshka, D.B. Hager, A multidimensional gas chromatography method for the analysis of hydrogen sulfide in crude oil and crude oil headspace, *J. Sep. Sci*, 37 (2014) 3649-3655.
- [10] H. Sid Kalal, A.A. Miran Beigi, M. Farazmand, S.A. Tash, Determination of trace elemental sulfur and hydrogen sulfide in petroleum and its distillates by preliminary extraction with voltammetric detection, *Analyst*, 125 (2000) 903-908.
- [11] N.S. Lawrence, R.P. Deo, J. Wang, Electrochemical determination of hydrogen sulfide at carbon nanotube modified electrodes, *Anal. Chim. Acta*, 517 (2004) 131-137.
- [12] S.K. Pandey, K.H. Kim, K.T. Tang, A review of sensor-based methods for monitoring hydrogen sulfide, *TrAC - Trends Anal. Chem.*, 32 (2012) 87-99.
- [13] Y. Zhao, T.D. Biggs, M. Xian, Hydrogen sulfide (H<sub>2</sub>S) releasing agents: chemistry and biological applications, *Chem. Commun.*, 50 (2014) 11788-11805.
- [14] J.F.S. Petrucci, A. Wilk, A.A. Cardoso, B. Mizaikoff, Online analysis of H<sub>2</sub>S and SO<sub>2</sub> via advanced mid-infrared gas sensors, *Anal. Chem.*, 87 (2015) 9605-9611.
- [15] O. Yassine, O. Shekhah, A.H. Assen, H<sub>2</sub>S sensors: fumarate-based fcu-MOF thin film grown on a capacitive interdigitated electrode, *Angew Chem.*, 55 (2016) 15879-15883.
- [16] N.E. Heshka, J.M. Choy, J. Chen, Gas chromatographic sulphur speciation in heavy crude oil using a modified standard D5623 method and microfluidic deans switching, *J. Chromatogr. A*, 1530 (2017) 241-146.
- [17] F. Huber, S. Riegert, M. Madel, K. Thonke, H<sub>2</sub>S sensing in the ppb regime with zinc oxide nanowires, *Sensor. Act. B. Chem.*, 239 (2017) 358-363.
- [18] N.S. Lawrence, J. Davis, R.G. Compton, Analytical strategies for the detection of sulfide: A review, *Talanta*, 52 (2000) 771-784.
- [19] R.A.K. Nadkarni, ASTM Test Methods for the Analysis of Petroleum Products and Lubricants, *World Refin.*, 6 (2000) 24-30

- [20] O.A. Habeeb, R. Kanthasamy, G.A.M. Ali, Hydrogen sulfide emission sources, regulations, and removal techniques: a review, *Rev. Chem. Eng.*, 34 (2017) 9-19.
- [21] R. Wedmann, S. Bertlein, I. Macinkovic, et al. Working with "H<sub>2</sub>S": Facts and apparent artifacts: nitric oxide, *Biol. Chem.*, 41 (2014) 85-96.



# Functionalized graphene-trimethoxyphenyl silane for toluene removal from workplace air by sorbent gas extraction method

Majid Bagheri Hosseinabadi<sup>a</sup>, Shahnaz Timoori<sup>b</sup> and Ali Faghihi Zarandi<sup>c\*</sup>

<sup>a</sup> School of Public Health, Shahrood University of Medical Sciences, Shahrood, Iran.

<sup>b</sup> Department of Environment and Natural Resources, Islamic Azad University, Science and Research Branch, Tehran, Iran.

<sup>c</sup> Occupational Health Engineering Department, School of Public Health, Kerman University of Medical Sciences, Kerman, Iran.

## ARTICLE INFO:

Received 14 Apr 2019

Revised from 28 Apr 2019

Accepted 20 May 2019

Available online 18 Jun 2019

## ABSTRACT

Inhalation exposure to toluene in the environment and workplace causes that some concerns about its adverse health effects on public and workers raise. So the implementation of high-performance methods to control toluene emission in industrial and environment settings is very important. Moreover, a new synthesized sorbent based on functionalizing graphene with N-Phenyl-3-aminopropyl trimethoxy silane (G-PhAPTMS, C<sub>12</sub>H<sub>21</sub>NO<sub>3</sub>Si) was developed as a novel sorbent for removal of toluene from air by sorbent gas extraction procedure (SGEP). By proposed method, the removal efficiency of G-PhAPTMS was compared with other sorbents such as activated carbon (AC), graphene (G), and graphene oxide (GO). In addition, the standard gas of toluene generated in pure air with different concentrations, and the effects of parameters such as temperature (10-90 °C), flow rate (50-500 mL min<sup>-1</sup>) and the amount of sorbent (2-30 mg) were investigated. According to the results, increasing the flow rate and temperature had negative effects on the removal efficiency of all sorbents. The highest removal efficiency of G-PhAPTMS was obtained up to 35 °C and less than 250 mL min<sup>-1</sup> (>95%). In optimized conditions, the amount of sorbent for toluene removal from air was achieved more than 10 mg of G-PhAPTMS. Finally, the results indicate that the G-PhAPTMS has high removal efficiency and surface area as compared to the AC, G, and GO. Furthermore, functionalizing graphene with N-Phenyl-3-aminopropyl trimethoxy silane improved the absorption of toluene due to chemical bonding ( $\pi$ - $\pi$  electron donor-acceptor) and introduced an environmentally friendly sorbent.

## Keywords:

Toluene

Chemical adsorption

Graphene

N-Phenyl-3-aminopropyl  
trimethoxy silane

Sorbent gas extraction  
procedure

## 1. Introduction

Toluene is one of the well-known air contaminants and widely used as an organic solvent in various industries such as petroleum refining, shipping, rubber manufacturing, automobile repairing, and shoe manufacturing [1]. It is estimated that toluene is consumed about 2.3 million tons in worldwide annually [2]. Moreover, public and occupational exposure to toluene can occur through the inhalation of toluene fumes from cigarette smoking

and vehicle emission [3]. In addition, it is likely to release from indoor sources such as paints, paint thinners, and adhesives [4]. The studies have been shown that chronic exposure to toluene can cause a wide variety of health problems including neurotoxic effects (from headache and fatigue to narcosis with increasing exposure level) and mucosal irritation [5, 6]. Because of the harmful effects of toluene, the implementation of high-performance methods to control toluene emission in industrial and environment settings is inevitable [7]. There are some different methods such as including adsorption, condensation, thermal

\* Corresponding Author: Ali Faghihi Zarandi

E-mail: [alifaghihi60@yahoo.com](mailto:alifaghihi60@yahoo.com)

DOI: <https://doi.org/10.24200/amecj>

oxidation, catalytic oxidation, photo catalytic oxidation and bio filtration that can be applied to reduce the concentration of toluene in air [8-11]. It seems that adsorption as a low operating cost and effective method can be used to remove toluene from air at low concentration [12, 13]. Adsorption is a process in which the molecules of pollutants are trapped at the surface of porous materials such as zeolites, silica gel and activated carbons by physical adsorption [14-16].

Among the different adsorbents, carbon adsorbing materials such as graphene oxide, activated carbons, carbon nanotubes, and porous carbon have demonstrated more advantage due to their low density, chemical stability and variety of structural forms [17-20]. The founding of new carbon materials is always one of the favorite subjects in the process of adsorption and sequestration [21]. Graphene, new two-dimensional carbon nanomaterial, as a new member of the carbon family with desirable properties such as low weight, small size, high surface area, and superior electrical, thermal and mechanical properties has attracted much attention [22-24]. The more advantage of graphene is the adsorption ability of chemicals with benzene rings like toluene through strong  $\pi$ - $\pi$  interaction [25, 26]. In addition, some functional groups has turned graphene into an excellent adsorbent [27].

On the other hand, graphene has high theoretic surface area up to  $2620 \text{ m}^2 \text{ g}^{-1}$  that it become an ideal adsorption [28, 29]. Furthermore, graphene can be easily obtained from the cheap natural graphite in large scale [29, 30]. In this regard, the high adsorption capacity of graphene and its derivatives was confirmed for dyes [31], pharmaceutical antibiotics [32], heavy metals, and VOCs in water [33, 34]. However, the studies on toluene adsorption characteristics and behaviors onto graphene from air are limited [35].

In this study, toluene removed from air based on G-PhAPTMS by SGEP. The different experimental conditions such as mass, flow rate, and temperature were investigated and optimized. By proposed procedure, the chemically adsorption

mechanism of toluene was achieved based on  $\pi$ - $\pi$  interaction between toluene and the surface of the G-PhAPTMS.

## **2. Experimental procedure**

### **2.1. Material and Instruments**

Toluene was purchased from Fluka (Germany) with purity above 99.5%. In addition, standard gas was obtained by injecting a certain amount of toluene into a 10 ml glass vial with PTFE cap to determine absorption capacity. In this study, helium and pure air were used as the dilution gas. Standard gas was prepared with a relative humidity of  $32 \pm 5\%$  for simulating the humidity in the workplace air. Thus, before filling the vial, the dilution gas was passed through deionized water. The concentrations of toluene in the standard gas were prepared from 9 to  $75 \text{ mg L}^{-1}$  (in batch system, high concentration up to  $400 \text{ mg L}^{-1}$ ).

In addition, a dynamic standard gas generation was designed to measure removal efficiency. This system consisted of impinger, adsorption tube, micro compressor, and sampling Tedlar bag (SKC Inc., USA). A certain amount of toluene was injected to the impinger, and then the dilution gas with a certain flow was passed through the adsorption tube. At the end of the system, unabsorbed toluene was collected into the Tedlar bag. The concentration of toluene in the Tedlar bag was measured by gas chromatography equipped with flame ionization detector (GC-FID) and air sample loop injection (Agilent GC, 7890A, FID, Netherland). Also, GC-MS was used for validation toluene concentration in air.

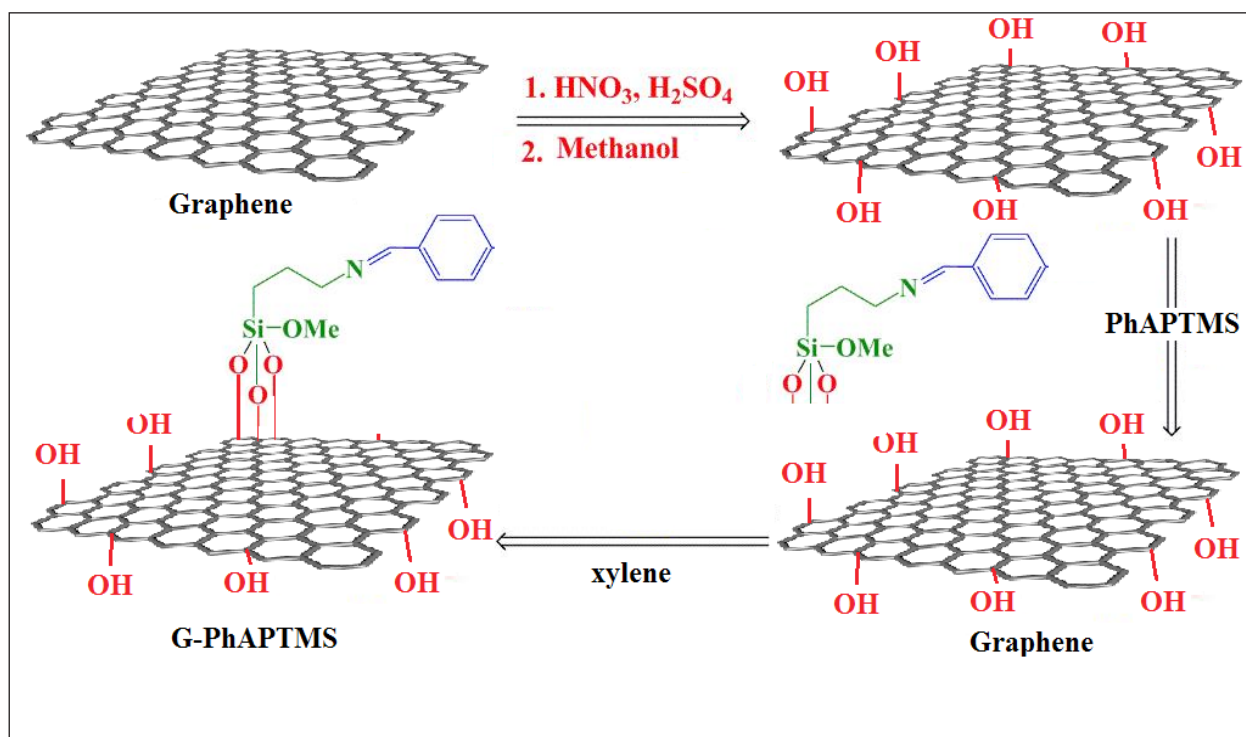
The crystal structure studies of the solids were carried out by X-ray diffractions (PW 1840, Phillips X-ray diffractometer, Netherland) with  $\text{Cu-K}_\alpha$  radiation source. Raman spectroscopy was performed using an Almega Thermo Nicolet and 532 nm Ar-ion laser excitation source. The Fourier transform infrared (FT-IR) spectrum was recorded on Bruker IFS 88 spectrometer (Bruker Optik GmbH, Ettlingen, Germany) with KBr pelleting method in the  $4000\text{--}400 \text{ cm}^{-1}$ . The morphology of the sorbent was examined using scanning electron

microscopy (SEM, Phillips, PW3710, Netherland) and transmission electron microscopy (TEM, CM30, Philips, Netherland).

## 2.2. Synthesis of functionalized graphene with N-Phenyl-3-aminopropyl trimethoxy silane

Graphene (G) was prepared by our special CVD (chemical vapor deposition) method by an electrical furnace consisting of a quartz tube. The furnace heating tuned up to 1000 °C for 25 min. The reaction between methane and hydrogen (4:1) was obtained. In order to pure grapheme without any metals, the product was stirred in HCl solution (ultra-trace) for about 20 h. The sample was then washed repeatedly with ultra-pure water until the solution became neutral. The treated product was finally dried in oven at 120 °C. For carboxylation process, 1 g of the as-prepared G was first mixed with a 200 mL mixture of concentrated H<sub>2</sub>SO<sub>4</sub> and HNO<sub>3</sub> (3:1 v/v) and stirred for 20 min at room temperature followed by sonication at 55 °C for 4 hours in an ultrasonic bath (50 kHz and 100 W). After cooling to room temperature, the reaction

mixture was diluted with 500 ml of deionized water and then vacuum-filtered through a filter paper (0.2 μm). Finally, G-COOH was dried in oven at 70 °C. In order to the formation of the free hydroxyl group, 0.5 g of filtered G-COOH was added to a methanolic solution of sodium borohydride. Then, the G bearing –OH group were allowed to disperse in xylene followed by addition of N-Phenyl-3-aminopropyl trimethoxy silane (PhAPTMS) to synthesize functionalized G in refluxing. After washing with xylene to remove the unreacted excess PhAPTMS, the product was dried for 10 h at 90 °C under reduced pressure. Morphology of the G-PhAPTMS was studied using scanning electron microscopy (SEM) and transmission electron microscopy (TEM). Graphite powder (5 g) and NaNO<sub>3</sub> (2.5 g) were mixed with 120 mL of concentrated H<sub>2</sub>SO<sub>4</sub> and stirred for 30 min in an ice bath (0-5 °C). KMnO<sub>4</sub> (15 g) was gradually added to the vigorously stirred suspension and the temperature of the mixture was kept to be below 15 °C. The ice bath was then removed, and the mixture was stirred at 35 °C until it gradually became



Scheme 1. Synthesis of functionalized graphene with N-Phenyl-3-aminopropyl trimethoxy silane

brownish slurry, and then it was diluted slowly with 250 mL of water. The reaction temperature was rapidly increased to 98 °C with effervescence, and the color changed to brown color. Later, H<sub>2</sub>O<sub>2</sub> solution (30%) was added to stop the oxidation process, and the color of the mixture changed to bright yellow, indicating fully oxidized graphite. The graphite oxide formed was washed by rinsing and centrifugation with diluted HCl solution and then repeatedly with deionized water until the filtrated solution became neutral. Graphene oxide nanosheets were obtained by ultra-sonication of the filtered graphite oxide suspension followed by centrifugation for 15 min at 3000 rpm to remove any un-exfoliated graphite oxide (Scheme 1). Finally, it was air-dried at 60 °C for 12 h. In this study, graphene oxide and activated carbon commercially were purchased from RIPI, Iran.

### 2.3. General procedure

Because the removal efficiency is highly affected by the amount of sorbent, the effects of amount of sorbents were studied in 1, 2, 4, 5, 10, 15, 20, 25, and 30 mg of different sorbents including G-PhAPTMS, G, GO and AC. The flow rate of the dilution gas was set from 50 to 500 ml min<sup>-1</sup>. The effects of temperature on the absorption of toluene were investigated in different temperature from 10 to 90 °C. The same concentration of standard gas of toluene was passed through the adsorption tube containing different amount of each sorbents in various thermal and flow rate conditions. The concentration of unabsorbed toluene collected in the Tedlar bag was analyzed by gas chromatography equipped with flame ionization detector. Removal efficiency was calculated as seen in Equation 1. The removal of toluene was evaluated in present of pure air in different flow rate by G-PhAPTMS, G, GO and AC as nanosorbents. In optimized conditions, the static and dynamic system was used by SGEP. The air was purified with electro air cleaner (EAC) and mixed with toluene in pilot. By proposed pilot, the pure air with and without toluene gas based on SGEP method was measured (5 times) by GC-FID and validated by GC-MS. The novel

G-PhAPTMS sorbent had chemical and physical adsorption between G and N-Phenyl with toluene, respectively. The mechanism of chemical adsorption was occurred based on  $\pi$ - $\pi$  interaction of N-Phenyl with toluene. Moreover, the G-PhAPTMS was more interaction than G for toluene removal from air. By new synthesis, G was functioned by PhAPTMS and improved the compatibility between toluene and surface of sorbent in optimized conditions as compared to G, Go, and AC.

$$\text{Removal Efficiency} = \frac{C_{in} - C_{out}}{C_{in}} \times 100 \quad \text{Eq 1}$$

$C_{in}$  (mg L<sup>-1</sup>) and  $C_{out}$  (mg L<sup>-1</sup>) were the concentration of toluene before and after adsorption respectively.

## 3. Results and discussion

Morphology of the G-PhAPTMS has been studied by SEM and TEM (Figure 1 and 2). After functionalizing of graphene with N-Phenyl-3-aminopropyl trimethoxy silane, it seems that the graphene has much more active surface to absorb toluene.

### 3.1. Effect of Temperature

The removal efficiency of G-PhAPTMS, G, GO and AC in temperature from 10 to 90 °C are shown in Figure 3. Functionalizing graphene could improve the properties of graphene in absorption of toluene from the air by increasing temperature. In addition, activated carbon had more removal efficiency rather than graphene oxide in the same conditions. The removal efficiency of G-PhAPTMS decreased

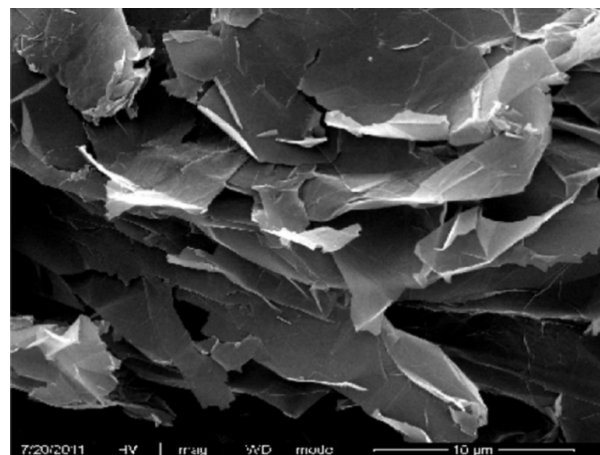


Fig. 1. SEM images of the G-PhAPTMS.

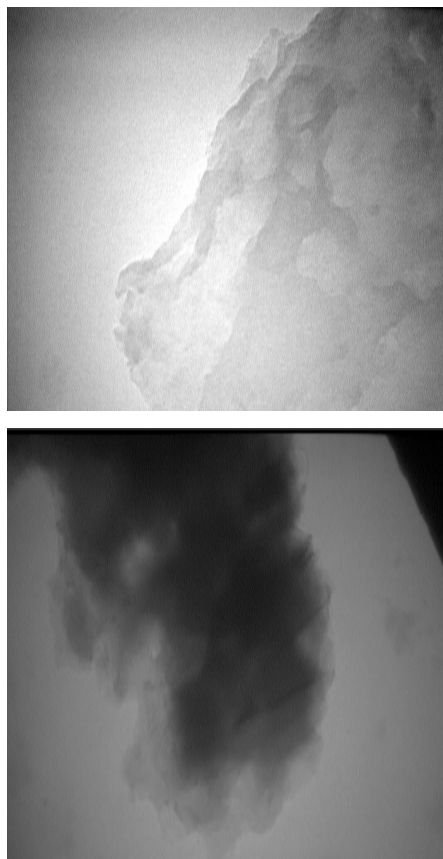


Fig. 2. TEM image of the G-PhAPTMS.

more than 50 °C, while, the removal efficiency of AC and GO decreased sharply from 68% and 40% in 45 °C to 5% and 2% in 90 °C respectively. Based on the results, the temperature can play a main role in removal efficiency of sorbents for toluene removal from air. By paying attention to previous

studies, the removal efficiency with increasing temperature was reported in other studies [36]. For instance, Sone et al. (2008) reported that absorption of VOCs can be highly influenced by increasing temperature. They found that when temperature was increased from 50 °C to 80 °C, the percentage of recovery of toluene decreased from 105.04 to 96.86 for charcoal [37]. Furthermore, it has been found out by Shih an Li in 2008 that lower temperature is a favorite condition for absorbing VOCs into the surface of carbon nanotube [38]. Overall, it can be argued the negative relation between increasing temperature and decreasing removal efficiency indicates that the sorption is an exothermic process, and decreasing temperature can improve the absorption properties of all investigated sorbents.

### 3.2. Effect of flow rate

The effect of flow rate on removal efficiency in 25 °C was investigated to optimize the flow rate conditions. The flow rate was set on 50 to 500 ml min<sup>-1</sup> for all sorbents. The results are presented in Figure 4.

The removal efficiency of G-PhAPTMS, G, GO, and AC decreased by increasing the flow rate, like temperature. The results showed, the more removal efficiency of G-PhAPTMS as compared to other sorbents, and the removal efficiency of G-PhAPTMS was decreased up to 62% in 500 ml

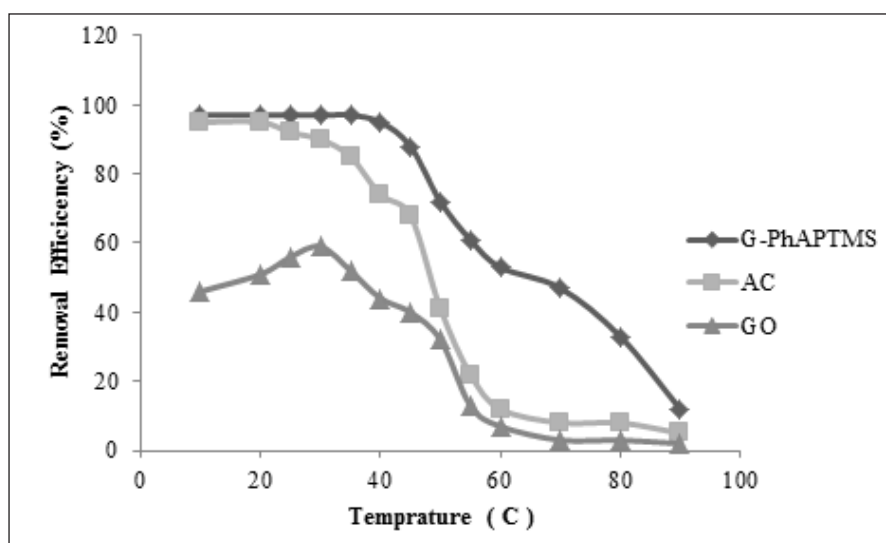


Fig. 3. the effects of temperature on removal efficiency of G-PhAPTMS, AC, and GO.

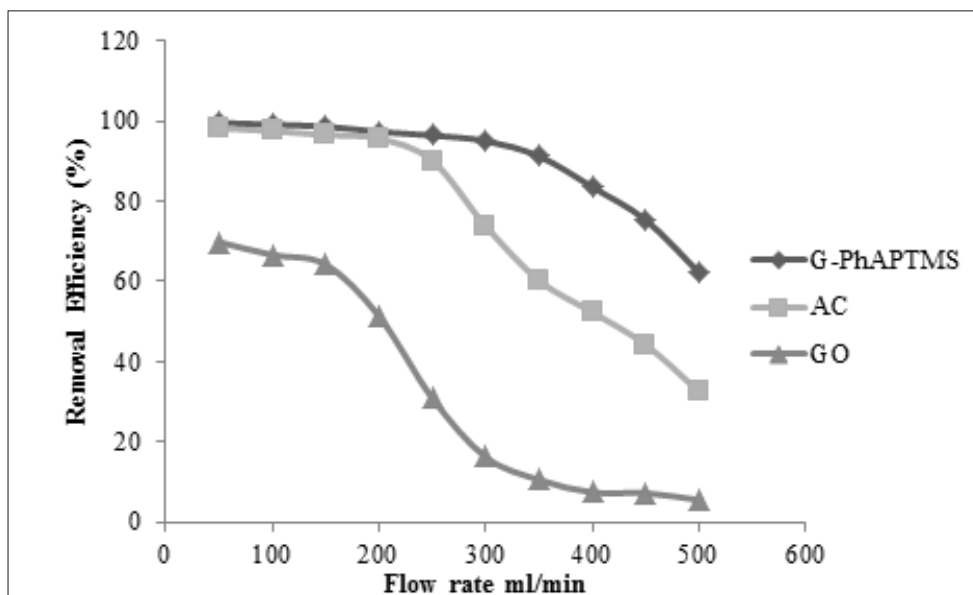


Fig. 4. the effects of flow rate on removal efficiency of G-PhAPTMS, AC, and GO.

$\text{min}^{-1}$ . However, the removal efficiency of AC and GO in this flow rate was 32% and 5% respectively. Increasing the flow rate affected on the removal efficiency of all sorbents, but this effect was lower for G-PhAPTMS. Similarly, the impact of flow rate (45, 92 and  $184 \text{ ml min}^{-1}$ ) on the removal efficiencies of toluene, limonene and methyl ethyl ketone was investigated by Yao et al in 2009. Their results showed that removal efficiency was decreased from 79% to 21% by increasing the flow rate [39]. Moreover, declining removal efficiency of fluoride by increasing the flow rate from 20 to  $30 \text{ ml min}^{-1}$  in activated alumina was reported by Ghorai and Pant [40]. The influence of flow rate on removal efficiency may be explained by reaction time. When the flow is high, the molecules of toluene have a little time to interact with the surface of absorbent, so they begin to escape from the end of the sorption tube [41].

### 3.3. Effect of mass sorbent

The amount of sorbent is another important parameter which was investigated in this study. The absorption tubes were loaded by different amounts of each absorbent from 1 to 30 mg by proposed

method. The temperature and flow rate were set on  $25 \text{ }^\circ\text{C}$  and  $200 \text{ ml min}^{-1}$ . The results are shown in Figure 5.

The removal efficiency of toluene with G-PhAPTMS increased by increasing the amount of sorbent and reached the highest point in 5 mg of sorbent. In addition, the removal efficiencies of AC and GO followed the same pattern as the G-PhAPTMS, while reached the highest point in 15 and 30 mg of sorbents respectively. The GO had the lowest removal efficiency rather than the G-PhAPTMS, G, and AC for all amount of sorbent. The positive impact of amount of sorbent on removal efficiency was reported by Samarghandi et al (2017) in the removal of reactive red from distilled water. They found that the removal efficiency increased when the amount of active carbon and graphene increase from 0.2 to  $4 \text{ g L}^{-1}$  and 0.02 to  $0.4 \text{ g L}^{-1}$  respectively [42]. Higher amount of sorbent provides much more chance for the molecule of toluene to react with the available surface of sorbent. So, the removal efficiencies of sorbents increase effectively. Based on the results, the more active absorption sites of  $\text{g L}^{-1}$  allow the molecules of toluene to absorb rapidly and

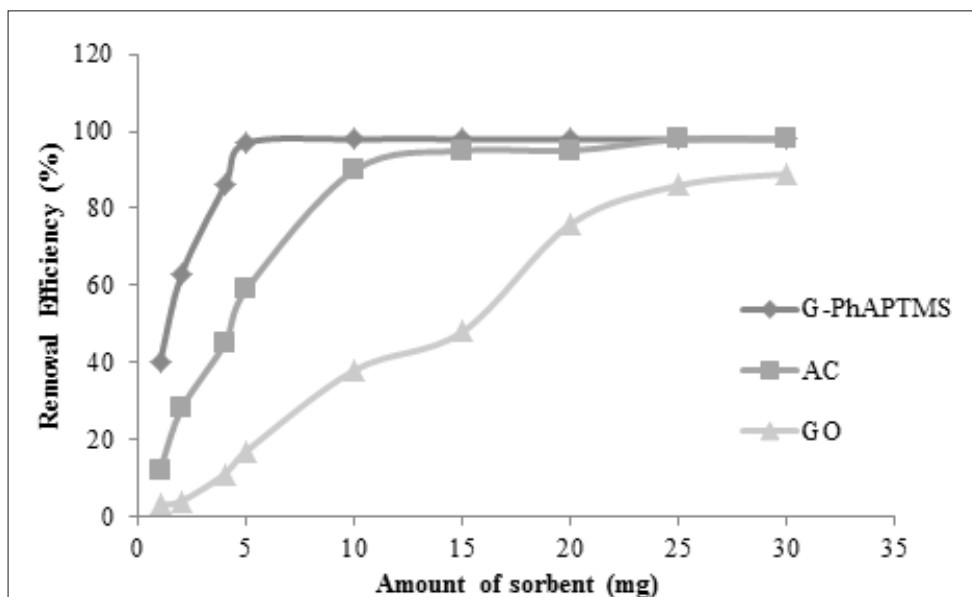


Fig. 5. the effects of amount of sorbent on removal efficiency of G-PhAPTMS, AC, and GO.

functionalizing graphene creates this opportunity that in the lower amount of sorbent, So we have maximum removal efficiency by G-PhAPTMS as compared with other sorbents. Repeatability of the sorbents was investigated in 25 °C, 200 ml min<sup>-1</sup> and from 2 to 30 mg of each sorbent (Figure 6). Each type of sorbent was used for twenty times and the mean of removal efficiencies were calculated.

The G-PhAPTMS had the highest removal efficiency for all investigated amount of sorbent compared with G, GO and AC sorbents after twenty times absorption and desorption. The mean of removal efficiency of AC experienced a downward pattern from 5 to 30 mg. Decreasing the removal efficiency for the GO happened from 20 mg to 30 mg where the removal efficiency fell from 64 to 42%. According to the results, functionalizing graphene with N-Phenyl-3-aminopropyl trimethoxy silane (G-PhAPTMS) can improve the absorption characteristics of graphene to absorb toluene from air.

### 3.4. Validation

The G-PhAPTMS was used as a novel and low-cost sorbent for removal of toluene vapor from air. By

proposed method, a mixture of 5-100 ppm of toluene vapor in artificial air with argon gas as a carrier gas passed through sorbent (G-PhAPTMS) by a pump. The concentration of toluene in standard gas was validated by highly sensitive and accurate GC-MS instrument in different concentration before using by proposed method. Since standard reference material for toluene in air is not currently available, the spiked of validated toluene concentration in a bag (GC-MS, 50 ppm, bag 5 Li, 0.2 L min<sup>-1</sup>) were prepared to demonstrate the reliability of the method by G-PhAPTMS. At optimum condition in one minute, 2.0 ppm of toluene vapor in air was almost removed by G-PhAPTMS. The efficient recovery of spiked samples was reasonable and was confirmed using addition method, which it indicates the capability of proposed method for removal of toluene from air (Table 1).

### 4. Conclusions

In this study, different absorbents such as G-PhAPTMS, G, GO, and AC were used to remove toluene from air. The results showed that functionalizing graphene with N-Phenyl-3-aminopropyl trimethoxy silane (G-PhAPTMS)

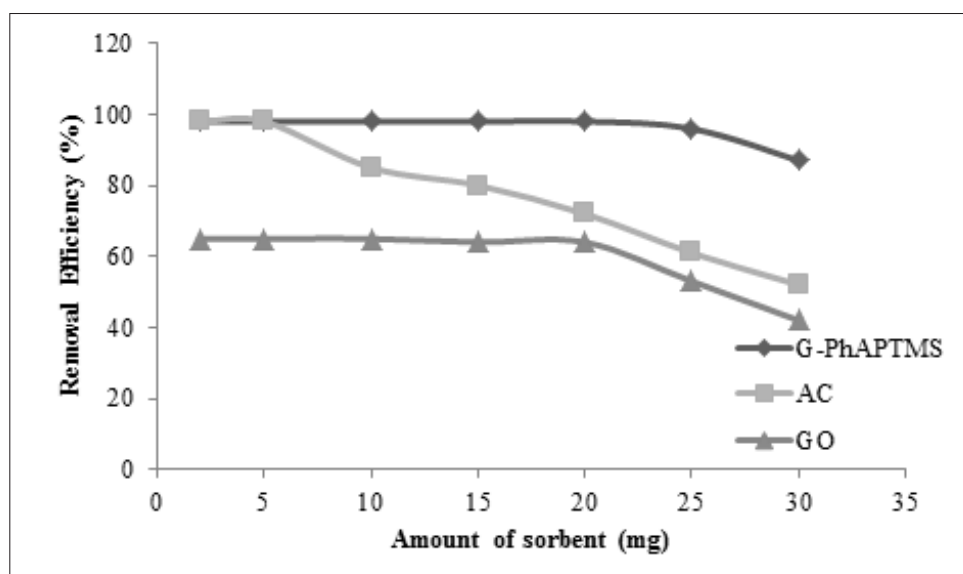


Fig. 6. The removal efficiency of different sorbents after using repeatedly.

**Table 1:** The recovery of G-PhAPTMS for removing toluene from air.

Samples	Toluene in air (ppm)*	Toluene in sorbent (ppm)**	Sorbent Recovery (%)
Sample A	2.63 ± 0.07	2.57 ± 0.11	97.7
Sample B	6.89 ± 0.14	6.48 ± 0.21	94
Sample C	10.72 ± 0.19	10.51 ± 0.32	98
Sample D	14.08 ± 0.34	13.52 ± 0.84	96
Sample E	18.73 ± 0.17	17.35 ± 0.28	92.6

\* Initial concentration in standard gas

\*\* Measured concentration in sorbent

promotes the removal efficiency of graphene by chemical bonding as  $\pi$ - $\pi$  electron donor-acceptor. Furthermore, increasing temperature and flow rate have negative effects of the removal efficiency of all sorbents, but the results of G-PhAPTMS showed high removal efficiency of toluene compared to the AC, G, and GO. The amount of sorbent was another parameter which was investigated. In optimized conditions, the amount of sorbent for the G-PhAPTMS, AC, and the GO were obtained 5, 5, and 30 mg respectively. This result shows that the G-PhAPTMS has many more available active sites for absorption of toluene. By lower amount

of G-PhAPTMS, high removal efficiency was achieved more than 95% by interaction between toluene and N-Ph. The results of repeatability of sorbents also indicate that functionalizing graphene with N-Phenyl-3-aminopropyl trimethoxy silane allows graphene to be used repeatedly, and it can be introduced as an environmentally friendly sorbent.

## 5. References

- [1] S.K. Lim, H.S. Shin, K.S. Yoon, Kwack SJ, Um YM, Hyeon JH, et al. Risk assessment of volatile organic compounds benzene, toluene, ethylbenzene, and xylene (BTEX) in consumer products, J. Toxicol.

- Environ. Health, 77 (2014) 22-24.
- [2] F. Yavari, C. Van, M.A. Nitsche, Effect of acute exposure to toluene on cortical excitability, neuroplasticity, and motor learning in healthy humans, *Arch. Toxicol.*, 92 (2018) 3149-3162.
- [3] P. Baltrėnas, E. Baltrėnaitė, V. Šerevičienė, P. Pereira, Atmospheric BTEX concentrations in the vicinity of the crude oil refinery of the Baltic region. *Environmental monitoring and assessment*, 182 (2011) 17-24.
- [4] J. Taylor, M. Fay, R.L. Williams, S.B. Wilbur, P.R. McClure, K. Zaccaria, Toxicological profile for toluene, *Stacks Cdc. Gov.*, 8 (2017) 1-62.
- [5] F. Yavari, C. van Thriel, M.A. Nitsche, M.F. Kuo, Effect of acute exposure to toluene on cortical excitability, neuroplasticity, and motor learning in healthy humans, *Arch. toxicol.*, 92 (2018) 3149-62.
- [6] D. Deschamps, C. Geraud, S. Dally, Cognitive functions in workers exposed to toluene: evaluation at least 48 hours after removal from exposure, *Int. Arch. Occup. Environ. Health*, 74 (2001) 285-288.
- [7] A. Romero-Anaya, M. Lillo-Ródenas, A. Linares-Solano, Spherical activated carbons for low concentration toluene adsorption, *Carbon*, 48 (2010) 53-59.
- [8] M. Lillo-Ródenas, J. Carratalá-Abril, D. Cazorla-Amorós, A. Linares-Solano, Usefulness of chemically activated anthracite for the abatement of VOC at low concentrations. *Fuel. Process. Technol.*, 77 (2002) 331-6.
- [9] L. Van De Beld, M.G. Bijl, A. Reinders, B. Van Der Werf, K. Westerterp, The catalytic oxidation of organic contaminants in a packed bed reactor, *Chem. eng. sci.*, 49 (1994) 61-73.
- [10] N. Bouazza, M. Lillo-Ródenas, A. Linares-Solano, Photocatalytic activity of TiO<sub>2</sub>-based materials for the oxidation of propene and benzene at low concentration in presence of humidity, *Appl. Catal. B*, 84 (2008) 691-8.
- [11] C. Hort, S. Gracy, V. Platel, L. Moynault, Evaluation of sewage sludge and yard waste compost as a biofilter media for the removal of ammonia and volatile organic sulfur compounds (VOSCs), *Chem. Eng. J.*, 152 (2009) 44-53.
- [12] A.J. Fletcher, Y. Yüzak, K.M. Thomas, Adsorption and desorption kinetics for hydrophilic and hydrophobic vapors on activated carbon, *Carbon*, 44 (2006) 989-1004.
- [13] J.H. Yun, K.Y. Hwang, D.K. Choi, Adsorption of benzene and toluene vapors on activated carbon fiber at 298, 323, and 348 K, *J. Chem. Eng. Data*, 43 (1998) 843-5.
- [14] Q. Hu, J.J. Li, Z.P. Hao, L.D. Li, S.Z. Qiao, Dynamic adsorption of volatile organic compounds on organofunctionalized SBA-15 materials, *Chem. eng. J.*, 149 (2009) 281-8.
- [15] M. Lillo-Ródenas, D. Cazorla-Amorós, A. Linares-Solano, Behaviour of activated carbons with different pore size distributions and surface oxygen groups for benzene and toluene adsorption at low concentrations, *Carbon*, 43 (2005) 1758-67.
- [16] A. Fuertes, G. Marban, D. Nevskaja Adsorption of volatile organic compounds by means of activated carbon fibre-based monoliths, *Carbon*, 41 (2003) 87-96.
- [17] A. Dhauadi, L. Monser, N. Adhoum, Removal of rotenone insecticide by adsorption onto chemically modified activated carbons, *J. hazad. mate*, 181 (2010) 692-9.
- [18] M. Seredych, T.J. Bandoz, Adsorption of ammonia on graphite oxide/Al<sub>13</sub> composites. *Colloids and Surfaces A*, 353 (2010) 30-6.
- [19] A. Silvestre-Albero, J. Ramos-Fernández, Martínez-Escandell M, Sepúlveda-Escribano A, Silvestre-Albero J, Rodríguez-Reinoso F. High saturation capacity of activated carbons prepared from mesophase pitch in the removal of volatile organic compounds, *Carbon*, 48 (2010) 48-56.
- [20] L. Wang, D. Zhu, L. Duan, W. Chen, Adsorption of single-ringed N-and S-heterocyclic aromatics on carbon nanotubes, *Carbon*, 48 (2010) 3906-3915.
- [21] T. Wu, X. Cai, S. Tan, H. Li, J. Liu, W. Yang, Adsorption characteristics of acrylonitrile, p-toluenesulfonic acid, 1-naphthalenesulfonic acid and methyl blue on graphene in aqueous solutions, *Chem. Eng. J.*, 173 (2011) 144-149.
- [22] X. Huang, X. Qi, F. Boey, H. Zhang, Graphene-based composites, *Chem. Soc. Rev.*, 41(2012) 666-86.
- [23] J.C. Meyer, A.K. Geim, M. Katsnelson, K. Novoselov, T. Booth, Roth S. The structure of suspended graphene sheets, *Nature*, 446(2007)60-3.
- [24] H. Wang, X. Yuan, Y. Wu, H. Huang, X. Peng, G. Zeng, et al. Graphene-based materials: fabrication, characterization and application for

- the decontamination of wastewater and wastegas and hydrogen storage/generation, *Adv. colloid interface sci.*, 195 (2013)19-40.
- [25] X. Cai, S. Tan, M. Lin, A. Xie, W. Mai, X. Zhang, et al. Synergistic antibacterial brilliant blue/reduced graphene oxide/quaternary phosphonium salt composite with excellent water solubility and specific targeting capability, *Langmuir*, 27(2011)28-35.
- [26] W. Wang, T. Sun, Y. Zhang, Y.B. Wang, Substituent effects in the  $\pi \cdots \pi$  interaction between graphene and benzene: An indication for the noncovalent functionalization of graphene, *Comput. Theor. Chem.*, 1046 (2014) 64-69.
- [27] D. Gu, J.B. Fein, Adsorption of metals onto graphene oxide: Surface complexation modeling and linear free energy relationships, *Colloid. Surf. A. Physicochem. Eng. Asp.*, 481 (2015) 319-27.
- [28] M.J. Allen, V.C. Tung, R.B. Kaner, Honeycomb carbon: a review of graphene. *Chemical reviews*, 110 (2009) 132-45.
- [29] S. Stankovich, D.A. Dikin, G.H. Dommett, K.M. Kohlhaas, E.J. Zimney, E.A. Stach, et al. Graphene-based composite materials. *Nature*, 442 (2006) 82-6.
- [30] K. Zhang, V. Dwivedi, C. Chi, J. Wu, Graphene oxide/ferric hydroxide composites for efficient arsenate removal from drinking water, *J. hazard. mater.*, 182 (2010) 162-8.
- [31] S.T. Yang, S. Chen, Y. Chang, A. Cao, Y. Liu, H. Wang, Removal of methylene blue from aqueous solution by graphene oxide. *Journal of colloid science*, 359(2011)9-24.
- [32] Y. Gao, Y. Li, L. Zhang, H. Huang, J. Hu, S.M. Shah, et al, Adsorption and removal of tetracycline antibiotics from aqueous solution by graphene oxide. *Journal of Colloid Sci.*, 368 (2012) 540-6.
- [33] G. Zhao, J. Li, X. Ren, C. Chen, X. Wang, Few-layered graphene oxide nanosheets as superior sorbents for heavy metal ion pollution management. *Environ sci. technol.*, 45 (2011) 54-62.
- [34] G. Zhao, X. Ren, X. Gao, X. Tan, J. Li, C. Chen, et al, Removal of Pb (II) ions from aqueous solutions on few-layered graphene oxide nanosheets, *Dalton Transactions*, 40 (2011) 45-52.
- [35] W. Wang, J. Yu, Q. Xiang, B. Cheng, Enhanced photocatalytic activity of hierarchical macro/mesoporous TiO<sub>2</sub>-graphene composites for photodegradation of acetone in air, *Appl. Catal. B*, 119 (2012) 9-16.
- [36] M.B.H. Abadi, H. Shir Khanloo, J. Rakhtshah, Air pollution control: The evaluation of TerphApm@MWCNTs as a novel heterogeneous sorbent for benzene removal from air by solid phase gas extraction, *Arab. J. Chem.*, 11 (2018) 287-301.
- [37] H. Sone, B. Fugetsu, T. Tsukada, M. Endo, Affinity-based elimination of aromatic VOCs by highly crystalline multi-walled carbon nanotubes, *Talanta*, 74(2008) 65-70.
- [38] Y.h. Shih, M.s. Li, Adsorption of selected volatile organic vapors on multiwall carbon nanotubes. *J. Hazard. Mater.*, 154 (2008) 8-21.
- [39] M. Yao, Q. Zhang, D.W. Hand, D. Perram, R. Taylor, Adsorption and regeneration on activated carbon fiber cloth for volatile organic compounds at indoor concentration levels. *J. Air. Waste. Manag. Assoc.*, 59 (2009) 31-6.
- [40] S. Ghorai, K. Pant, Equilibrium, kinetics and breakthrough studies for adsorption of fluoride on activated alumina, *Sep. Purif. Technol.*, 42 (2005) 65-71.
- [41] N. Mohan, G. Kannan, S. Upendra, R. Subha, N. Kumar, Breakthrough of toluene vapours in granular activated carbon filled packed bed reactor. *J. hazard. mater.*, 168 (2009) 77-81.
- [42] M.R. Samarghandi, A. Poormohammadi, S. Shanesaz, K. Godini, Comparison Between the Performance of Activated Carbon and Graphene in Removal of Reactive Red 198, *Avicenna, J. Environ. Health. Eng.*, 4 (2017) 17-23.



# Food Analysis: Task specific ionic liquids for separation of nickel and cadmium from olive oil samples by thermal ultrasound-assisted dispersive multiphasic microextraction

Hamid Shir Khanloo<sup>a,\*</sup> and Aisan Khaligh<sup>b</sup>

<sup>a</sup>Research Institute of Petroleum Industry (RIPI), West Entrance Blvd., Olympic Village

<sup>b</sup>Department of Chemistry, Semnan University, Semnan

## ARTICLE INFO:

Received 17 Apr 2019

Revised form 4 May 2019

Accepted 25 May 2019

Available online 20 Jun 2019

## Keywords:

Olive oil

Cadmium and nickel

Thermal ultrasound-assisted  
dispersive multiphasic  
microextraction

Task specific ionic liquid

Atom trap flame atomic  
absorption spectrometry

## ABSTRACT

In this study, a novel task-specific ionic liquid (TSILs) was used for highly sensitive extraction and separation of nickel and cadmium in olive oil by thermal ultrasound-assisted dispersive multiphasic microextraction (TUSA-DMP $\mu$ E). By proposed method, a mixture containing of hydrophilic TSILs ( $\alpha$ - Cyano-4-hydroxycinnamic acid diethylamine; [CHCA] [DEA] and 1-(2-Hydroxyethyl)-3-methylimidazolium tetrafluoroborate; [HEMIM] [BF<sub>4</sub>]) as a complexing and extracting solvent, acetone as a dispersant of TSILs was added to diluted olive oil with n-hexane containing Cd (II) and Ni (II) that was already complexed by TSILs in 60°C at pH 6.0-7.5. After optimized conditions, the enrichment factor (EF), Linear range (LR) and limit of detection (LOD) were obtained (19.3; 19.6), (5.0- 415  $\mu$ g L<sup>-1</sup>; 2.7- 92  $\mu$ g L<sup>-1</sup>) and (1.3  $\mu$ g L<sup>-1</sup>; 0.6  $\mu$ g L<sup>-1</sup>) with [CHCA] [DEA] and (13.7; 14.2), (7.5- 600  $\mu$ g L<sup>-1</sup>; 3.6- 128  $\mu$ g L<sup>-1</sup>) and (2.2 ng L<sup>-1</sup>; 0.9  $\mu$ g L<sup>-1</sup>) with [HEMIM][BF<sub>4</sub>] for Ni and Cd ions in olive oil samples respectively. In addition, the ions extraction with [CHCA] [DEA] is more efficient than [HEMIM][BF<sub>4</sub>] by TUSA-DMP $\mu$ E method (less than 60%). Moreover, the validation of methodology was achieved by standard oil by microwave digestion/ETAAS technique and spike samples with atom trap flame atomic absorption spectrometry (AT-FAAS)

## 1. Introduction

The edible oil toxicity by cadmium (Cd) and nickel (Ni) ions is very important problem in food industry because of bioaccumulation in human body and cause damage to organs such as kidney dysfunction, hypertension, liver damage, lung damage, cancer and adverse DNA modifications [1-3]. The presence of high concentration of Cd (II) and Ni (II) in edible oils may also have deleterious effects on the quality of the product, causing changes to their taste and smell [4]. Cd (II) and Ni (II) ions are easily transferred from arable land to oil plants,

which are increasingly contaminated by cadmium and nickel from phosphate-based fertilizers. These toxic elements can also be present in edible oils, as a result of contamination from the environment, the refining process, the storage tank, and the packing with different materials [5-7]. The U.S. Food and Drug Administration (USFDA) reported that the permissible limits of nickel and cadmium in the vegetables oils are less than 1.0 mg/kg and 0.1 mg/kg, respectively. For healthy people, the mean of cadmium and nickel concentration in human serum samples is less than 0.2  $\mu$ g L<sup>-1</sup>. Therefore, the accurate determination of trace cadmium and nickel ions in edible oils is an important concern because

\*Corresponding Author: Hamid Shir Khanloo

Email: [hamidshirkhanloo@yahoo.ca](mailto:hamidshirkhanloo@yahoo.ca)

DOI: <https://doi.org/10.24200/amecj.v2.i01.44>

of their toxic role in human body and possibilities for adulteration detection and oil characterization [8-10]. The presence of trace metal ions in edible oils were quantitatively determined by different techniques such as flame atomic absorption spectrometry (FAAS) [1, 3, 11], electro-thermal atomic absorption spectrometry (ETAAS) [12], inductively coupled plasma atomic emission spectrometry (ICP-AES) [12, 13], inductively coupled plasma mass spectrometry (ICP-MS) [4, 14], and adsorptive stripping square wave voltammetry (AdSSWV) [15]. Sample preparation is a critical step in the whole analytical procedure due to low concentration levels of metal ions and high organic matrix of oils [3, 16]. Moreover, many of conventional methods employed for the sample pretreatment such as acid digestion, wet or dry ashing of oil matrix, closed-vessel, and focused open-vessel microwave dissolution, dilution as well as basic alcoholic solubilization are not recommended because of associated safety hazards, a potential risk of sample contamination, analyte losses and being time-consuming [17]. In this regard, preconcentration and separation steps are required prior to analyte determination. Recently, dispersive liquid-liquid microextraction (DLLME) has introduced by Rezaee et al [18] has gained increasing popularity for the trace metal ions preconcentration-separation in food and biological samples because of its simplicity, rapidity, low cost, low consumption of toxic organic solvents as well as the high preconcentration factor and extraction efficiency that are achieved [19, 20]. DLLME uses an extraction solvent, immiscible in the aqueous phase, and a disperser solvent, miscible in both the extraction solvent and in the aqueous sample solution. In this method, the contact area between the extraction solvent and the sample solution is extremely large, so the extraction equilibrium is reached rapidly. In the DLLME, the choice of the appropriate mixture of the extraction and dispersive solvents is critical for achieving high enrichment factor [21]. Ionic liquids (ILs), as an alternative to traditional organic solvents in sample preparation, are one of the mostly considered

extraction solvents in DLLME due to their low volatility, high viscosity, dual natural polarity, good thermal stability, and miscibility with water and organic solvents (TSIL, chempaper) without requiring a dispersive solvent [20, 22, 23]. It has been demonstrated that organic analytes can be partitioned to ILs based on the hydrophobicity of the analytes and ILs, but metal ions cannot be extracted in liquid/liquid systems owing to negligible partitioning and the tendency of metal cations to remain hydrated in the aqueous phase [21]. Therefore, it is necessary to use chelating agents which firstly form hydrophobic complex with metal ions, and then the formed complex extract into extraction solvent. In recent years, task specific ionic liquid (TSIL), a new group of ionic liquids, has been introduced in which thiol or urea groups are covalently attached to the cationic or anionic part of the IL. TSIL can be used as a dispersive and extraction solvent for metal ions in DLLME method without any chelating agents [23]. In the TSIL-DLLME, extraction and complexation of metal ions were done simultaneously and this newly developed procedure is a very fast and easy single-step method without needing chelating agents compared to the traditional DLLME method [24]. To date, different DLLME modes based on the ILs have been developed such as temperature controlled, ultrasonic-assisted, microwave-assisted and vortex-assisted [25]. Zhou et al. made the most preferred modifications in IL-DLLME which are ultrasound-assisted (US) and temperature-controlled (TC) techniques [26, 27]. In TC, IL-dispersive liquid-liquid microextraction, the extraction solvent is heated until it is completely solubilized in the water matrix. The heating improves the mass transfer of the analyte to the IL [28]. In US, IL-dispersive, liquid-liquid microextraction, ultrasound and dispersive solvents are used to increase the extraction ability of ILs [28]. The motivation behind the present work is that a great number of the TSIL-DLLME analytical procedures reported to date have dealt with water analysis or relatively simple matrices. For example, Werner developed TSIL-USA-DLLME combined

with liquid chromatography for preconcentration and determination of Cd (II), Co(II) and Pb (II) ions in tea samples [22]. However, application of this method in edible oil samples has not been studied yet. Therefore, the main aim of the current study is to develop a simple, rapid, reliable and economic method for the determination of trace Cd<sup>2+</sup> and Ni<sup>2+</sup> ions in olive oil samples without chelating agents. This method is based on the combination of the thermal ultrasound-assisted-task specific ionic liquid-dispersive multiphasic microextraction technique (TUS-TSIL-DMP<sub>μ</sub>E) and AT-FAAS. In the present approach, two hydrophilic TSILs, ([CHCA] [DEA]) and [HEMIM][BF<sub>4</sub>]), were used and compared not only as an extraction solvent but also as a selective chelating agent. Experimental parameters including sample pH, amount of sorbent, sample volume, eluent type and volume, and time of ultrasound, etc., have been studied and optimized.

## 2. Experimental procedure

### 2.1. Apparatus

The measurements of Cd (II) and Ni(II) ions were performed with a spectra GBC 906 double beam atomic absorption spectrophotometer equipped with atom trap, air-acetylene flame and ultra-pulse deuterium as a background correction (AT-FAAS, GBC, Model; Plus 906, Australia). The atom trap was installed on an air-acetylene burner. A data station (AT-compatible computer) with 906 AAS operating software was utilized for collecting and storing data. For the matter of interest, the operating parameters were set as recommended by the manufacturer. A Cd and Ni hollow cathode lamps as the radiation sources were used at a current of 10 mA and 3 mA, and a wavelength of 279.5 nm and 228.8 nm, respectively, with a spectral bandwidth of 0.5 nm. The pH values of the solutions were measured by a Metrohm pH-meter (model 744, Herisau, Switzerland) supplied with a glass-combined electrode. Phase separation was carried out by a Demerd centrifuge (model LC8-12). A Kunshan ultrasonic bath with temperature control (model KQ-100DE, Kunshan, China) was used throughout this study.

### 2.2. Chemical Reagents and Material

A standard stock solutions (1000 mg L<sup>-1</sup>) of Ni (II) and Cd (II),  $\alpha$ - Cyano- $\epsilon$ -hydroxycinnamic acid diethylamine ([CHCA] [DEA]) ionic liquid, acetone, sodium tetrafluoroborate (NaBF<sub>4</sub>), ethyl acetate, chloroethanol, 1-methylimidazole and all of the other chemical compounds and reagents were of analytical grade and purchased from Merck (Darmstadt, Germany). Ultra-pure deionized water (DW, 18 M $\Omega$  cm<sup>-1</sup>) from Milli-Q plus water purification system (Millipore, Bedford, MA, USA) was used for preparing all aqueous solutions. The standard and experimental solutions of Ni<sup>2+</sup> and Cd<sup>2+</sup> were prepared daily by appropriate dilution of the stock solutions with DW. The pH adjustments of samples were made using appropriate buffer solutions including sodium acetate (CH<sub>3</sub>COONa/CH<sub>3</sub>COOH, 1-2 mol L<sup>-1</sup>) for pH 3.8–5.8, sodium phosphate (Na<sub>2</sub>HPO<sub>4</sub>/NaH<sub>2</sub>PO<sub>4</sub>, 0.2 mol L<sup>-1</sup>) for pH of 5.8–8.0, and ammonium chloride (NH<sub>3</sub>/NH<sub>4</sub>Cl, 0.2 mol L<sup>-1</sup>) for pH 8–10. All the laboratory glassware and plastic tubes were cleaned by soaking in 10% (v/v) nitric acid for at least 24 h and then rinsed several times with deionized water and dried in a clean oven prior to use. In this study, five olive oils (Cooking and skin) was selected and used for investigation.

### 2.3. Synthesis of TSIL

The hydrophilic TSILs, ( $\alpha$ - Cyano-4-hydroxycinnamic acid diethylamine; [CHCA] [DEA] purchased from Merck and [HEMIM] [BF<sub>4</sub>] was prepared according to the synthesis method [27]. The general procedure for synthesis of [HEMIM][BF<sub>4</sub>] TSIL is described as follows: First, 13.9 g (0.169 mol) of 1-methylimidazole (99 %), distilled over KOH, was slowly added to 15.0 g (0.186 mol) of freshly distilled 2-chloroethanol in a round-bottomed flask equipped with a magnetic stirrer and a condenser, under nitrogen atmosphere. The mixture was refluxed at 100 °C for 4 h. After cooling to 70 °C, the reaction mixture was washed four times with ethyl acetate, and then dried in vacuo at 70 °C for 8 h. The product, 1-(2-hydroxyethyl)-3-methylimidazolium chloride ([HEMIM][Cl]), was

obtained in form of white crystalline solid (65% yield, 17.9 g). This compound was characterized by  $^1\text{H}$  NMR (500 MHz,  $\text{D}_2\text{O}$ , 25 °C,  $\delta$ ; ppm). The obtained data are here: 3.87 (3H, s,  $\text{NCH}_3$ ), 3.89 (2H, t,  $\text{NCH}_2\text{CH}_2\text{OH}$ ), 4.28 (2H, t,  $\text{NCH}_2\text{CH}_2\text{OH}$ ), 7.42 (1H, d, H-4), 7.47 (1H, d, H-5), and 8.71 (1H, s, H-2).

Then 30.0 g (0.185 mol) of  $[\text{HEMIM}][\text{Cl}]$  was reacted with 26.4 g (0.24 mol) of  $\text{NaBF}_4$  in acetonitrile solvent at room temperature for 48 h, under nitrogen atmosphere. The reaction mixture was then cooled to 18 °C overnight and filtered through a short column of Celite to remove  $\text{NaCl}$ . The solvent was removed using a rotary evaporator, and the residual chloride test (a concentrated  $\text{AgNO}_3$  solution test) performed on product was negative. The product, 1-( $\gamma$ -hydroxyethyl)-3-methylimidazolium tetrafluoroborate ( $[\text{HEMIM}][\text{BF}_4]$ ), was obtained as a viscous material (62% yield). Karl Fischer test showed < 100 ppm of water and the absence of chloride ion confirmed the product purity (> 99.5 %). This compound was also characterized by  $^1\text{H}$  NMR (500 MHz,  $\text{D}_2\text{O}$ , 25 °C,  $\delta$ ; ppm): 3.83 (3H, s,  $\text{NCH}_3$ ), 3.87 (2H, t,  $\text{NCH}_2\text{CH}_2\text{OH}$ ), 4.24 (2H, t,  $\text{NCH}_2\text{CH}_2\text{OH}$ ), 7.38 (1H, d, H-4), 7.43 (1H, d, H-5), and 8.66 (1H, s, H-2).

#### 2.4. General procedure

In this procedure,  $[\text{CHCA}]$   $[\text{DEA}]$  and  $[\text{HEMIM}][\text{BF}_4]$  were used as hydrophilic task-specific ionic

liquids (TSILs) to complex the ultra-trace amounts of Ni (II) and Cd (II) ions in Olive oil samples and extract them. The TUSA-DMP $\mu\text{E}$  of metal ions was performed as follows: In a 100 mL glass centrifuge tube with a conical bottom, 26.0 g (20 mL) of olive oil sample containing Cd and Ni ions was diluted with n-hexane up to 40 mL. Then, the mixture of 0.25 g of the mentioned above TSILs and 0.5 mL of acetone (as a dispersive solvent) which was diluted with DW up to 5.0 mL was prepared and then, the pH adjusted between 2 to 10 by buffer solution. Afterwards, the mixture was injected rapidly into 40 mL of edible oil samples with HPLC autosampler syringe (5 mL, gastight, CTC-PAL, Trajan, AUS) and stirred for 5 min at 85 °C. The cloudy phases were then separated by centrifuging of the turbid solution for 4 min at 4000 rpm (25°C). The Cd/Ni complexes were settled down at the bottom of the conical tube into droplets of TSILs. The upper phase of the sample (edible oil) was removed with a pipette, the metal complexes was back extracted from TSIL with  $\text{HNO}_3$  (0.2 mL, 0.5 M) and finally the concentration of Ni (II) and Cd (II) ions in the resulting solution was determined by AT-FAAS after dilution with deionized water up to 1 mL. For validation, 1 mL of sample oils was digested with microwave accessory for 1 hour (UV, 5:1 mL;  $\text{HNO}_3/\text{H}_2\text{O}_2$ , 220°C) and concentration of Ni and Cd ions determined by F-AAS/ET-AAS/ICP-MS (Figure 1).

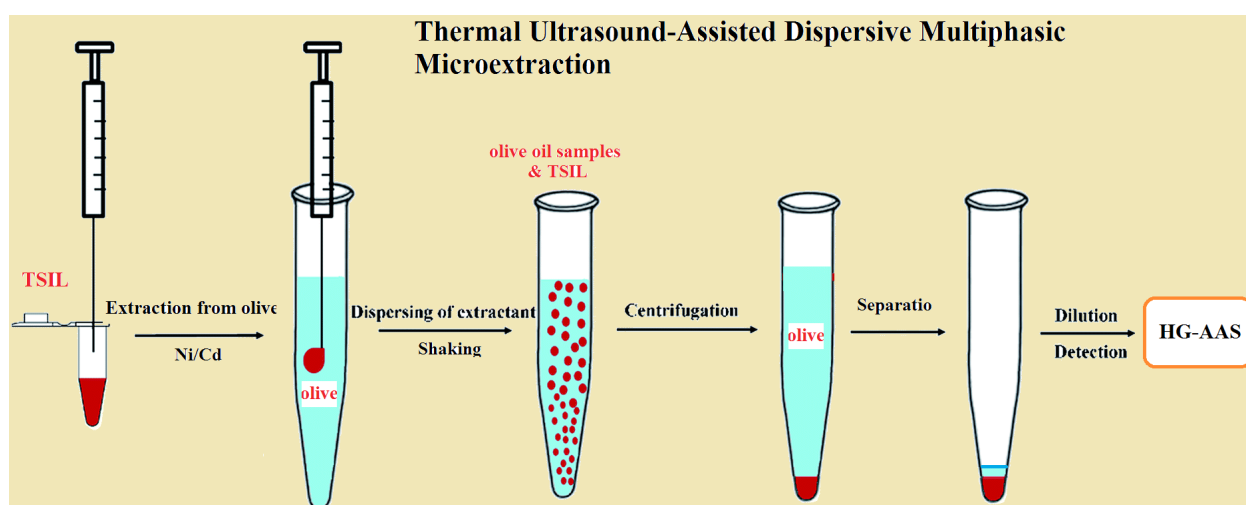


Fig. 1. General procedure for extraction of Ni/Cd from olive oil by TUSA-DMP $\mu\text{E}$

### 3. Results and Discussion

#### 3.1. Effect of sample pH

Complexation was strongly conditioned by the pH of the solutions. In the present work, the solution pH affected the extraction process through the functional group moieties of the TSIL. The influence of sample pH on the complex formation and the extraction of Ni (II) and Cd (II) ions with [CHCA] [DEA] and [HEMIM][BF<sub>4</sub>] TSILs was separately investigated at different pH values from 2 to 10 for 40 mL buffered diluted olive oil samples, according to the general procedure. The results were depicted in figures 2a and 2b. Obviously, the maximum extraction efficiencies for Ni (II) and Cd

(II) ions were obtained with [CHCA] [DEA] TSIL in pH range of 6-8, and then the recoveries were decreased by increasing of pH (Fig. 2a). Whereas, by using [HEMIM][BF<sub>4</sub>] TSIL (Fig. 2b), the quantitative recoveries were less than 40-70% at pH 7.5-10.

#### 3.2. Effect of sample volume

The sample volume is one of the most important parameters to be studied by TUSA-DMP $\mu$ E method, since it determines the sensitivity and enhancement of the technique. The effect of sample volume was studied in the range of 5–40 mL for 5 - 100  $\mu$ g L<sup>-1</sup> of standard solution of Ni and Cd (Fig. 3).

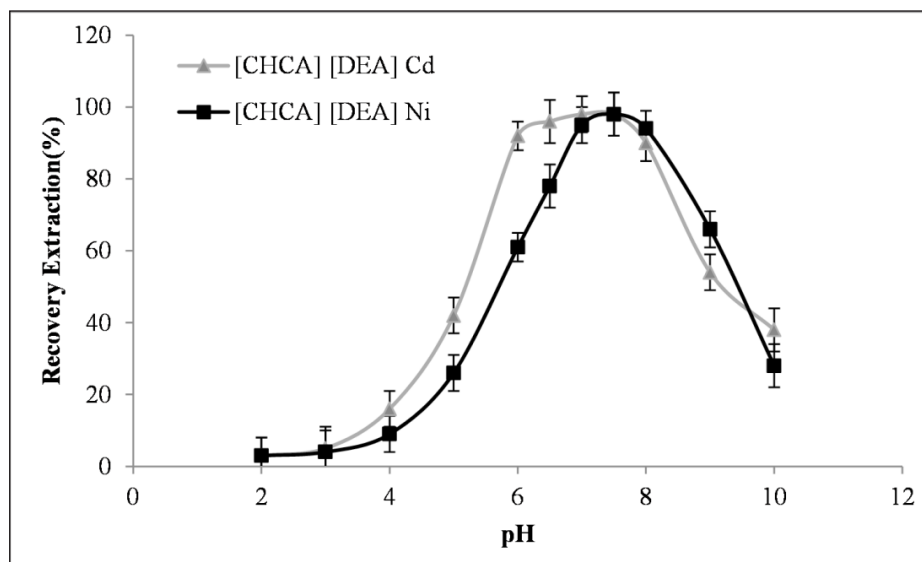


Fig. 2a. Effect of pH on extraction of Ni (II) and Cd (II) ions in olive oil with [CHCA] [DEA] by TUSA-DMP $\mu$ E

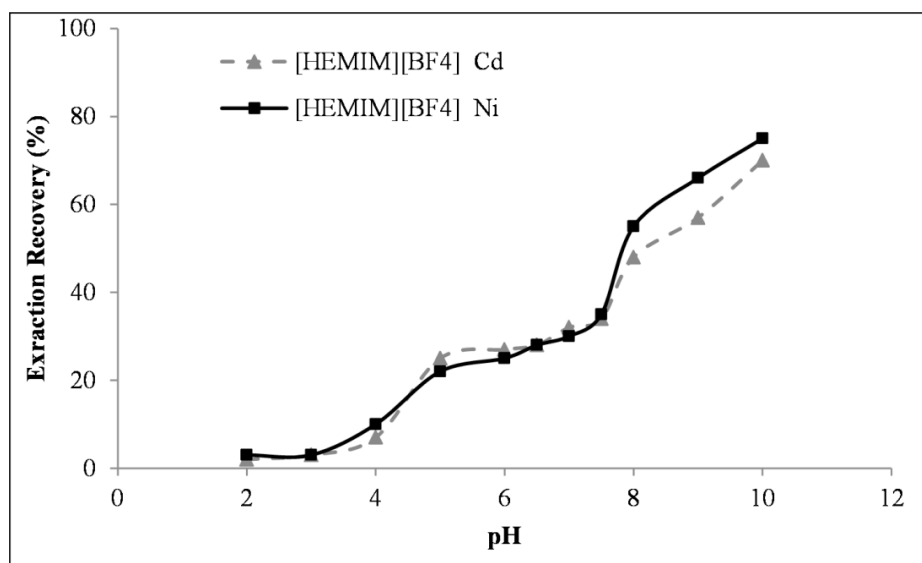


Fig. 2b. Effect of pH on extraction of Ni (II) and Cd (II) ions in olive oil with [HEMIM][BF<sub>4</sub>] by TUSA-DMP $\mu$ E.

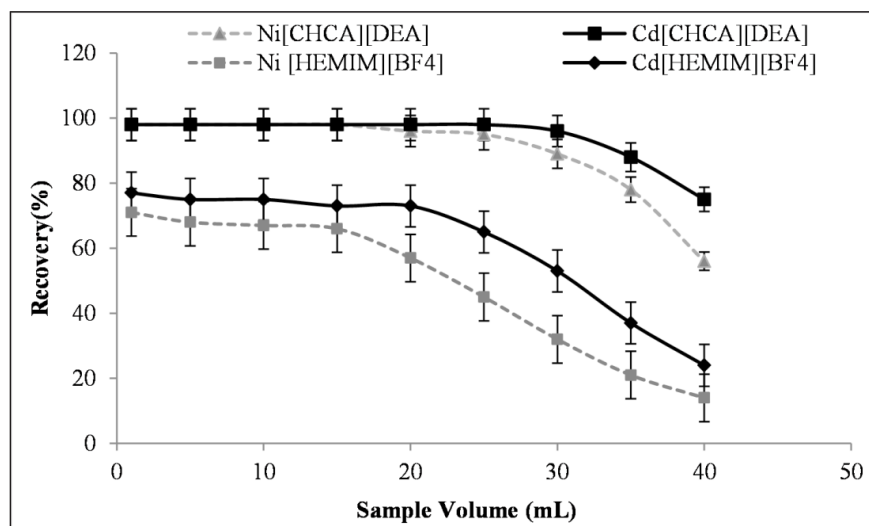


Fig. 3. Effect of sample volume on extraction of Ni (II) and Cd (II) ions in olive oil by TUSA-DMP $\mu$ E.

### 3.3. Effect of TSIL amount on Ni and Cd extraction

The amounts of ILs on the extraction efficiencies of Ni/Cd in Olive oil by TUSA-DMP $\mu$ E method was studied and optimized. For this purpose, the range of 0.01-0.1 g of [CHCA] [DEA] and [HEMIM] [BF<sub>4</sub>] as a TSIL was used in human biological samples and standard solution containing; 5-100  $\mu$ g L<sup>-1</sup> of Ni (II) and Cd(II) (Fig. 3). The results show that the quantitative recoveries were obtained with 20-40 mg of [CHCA] [DEA] as a 98% recovery. Therefore, in order to achieve a suitable preconcentration, 50 mg of [CHCA] [DEA] was chosen as optimum leading to a final IL for blood/urine and standard solution analysis. Also,

the effect of IL used on the recovery efficiencies of Ni/Cd ions with TSIL of [HEMIM][BF<sub>4</sub>] was investigated by TUSA-DMP $\mu$ E method. The results showed us, the maximum recoveries of Ni/Cd in olive oils were less than 64% by using [HEMIM][BF<sub>4</sub>], therefore the [HEMIM][BF<sub>4</sub>] had lower recovery as compared to [CHCA] [DEA]. Moreover, by increasing the ultra-sonication time up to 60 min and 150 mg of [HEMIM][BF<sub>4</sub>], the almost 73% of Ni/Cd ions from olive oils can be extracted by [HEMIM][BF<sub>4</sub>] in standard solution (Fig. 4). So, the recovery extraction of ions with [HEMIM][BF<sub>4</sub>] cannot be increased by long time or amount of IL.

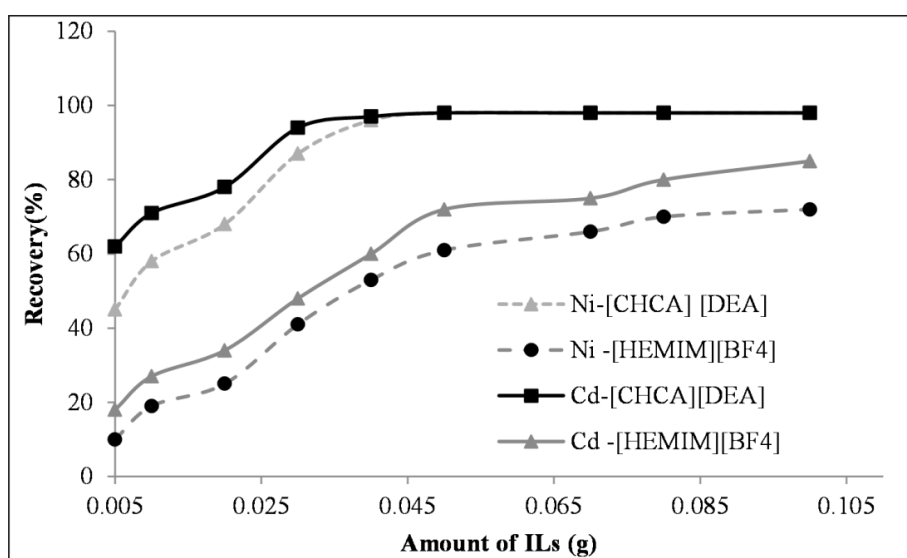


Fig. 4. Effect of amount of TSILs on extraction of Ni (II) and Cd (II) ions in olive oil by TUSA-DMP $\mu$ E

### 3.4. Effect of ultra-sonication time for Ni and Cd extraction

The ultra-sonication time during the extraction process can improve the extraction recovery since it enhances the complexation of Ni/Cd ions to TSIL. Based on procedure, kind of TSILs are the most important factors for sonication time by TUSA-DMP $\mu$ E method. Therefore, the effect of sonication type, shaker tube or ultrasound bath, on the recovery efficiencies of Ni/Cd ions in olive oils was examined by [CHCA] [DEA] and [HEMIM] [BF<sub>4</sub>]. The results showed, the maximum recovery was obtained using sonication at 5 min. The optimization of sonication time increased the extraction recovery and decreased the time and IL mass. This fact can be related to the large contact area between dispersion of TSILs with olive oil samples. In this study, ultrasound assisted extraction times ranging from 1 to 25 min were evaluated. Therefore, the ultrasonic time of 5 min was selected as optimum time (Fig. 5).

### 3.5. Interference study

The determination of Ni/Cd ions in different olive oil samples in the presence of interfering matrix ions was examined. In order to get the acceptable analytical technique by TUSA-DMP $\mu$ E procedure, various interfering cations such as; Na<sup>+</sup>, K<sup>+</sup>, V<sup>3+</sup>, Cu<sup>2+</sup>, Zn<sup>2+</sup>, Al<sup>3+</sup>, Co<sup>2+</sup>, Cr<sup>3+</sup>, Hg<sup>2+</sup>, As<sup>3+</sup>, Mn<sup>2+</sup>

and anions, SO<sub>3</sub><sup>2-</sup>, NO<sub>3</sub><sup>-</sup>, Cl<sup>-</sup>, F<sup>-</sup>, PO<sub>4</sub><sup>3-</sup> (1-3 mgL<sup>-1</sup>) were added individually to real olive oil and standard solutions containing 5–100  $\mu$ gL<sup>-1</sup> of Ni<sup>2+</sup> and Cd<sup>2+</sup> in optimized conditions. Interfering ions concentration causing less than  $\pm$  5% deviation in the recovery of Ni(II) and Cd(II) was considered as the tolerance limit. Based on the results, the presence of interfering ions has no considerable effect on the recovery efficiencies of Ni(II) and Cd(II) in olive oil samples.

### 3.6. Effect of Temperature on Ni and Cd extraction

The temperature has a critical role in extraction recovery of Ni(II) and Cd(II) in olive oil samples by TSILs. As evaluation of TSILs, the effect of temperature was studied and optimized between 20–90 °C. The results showed us, the extraction efficiency of Ni(II) and Cd(II) by [CHCA] [DEA] and [HEMIM][BF<sub>4</sub>] was depended to temperature. The results showed us, the optimized temperature was obtained between 40- 60 °C. In optimized temperature, the extraction ions in olive oils with [CHCA] [DEA] was more than [HEMIM][BF<sub>4</sub>].

### 3.7. Effect of mineral acids on the back-extraction ions

Because of high viscosity of TSILs, the direct injection of ILs into AT-FAAS is not possible. So, the Ni and Cd ions back extracted from TSILs with

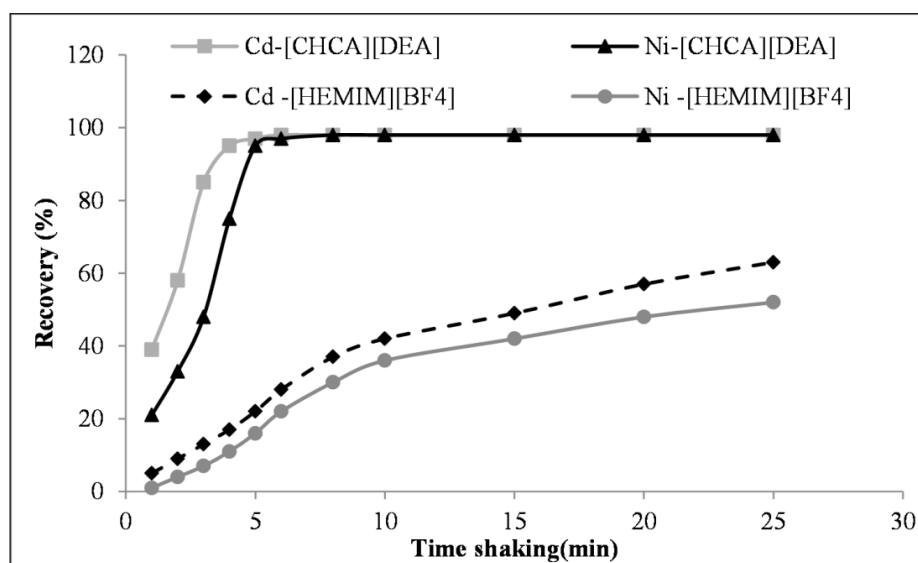


Fig. 5. Effect of shaking time on extraction of Ni (II) and Cd (II) ions in olive oil by TUSA-DMP $\mu$ E

a mineral acidic solution. Decreasing the pH leads to dissociation and releasing of Ni(II) ions into the aqueous phase. Different mineral acids such as HCl, HNO<sub>3</sub>, CH<sub>3</sub>COOH and H<sub>2</sub>SO<sub>4</sub> (0.1–0.5 M) were studied for Ni/Cd back-extraction from the TSILs. The research showed that 0.1 mL of HNO<sub>3</sub> (0.5 M) quantitatively back-extracted Ni/Cd ions from the olive oil samples before diluted with DW up to 1 mL.

### 3.8. Validation of Method

The analytical characteristics of the developed TUSA-DMPμE method at the optimum conditions were shown in table 1. After sample preparation, Ni/Cd in olive oils and standard samples was determined by proposed method. The olive oils samples as a real sample was used for determination of Ni/Cd as the average of three separate determinations. The accuracy of the results was verified by analyzing the spiked samples with known concentration of Ni/Cd (II) in olive oils samples (Tables 2). Based on the obtained results, a good agreement was obtained between the added and measured Ni/Cd amount, which confirms the accuracy of the procedure and its independence from the matrix effects. The

recoveries of spiked samples demonstrated that the developed method was satisfactory for Ni/Cd analysis. In order to validate the method described, certified reference materials in olive oils (CRM, A-D) which was determined with ET-AAS after microwave digestion with pure acid and H<sub>2</sub>O<sub>2</sub>, were analyzed by proposed method (Table 3). Analytical results of the CRM samples were satisfactorily in agreement with the certified values. Moreover, a good agreement was obtained between added and found values of the Ni/Cd ions in spiked samples by CRM samples.

### 4. Conclusions

A novel, reliable and efficient method was used for preconcentration, separation and determination of trace Ni/Cd in olive oil samples by TUSA-DMPμE procedure. The proposed method was developed based on hydrophilic TSILs ( $\alpha$ -Cyano-4-hydroxycinnamic acid diethylamine; [CHCA] [DEA] and 1-(2-Hydroxyethyl)-3-methylimidazolium Tetrafluoroborate; [HEMIM] [BF<sub>4</sub>]) as a complexing and extracting solvent which was coupled by AT-FAAS technique. Finally, the newly developed method was low interference,

**Table 1.** Analytical characteristics of the developed TUSA-DMPμE method at the optimum conditions by [CHCA] [DEA].

Metal ions	Sample volume (mL)	Linear range ( $\mu\text{g L}^{-1}$ )	Regression coefficient ( $R^2$ )	LOD <sup>a</sup> (n = 10) ( $\mu\text{g L}^{-1}$ )	RSD <sup>b</sup> (n = 10) (%)	PF <sup>c</sup>
Cd <sup>2+</sup>	20	2.7- 92	0.9996	0.6	4.4%	19.6
Ni <sup>2+</sup>	20	5.0- 415	0.9998	1.3	5.1%	19.3

<sup>a</sup> Limit of detection, <sup>b</sup> Relative standard deviation, <sup>c</sup> Preconcentration factor

**Table 2.** Analytical results for determination of analytes in spiked olive oil samples.

Sample	Added ( $\mu\text{g L}^{-1}$ )		Found <sup>a</sup> ( $\mu\text{g L}^{-1}$ )		RSD <sup>b</sup> (%)		Recovery (%)	
	Cd <sup>2+</sup>	Ni <sup>2+</sup>	Cd <sup>2+</sup>	Ni <sup>2+</sup>	Cd <sup>2+</sup>	Ni <sup>2+</sup>	Cd <sup>2+</sup>	Ni <sup>2+</sup>
Olive 1	-----	-----	3.6	65.7	4.2	5.7	-----	-----
	5.0	50.0	8.4	114.8	5.3	4.7	0.96	98.2
Olive 2	-----	-----	18.5	98.4	3.9	4.8	-----	-----
	20.0	100.0	39.1	197.7	4.5	5.1	103	99.3
Olive 3	-----	-----	2.5	32.2	4.9	5.3	-----	-----
	2.0	30.0	4.4	61.4	5.7	5.4	95.0	97.4
Olive 4	-----	-----	22.6	45.8	5.4	5.3	-----	-----
	20.0	50.0	41.8	95.9	4.4	4.7	96.0	102

<sup>a</sup> Mean of three determinations  $\pm$  confidence interval (P = 0.95, n = 5), <sup>b</sup> Relative standard deviation.

**Table 3.** Validation of developed TUSA-DMP $\mu$ E method with Standard Reference Material (CRM).

sample	Certified <sup>a</sup> ( $\mu\text{g L}^{-1}$ )		Added ( $\mu\text{g L}^{-1}$ )		Found <sup>b</sup> ( $\mu\text{g L}^{-1}$ )		Recovery (%)	
	Cd(II)	Ni(II)	Cd(II)	Ni(II)	Cd(II)	Ni(II)	Cd(II)	Ni(II)
A	4.5	10.5	5	10	9.3	19.9	97.9	97.1
B	12.8	45.6	10	50	22.1	94.4	96.9	98.7
C	55.2	117.9	50	100	99.9	209.7	94.9	96.2
D	88.6	267.9	100	200	191.1	460.2	101.0	98.3

<sup>a</sup> Certified by ETAAS after digestion with micro wave of oils

<sup>b</sup> Mean of three determinations  $\pm$  confidence interval ( $P = 0.95$ ,  $n = 5$ ),

easy usage for sample preparation in olive oil samples and also provides low LOD, and RSD values as well as good PF values and quantitative recoveries for Ni/Cd extraction in difficulty olive oil matrix (>95%). Therefore, the proposed method can be considered as simple and applied sample preparation techniques with TSILs for Ni/Cd separation / determination in olive oil samples by AT-FAAS.

## 5. Acknowledgements

The authors wish to thank the Iranian Research Institute of Petroleum Industry (RIPI) for this work (No grant or fund by RIPI).

## 6. References

- [1] O. Acar, Evaluation of cadmium, lead, copper, iron and zinc in Turkish dietary vegetable oils and olives using electrothermal and flame atomic absorption spectrometry, *grasas y aceites*, 63 (2012) 383-393.
- [2] A. Palizban, A. Badii, G. Asghari, H. Mardani-Nafchi, Lead and cadmium contamination in seeds and oils of Brassica napus L and Carthamus tinctorius grown in Isfahan Province/Iran, *Iranian J. Toxicol.*, 8 (2015) 1196-1202.
- [3] E.K. Baran, S.B. Yaşar, Zinc and nickel determination in liquid edible oils by FAAS after the extraction, *Eur. j. lipid sci. technol.*, 114 (2012) 1320-1326.
- [4] K. Bakkali, N.R. Martos, B. Souhail, E. Ballesteros, Determination of heavy metal content in vegetables and oils from Spain and Morocco by inductively coupled plasma mass spectrometry, *Anal. Lett.*, 45 (2012) 907-919.
- [5] M.Y. Aşci, A. Efendioğlu, B. Bati, Solid phase extraction of cadmium in edible oils using zinc piperazinedithiocarbamate and its determination by flame atomic absorption spectrometry, *Turkish J. Chem.*, 32 (2008) 431-440.
- [6] C. Onyema, K. Ibe, Effects of Refining Processes on the Physicochemical Properties of Some Selected Vegetable Oils, *Am. Chem. Sci. J.*, 12 (2016) 1-7.
- [7] S.U. Okorie, C.N. Nwachukwu, Comparative Evaluation Of Quality Characteristics Of Oils Extracted From Some Selected Legumes And A Cereal, *IOSR J. Environ. Sci., Toxicol. Food Technol.*, 8 (2014) 66-69.
- [8] H. Well, Agency for Toxic Substances and Disease Registry (ATSDR), 2015.
- [9] M. Hezbullah, S. Sultana, S. Chakraborty, M. Patwary, Heavy metal contamination of food in a developing country like Bangladesh: An emerging threat to food safety, *J. Toxicol. Environ. Health Sci.*, 8 (2016) 1-5.
- [10] F. Zhu, W. Fan, X. Wang, L. Qu, S. Yao, Health risk assessment of eight heavy metals in nine varieties of edible vegetable oils consumed in China, *Food chem. toxicol.*, 49 (2011) 3081-3085.
- [11] D. Mendil, Ö.D. Uluözülü, M. Tüzen, M. Soylak, Investigation of the levels of some element in edible oil samples produced in Turkey by atomic absorption spectrometry, *J. Hazard. Mater.*, 165 (2009) 724-728.
- [12] M. Zeiner, I. Steffan, I.J. Cindric, Determination of trace elements in olive oil by ICP-AES and ETA-AAS: A pilot study on the geographical characterization, *Microchem. J.*, 81 (2005) 171-176.
- [13] I.J. Cindric, M. Zeiner, I. Steffan, Trace elemental characterization of edible oils by ICP-AES and GFAAS, *Microch. J.*, 85 (2007) 136-139.
- [14] E. Llorent-Martínez, P. Ortega-Barrales, M. Fernández-de Córdoba, A. Domínguez-Vidal, A. Ruiz-Medina, Investigation by ICP-MS of trace

- element levels in vegetable edible oils produced in Spain, *Food Chem.*, 127 (2011) 1257-1262.
- [15] T.G. Díaz, A. Guiberteau, M.L. Soto, J. Ortiz, Determination of copper with 5, 5-dimethylcyclohexane-1, 2, 3-trione 1, 2-dioxime 3-thiosemicarbazone in olive oils by adsorptive stripping square wave voltammetry, *Food Chem.*, 96 (2006) 156-162.
- [16] F. Tokay, S. Bağdat, Spectrometric determination of iron and copper in vegetable oils after separation with Schiff base impregnated silica gel column: A simple approach for eliminating the high organic matrix, *Int. j. food sci. technol.*, 50 (2015) 2694-2699.
- [17] F. Tokay, S. Bağdat, Determination of iron and copper in edible oils by flame atomic absorption spectrometry after liquid-liquid extraction, *J. Am. Oil Chem. Soc.*, 92 (2015) 317-322.
- [18] M. Rezaee, Y. Assadi, M.-R.M. Hosseini, E. Aghaee, F. Ahmadi, S. Berijani, Determination of organic compounds in water using dispersive liquid-liquid microextraction, *J. Chromatogr. A*, 1116 (2006) 1-9.
- [19] I. López-García, Y. Vicente-Martínez, M. Hernández-Córdoba, Determination of cadmium and lead in edible oils by electrothermal atomic absorption spectrometry after reverse dispersive liquid-liquid microextraction, *Talanta*, 124 (2014) 106-110.
- [20] H. Shirkhanloo, A. Khaligh, H.Z. Mousavi, M.M. Eskandari, A.A. Miran-Beigi, Ultra-trace arsenic and mercury speciation and determination in blood samples by ionic liquid-based dispersive liquid-liquid microextraction combined with flow injection-hydride generation/cold vapor atomic absorption spectroscopy, *Chem. Papers*, 69 (2015) 779-790.
- [21] H. Shirkhanloo, M. Ghazaghi, H.Z. Mousavi, Cadmium determination in human biological samples based on trioctylmethyl ammonium thiosalicylate as a task-specific ionic liquid by dispersive liquid-liquid microextraction method, *J. Mol. Liq.*, 218 (2016) 478-483.
- [22] J. Werner, Determination of metal ions in tea samples using task-specific ionic liquid-based ultrasound-assisted dispersive liquid-liquid microextraction coupled to liquid chromatography with ultraviolet detection, *J. sep. sci.*, 39 (2016) 1411-1417.
- [23] S. Sadeghi, A.Z. Moghaddam, Task-specific ionic liquid based in situ dispersive liquid-liquid microextraction for the sequential extraction and determination of chromium species: optimization by experimental design, *RSC Adv.*, 5 (2015) 60621-60629.
- [24] N. Khan, T.G. Kazi, H.I. Afridi, M.B. Arain, Determination of cadmium in human serum and blood samples after dispersive liquid-liquid microextraction using a task specific ionic liquid, *Anal. Lett.*, (2017).
- [25] M.J. Trujillo-Rodríguez, P. Rocío-Bautista, V. Pino, A.M. Afonso, Ionic liquids in dispersive liquid-liquid microextraction, *TrAC Trends in Anal. Chem.*, 51 (2013) 87-106.
- [26] Q. Zhou, H. Bai, G. Xie, J. Xiao, Temperature-controlled ionic liquid dispersive liquid phase micro-extraction, *J. Chromatogr. A*, 1177 (2008) 43-49.
- [27] Q. Zhou, X. Zhang, J. Xiao, Ultrasound-assisted ionic liquid dispersive liquid-phase micro-extraction: A novel approach for the sensitive determination of aromatic amines in water samples, *J. Chromatogr. A*, 1216 (2009) 4361-4365.
- [28] J. Zhang, H. Gao, B. Peng, S. Li, Z. Zhou, Comparison of the performance of conventional, temperature-controlled, and ultrasound-assisted ionic liquid dispersive liquid-liquid microextraction combined with high-performance liquid chromatography in analyzing pyrethroid pesticides in honey samples, *J. Chromatogr. A*, 1218 (2011) 6621-6629.



# The use of zinc metalloporphyrin grafted magnetic nanoparticles for the removal of sulfate ions from wastewaters

Tahereh Poursaberi<sup>a</sup> and Ali Akbar Miran Beigi<sup>b,\*</sup>

<sup>a</sup> Analytical Research Group, Research Institute of Petroleum Industry, Tehran, Iran

<sup>b</sup> Oil Refining Research Division, Research Institute of Petroleum Industry, Tehran, Iran

## ARTICLE INFO:

Received 25 March 2019

Revised form 22 Apr 2019

Accepted 16 Mar 2019

Available online 16 Jun 2019

## ABSTRACT

This study investigates an application of zinc metalloporphyrin grafted  $\text{Fe}_3\text{O}_4$  nanoparticles as a new adsorbent for removal of sulfate ions from wastewaters. The modification of magnetite nanoparticles was conducted by 3-aminopropyltriethoxysilane followed by zinc (II) porphyrin in order to enhance the removal of sulfate ions. Moreover, Fourier Transform Infrared Spectroscopy (FT-IR), X-ray diffraction (XRD), Transmission Electron Microscopy (TEM) and Scanning Electron Microscopy (SEM) were used to characterize the synthesized nanosorbent. The effect of important experimental factors such as pH, contact time, sorbent dosage and some co-existing anions present in aqueous solutions were investigated. Under optimal conditions (i.e. contact time: 30 min, pH: 6.5 and nanosorbents dosage: 100 mg) for a sulfate sample (50 mL, 50  $\text{mgL}^{-1}$ ), the percentage of the extracted sulfate ions was 94.5%. Regeneration of sulfate adsorbed material could be possible by NaOH solution and the modified magnetic nanosorbent exhibited good reusability. The proposed system can provide a fast and efficient removal of the sulfate ion by using just an external magnetic field. In addition, the competitive adsorption tests verified that this system has good adsorption selectivity for sulfate ion. Finally, the synthesized sorbent was successfully applied for treating a wastewater sample from glass industry..

## Keywords:

Magnetic nanoparticles

Water samples

Sulfate removal

Zinc (II) porphyrin

Nanosorbent

## 1. Introduction

Sulfate is a common constituent of many natural waters and wastewaters [1], which it is present as a dissolved compound in seas and oceans or as insoluble salt (e.g., gypsum layers). Industrial wastewaters are responsible for most anthropogenic emissions of sulfate into the environment. Domestic sewage typically contains between 20 and 500  $\text{mg L}^{-1}$  sulfate [2] while certain industrial effluents may contain several thousands of milligrams per

liter. The main source of sulfate in the laboratory wastewaters is the use of sulfuric acid in many routine chemical analyses. Sulfur compounds are also present in wastewaters used in the research activities such as those from the pulp and paper industry, the food processing industry, and the photographic sector, among others [3].

The damage which is caused by sulfate emissions is not direct, since sulfate is a chemically inert, non-volatile, and non-toxic compound. However, high sulfate concentrations can unbalance the natural sulfur cycle [1, 2], and also endanger human health when excessive ingestion. The accumulation of

\*Corresponding Author: Ali Akbar Miran Beigi

E-mail: [amiranbeigi@yahoo.com](mailto:amiranbeigi@yahoo.com) ; [miranbeigiaa@ripi.ir](mailto:miranbeigiaa@ripi.ir)

DOI: <https://doi.org/10.24200/amecj.v2.i01.53>

sulfate-rich sediments in lakes, rivers and sea may cause the release of toxic sulfides that can provoke damages to the environment [4]. The World Health Organization (WHO) has established the maximum tolerable level of sulfate in water as 500 mg L<sup>-1</sup> [5]. The current U.S. EPA national Secondary Maximum Contaminant Level for sulfate, based on organoleptic effects, is 250 mg L<sup>-1</sup> [6].

A number of methods are currently used to promote the removal of dissolved sulfate. They include reversed osmosis, electrodialysis, or nanofiltration, which are expensive, can be poisoned by impurities, and require a post-treatment of the brine [2]. In addition, established methods for removal of sulfate from industrial effluents include chemical precipitation, biological treatment and adsorption technologies. Chemical precipitation, for example, to add barium or calcium salts, is rapid and effective, but it may produce another kind of pollution and secondary treatment for solid phase is necessary [1]. Removal of sulfate by sulfate-reducing bacteria is another alternative; however, the efficiency of biological treatment is susceptible to environmental conditions because the growth requirements of this microbial are relatively rigid [7]. Adsorption method may be preferred for their rapid and high selectivity, and sulfur can be recovered.

More recently, the use of NPs for sample extraction is gaining researchers interest [8-16]. Compared with micrometer-sized particles used in the SPE, the NPs offer a multitude of benefits that make it a better choice. They have a significantly higher surface area-to-volume ratio and a short diffusion route, resulting in a higher extraction capacity; rapid dynamics of extraction and its higher extraction efficiencies [17, 18]. Also, the main advantage of magnetic nanoparticles is their separation by application of external magnetic field. In addition, combination of the molecular scale recognition and nano scale surface modification creates a powerful tool for the development of selective separation systems. Depending on the usage, surface modification can be performed by physical / chemical sorption or surface coating of

specific ligands [19-23].

Supramolecular chemistry of anions has been widely studied and created a lot of artificial anionophores [24, 25] among them; in addition, metalloporphyrins (MP) are well known for their ability as anion carriers. The coordinating site of MPs is an acidic metal and the anion recognition is the result of specific anion coordination with this central metal ion [26]. Previously, it has been reported by us that the application of magnetic nanoparticles modified by Zr(IV) porphyrin and oxovanadium(IV) porphyrin for removal of fluoride and nitrate respectively [27, 28].

Herein, we have combined the sulfate selectivity of zinc (II) porphyrin with the advantages of magnetic nanoparticles has been combined by us to fabricate a new kind of magnetic nanosized sorbent with high affinity toward sulfate ion and good magnetic separability. The effect of pH, contact time, nanosorbent dosage and some co-existing anions present in aqueous solutions on sulfate removal efficiency were investigated.

## 2. Experimental procedure

### 2.1. Materials

Ferric chloride hexahydrate, ferrous chloride tetrahydrate, APTES, dichloromethane (DCM), *N,N*-dimethylformamide (DMF), dicyclohexylcarbodiimide (DCHC), methanol, ammonia, sodium salts of indicated anions were all analytical grade from Merck Chemical Co. *Meso*-Tetrakis (4-carboxyphenyl) porphyrinato zinc (II) (ZnTCPP) was obtained by metallation of the free ligand porphyrin tetrakis (4-carboxyphenyl) porphine H<sub>2</sub> (TCPP) (Aldrich)

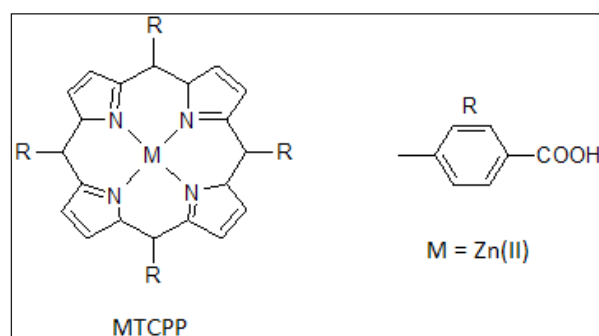


**Fig. 1.** Schematic representation of the Zinc (II) porphyrin used in this work.

according to the methods described in the literature [29]. Schematic of the Zinc (II) porphyrin is shown in Figure 1.

## 2.2. Equipments

The morphology and dimension of  $\text{Fe}_3\text{O}_4$ /APTES/ $\text{ZnTCPP}$  were examined by transmission electron microscope (TEM) using Zeiss 900 TEM at a voltage of 80 kV. Size and morphology of the nanosorbent were investigated by Tescan Mira LMU SEM. The phase purity was characterized by X-ray powder diffraction (XRD) (PW-1840 diffractometer from Philips Co) using Cu-K $\alpha$  radiation ( $\lambda=1.54178 \text{ \AA}$ ). Ion chromatography (IC) determinations were carried out in a S 1122 Sykam ion chromatograph. **In addition**, pH measurements were performed with a Metrohm 691 pH meter. FTIR spectra were recorded on a Vertex 70 FT-IR spectrophotometer from Bruker Co. using standard KBr pellet technique.

## 2.3. Sorbent preparation

### 2.3.1. Synthesis of $\text{Fe}_3\text{O}_4$ nanoparticles

The chemical co-precipitation method was used in the preparation of the  $\text{Fe}_3\text{O}_4$  NPs [30]. First, for preparing a stock solution, 10.4 g of  $\text{FeCl}_3 \cdot 6\text{H}_2\text{O}$ , with 4.0 g of  $\text{FeCl}_2 \cdot 4\text{H}_2\text{O}$  and 1.7 mL of HCl ( $12 \text{ mol L}^{-1}$ ) were mixed and dissolved in 50 mL of deionized water in a beaker which was then

degassed using nitrogen gas for 20 min before use. Simultaneously, 500 mL of  $1.5 \text{ mol L}^{-1}$  NaOH solution was degassed (for 15 min) and heated to  $80 \text{ }^\circ\text{C}$  in a reactor. The stock solution was then added dropwise using a dropping funnel for 30 min under nitrogen gas protection and vigorously stirring (1000 rpm) using a glassware stirrer. During the whole process, the solution temperature was maintained at  $80 \text{ }^\circ\text{C}$ , and nitrogen gas was used to prevent the intrusion of oxygen. After the reaction, the obtained  $\text{Fe}_3\text{O}_4$  NPs precipitate was separated from the reaction medium by using a magnetic field, and then washed four times with 500 mL of deionized water. Finally,  $\text{Fe}_3\text{O}_4$  nanoparticles were dried.

### 2.3.2. Modification of $\text{Fe}_3\text{O}_4$ nanoparticles with APTES groups

$\text{Fe}_3\text{O}_4$ /APTES nanoparticles were synthesized via the reaction of APTES and hydroxyl groups on the surface of magnetite. 2.3 g of  $\text{Fe}_3\text{O}_4$  nanoparticles were dispersed in 100 mL of ethanol by sonication for about 1 h. Then under continuous mechanical stirring, 20.34 mL of APTES was added dropwise to the suspension. The reaction mixture was kept at  $40 \text{ }^\circ\text{C}$  for 20 h under nitrogen atmosphere with vigorous mechanical stirring. The prepared APTES nanoparticles were collected with a magnet, and washed with ethanol and deionized water. Finally,

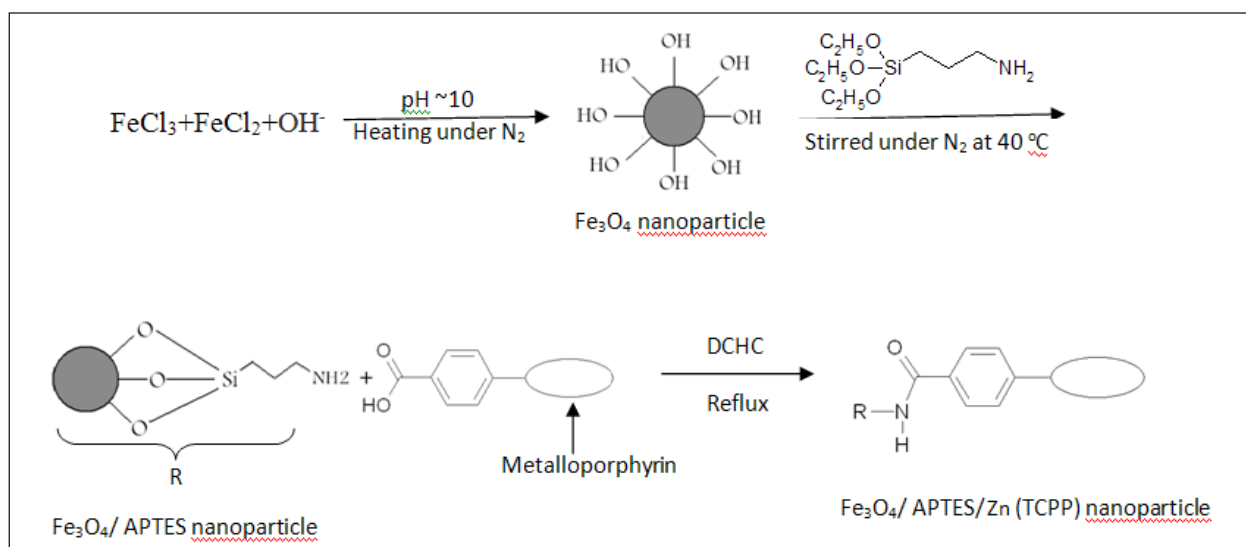


**Fig. 2.** A scheme of the magnetite synthesis and surface modification process using APTES followed by metalloporphyrin insertion.

$\text{Fe}_3\text{O}_4/\text{APTES}$  nanoparticles were dried under vacuum at  $50\text{ }^\circ\text{C}$ .

### 2.3.3. Grafting of Zn (TCPP) groups at the surface of $\text{Fe}_3\text{O}_4/\text{APTES}$

Functionalization of the modified nanoparticles was carried out by suspension of  $\text{Fe}_3\text{O}_4/\text{APTES}$  and DCHC in DMF under nitrogen [31]. Then Zn (TCPP) was dissolved in DMF and added to the suspension. The mixture was refluxed at  $140\text{ }^\circ\text{C}$  for 8 h. In order to prevent the presence of volatile dimethylamine, a product of DMF decomposition, a high flux of nitrogen is recommended. After reaction, the solid  $\text{Fe}_3\text{O}_4/\text{APTES}/\text{Zn}$  (TCPP) nanoparticles were separated magnetically and washed with DMF,  $\text{CH}_2\text{Cl}_2$ , and methanol to remove non-covalently bonded porphyrins from  $\text{Fe}_3\text{O}_4/\text{APTES}$ . A scheme of the magnetite synthesis and surface modification process is shown in Figure 2.

### 2.4. Removal of sulfate ions by $\text{Fe}_3\text{O}_4/\text{APTES}/\text{Zn}$ (TCPP)

Adsorption of sulfate by  $\text{Fe}_3\text{O}_4/\text{APTES}/\text{ZnTCPP}$  has been studied in batch experiments. A known amount of nanosorbent (100 mg) was mixed with 50 ml of  $50\text{ mgL}^{-1}$  aqueous sulfate solution and

was shaken at room temperature with 200 rpm for a 30 min. The sorbent was separated before measurement. The residual sulfate concentration of aqueous solution was determined by ion chromatography. The sulfate removal efficiency was calculated according to Eq. (1):

$$\text{Sulfate removal efficiency (\%)} = \left[ \frac{C_0 - C_r}{C_0} \right] \times 100 \quad (1)$$

where  $C_0$  and  $C_r$  are the initial and final concentrations of the sulfate ion before and after the sorption, respectively.

## 3. Results and discussion

### 3.1. Characterization of the synthesized nanosorbent

#### 3.1.1. X-ray powder Diffraction (XRD)

XRD analysis was used to investigate the crystalline structure of synthesized nanoparticles (Figure 3).

The Joint Committee on Powder Diffraction Standards (JCPDS) reference pattern of magnetite (No. 19-629) was used for comparison. As seen, the XRD pattern of magnetite nanoparticles was in good agreement with that of the standard  $\text{Fe}_3\text{O}_4$  structure. The same set of characteristic peaks were also observed for  $\text{Fe}_3\text{O}_4/\text{APTES}$  and  $\text{Fe}_3\text{O}_4/\text{APTES}/\text{ZnTCPP}$ , indicating the stability of the

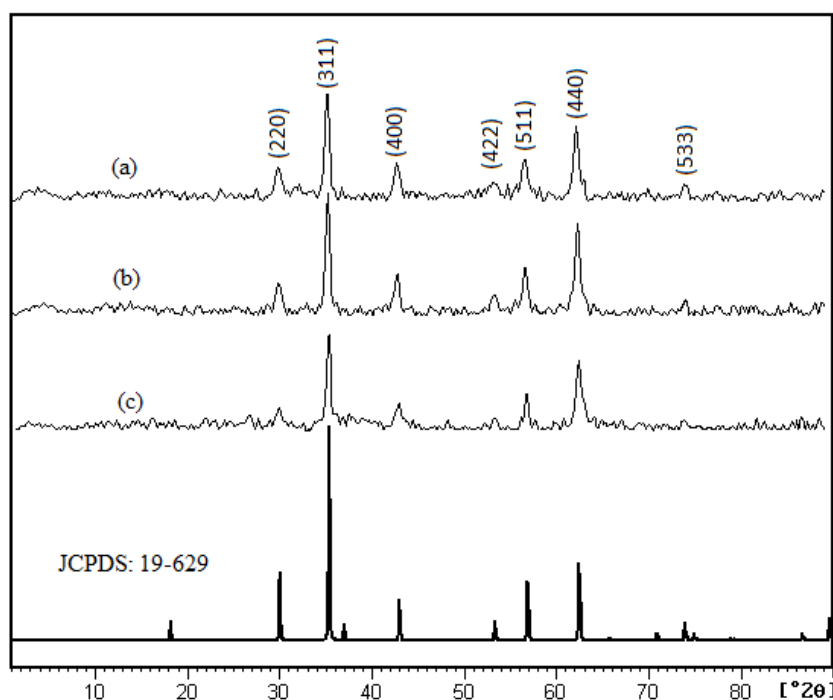


Fig. 3. XRD patterns of  $\text{Fe}_3\text{O}_4$  (a),  $\text{Fe}_3\text{O}_4/\text{APTES}$  (b), and  $\text{Fe}_3\text{O}_4/\text{APTES}/\text{Zn(TCPP)}$  (c).

crystalline phase of  $\text{Fe}_3\text{O}_4$  nanoparticles during functionalization and revealed that the APTES coating and metalloporphyrin grafting did not result in the phase change of  $\text{Fe}_3\text{O}_4$ .

The Single formula given by Debye Scherre (Eq. 2) can be used to calculate the crystalline size from the available XRD data. The average size of the  $\text{Fe}_3\text{O}_4$  nanoparticles using Debye Scherre was about 27 nm.

$$D = K\lambda / \beta\cos(\theta) \quad (2)$$

### 3.1.2. Scanning Electron Microscopy (SEM)

The particle size and morphological characteristics of the magnetite nanoparticles, before and after surface modification, were investigated by using SEM (Fig. 4). As can be seen from figure 4a, the bare magnetic nanoparticles show spherical shape with some aggregates due to the lack of any repulsive force between the magnetite nanoparticles. This is mainly due to the nano-size of the  $\text{Fe}_3\text{O}_4$ , which is about 27 nm. After APTES introduction (Fig. 4b),

particles with an approximate spherical shape and an average diameter of 30 nm were observed. This may be considered as indirect evidence that the magnetite core of the APTES magnetite particles consisted of a single magnetite crystallite with a typical diameter of 27 nm; and that the difference of 3 nm corresponds the APTES-coating. After metalloporphyrin immobilization (Fig. 4c), the dispersion of particles were improved greatly. It can easily be explained by the electrostatic repulsion force and steric hindrance between the metalloporphyrin on the surface of  $\text{Fe}_3\text{O}_4$  nanoparticles. Figure 4c shows that the morphology of the functionalized magnetic nanoparticles almost maintains the original state.

### 3.1.3. Transmission Electron Microscopy (TEM)

The introduction of Zn (TCPP) into the magnetite nanoparticles was evident from TEM results. The dark nano- $\text{Fe}_3\text{O}_4$  cores surrounded by a grey shell could be observed in Figure 5. Moreover, the

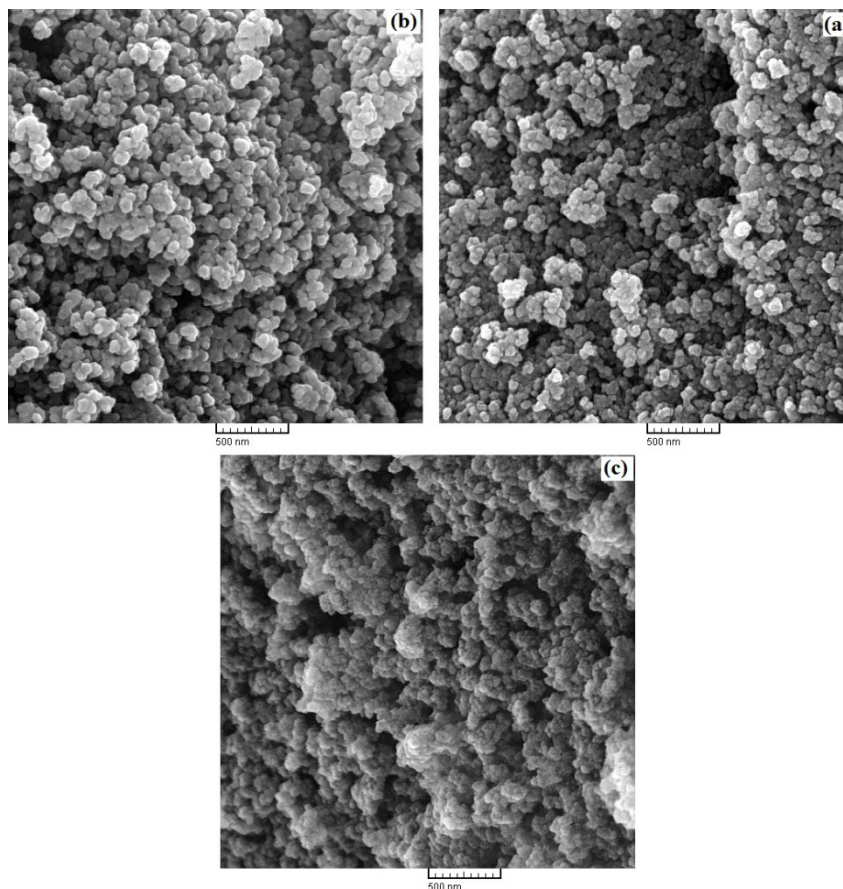


**Fig. 4.** SEM images of  $\text{Fe}_3\text{O}_4$  (a),  $\text{Fe}_3\text{O}_4/\text{APTES}$  (b) and  $\text{Fe}_3\text{O}_4/\text{APTES}/\text{Zn}(\text{TCPP})$  (c).

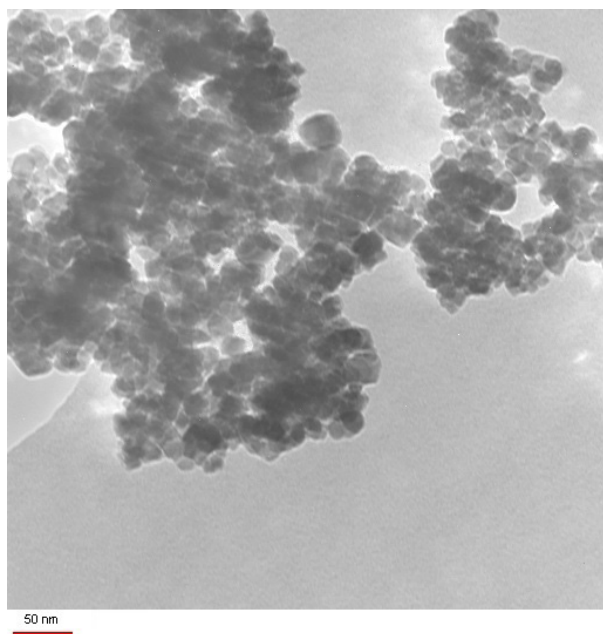


**Fig. 5.** TEM micrograph of  $\text{Fe}_3\text{O}_4/\text{APTES}/\text{Zn}$  (TCPP) nanosorbents.

particles have special characteristics such as an approximate spherical shape and an average size of 45 nm, which their characteristics complement the SEM data.

#### 3.1.4. FT-IR spectrum

FT-IR is a reliable technique for the monitoring of the variations in the functional groups. Therefore, the structures of the synthesized nanosorbent ( $\text{Fe}_3\text{O}_4/\text{APTES}/\text{Zn}$  (TCPP)) were characterized by

FTIR spectroscopy (Fig. 6). Fe–O stretching band at  $580\text{ cm}^{-1}$  is the characteristic peak of magnetite. Moreover, absorption bands at 2925 and  $2860\text{ cm}^{-1}$  assigned to stretching vibration of C–H bond of the propyl amine group. The silica network adheres to the particle surface via Fe–O–Si bond. The introduction of APTES to the surface of  $\text{Fe}_3\text{O}_4$  nanoparticles was confirmed by the bands around 1012 and  $1115\text{ cm}^{-1}$  from the SiO–H and Si–O–Si groups. A band at  $3430\text{ cm}^{-1}$  can be ascribed to the N–H stretching vibration. A peak at  $1647\text{ cm}^{-1}$  relating to the amide group stretching band, which proves that the metalloporphyrin can be covalently attached to the amine groups of APTES through the formation of a stable amide bond. The spectrum also showed the C=C stretching vibrations of carbon-carbon bonds of the aromatic ring about  $1500\text{ cm}^{-1}$ .

### 3.2. Adsorption experiments

#### 3.2.1. Optimization of the parameters

##### 3.2.1.1. Effect of the solution pH

It is well known that pH is one of the most important factors which affect the sorption process. Experiments were performed to find the optimum pH on the sorption of sulfate ions onto proposed nanosorbents using different pH values changing from 4.0 to 9.0.

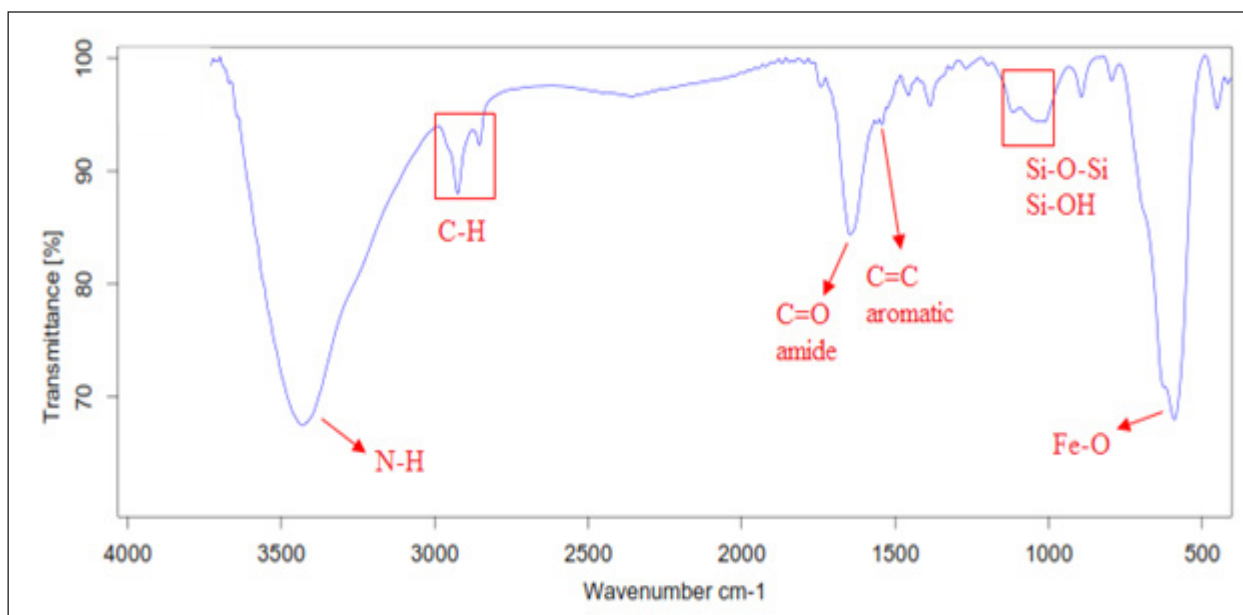


**Fig. 6.** FTIR spectra of  $\text{Fe}_3\text{O}_4/\text{APTES}/\text{Zn}$  (TCPP) nanoadsorbents.

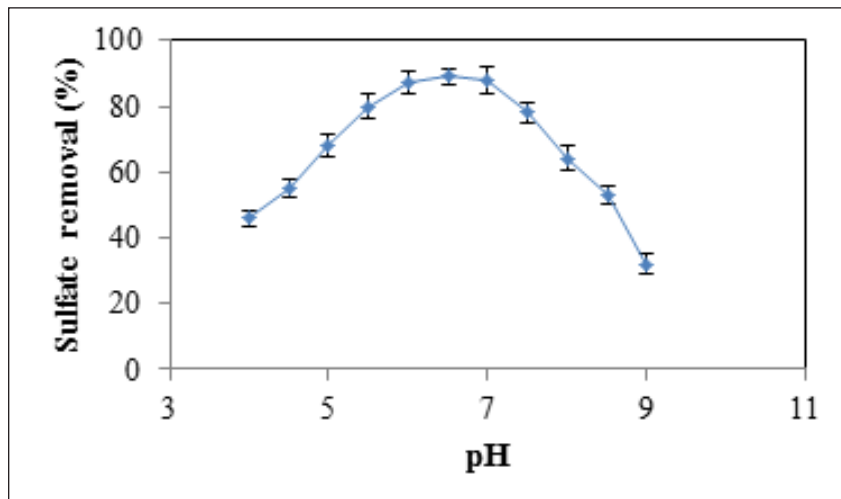


**Fig. 7.** The pH influence on the removal efficiency of sulfate (amount of adsorbent: 100 mg; sulfate concentration: 50 mg L<sup>-1</sup>).

As presented in Figure 7, while the sulfate removal depends on the pH of the sample, there is only a slight variation of the sulfate removal percentage with the pH values in the 6.0 – 7.0 pH range. In the acidic region the sulfate removal is decreased as a result of partial demetallation of the metalloporphyrin complex during the contact with the low pH test solution [32, 33]. At high pH values, sulfate and OH<sup>-</sup> ions are in competition to coordinate to the central metal ion (Zinc) of the porphyrin and therefore the sorption of nitrite ions is decreased [34]. Therefore, pH=6.5 was selected for all subsequent experiments.

### 3.2.1.2. Effect of the contact time

Contact time studies were performed to obtain

the optimum time with the maximum amount of sulfate removed. The adsorption of sulfate onto nanoadsorbents was monitored for 120 min. Sulfate was adsorbed onto nanosorbents quickly, and equilibrium was achieved within 30 min and thereafter remains constant (Fig. 8). Therefore, the time of 30 min was chosen as optimum value for all subsequent experiments.

### 3.2.1.3. Effect of the adsorbent dosage

To find the optimum amount of nanosorbents which can remove sulfate ions from aqueous solution, a batch-mode sorption study was performed using various amounts (25–250 mg) of Fe<sub>3</sub>O<sub>4</sub>/APTES/Zn (TCPP) nanosorbents. The sulfate removal efficiency as a function of nanosorbents dosage

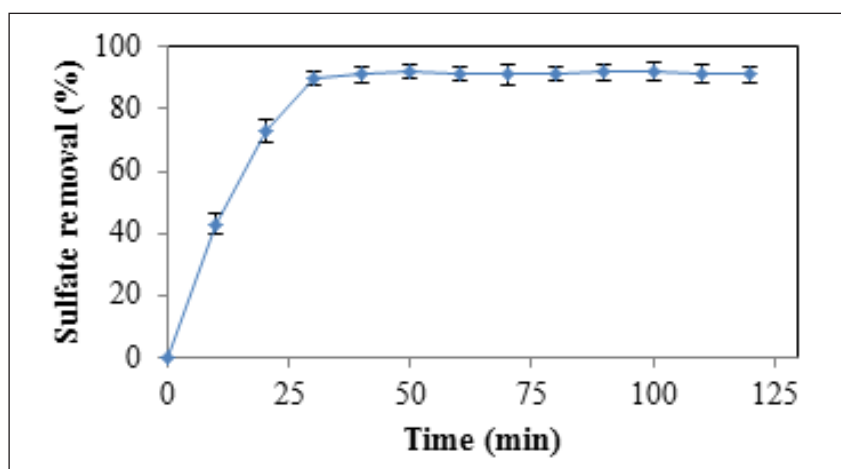


**Fig. 8.** Effect of contact time on the adsorption of sulfate by modified nanosorbent (pH of the solution: 6.5, amount of adsorbent: 100 mg; sulfate concentration: 50 mg L<sup>-1</sup>).

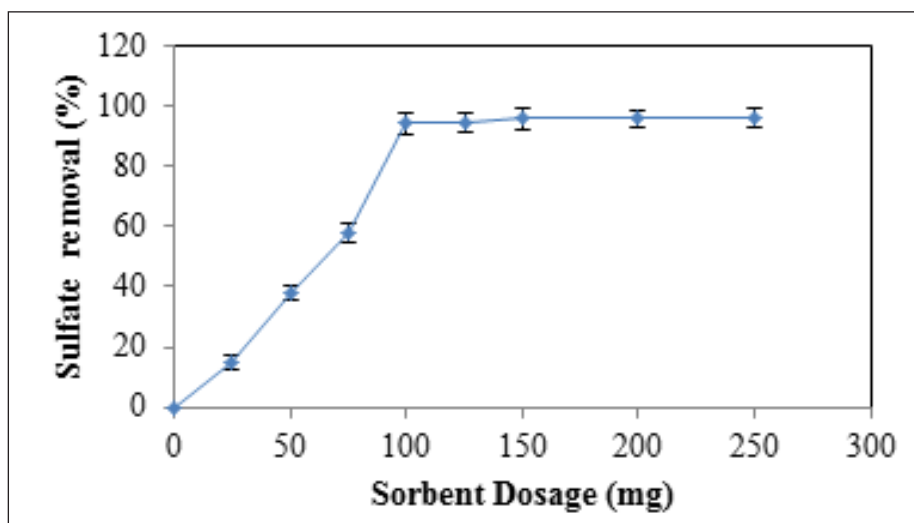


**Fig. 9.** Effect of nanosorbents dosage on the sulfate removal by modified nanosorbent (pH of the solution: 6.5, contact time: 30 min, sulfate concentration: 50 mg L<sup>-1</sup>).

is presented in Figure 9. Moreover, it is evident that the percent of sulfate removal increased with the increase of the sorbent dosage which is due to the fact that a greater amount of sorbent implies a greater amount of available binding sites. As seen in Figure 9, the percent removal reached steady state value after 100 mg of Fe<sub>3</sub>O<sub>4</sub>/APTES/ Zn (TCPP) nanosorbents for 50 mL of aqueous solution containing 50 mg L<sup>-1</sup> sulfate ion. Therefore, in all the experiments, 0.1 g of the nanoadsorbents was fixed as the optimum dose.

### 3.2.2. Removal studies

#### 3.2.2.1. Removal of sulfate from spiked sample

In order to evaluate the performance of the synthesized nanosorbent for sulfate removal, solid-phase extraction was used under optimal conditions. The deionized water was spiked with sulfate ion to make a 50.0 mg L<sup>-1</sup> solution. The batch adsorption experiment was carried out on 50 mL of this spiked sample under optimal conditions; i.e. contact time: 30 minutes, pH=6.5 and sorbent dosage: 100 mg. It was found that the sulfate content decreased from 50.0 mg L<sup>-1</sup> to 2.75 mg L<sup>-1</sup> (94.5 ± 2.7% removal efficiency, (n=5)).

#### 3.2.2.2. Effect of co-existing anions

Depending on the water source, more than one anion might be present. By considering the competition

for the binding sites between sulfate ions and such anions, they may affect the extraction efficiency of the proposed nanosorbent and might interfere with the removal efficiency of sulfate. In due course, prior to the application of proposed method on real samples, it is essential to investigate the effect of some of the interfering ions on the recovery percentage of sulfate; therefore, the adsorption of sulfate ion is tested in the presence of spiked known amounts of interfering ions. The tolerance limit was defined as the amount of the foreign ion causing a change of ±5% in the removal efficiency. As seen from figure 10, the removal percentage of sulfate was remained within the tolerance limit in the presence of fifty-fold of nitrite and nitrate and one hundred-fold of fluoride, chloride and bromide concentrations. These experimental results indicated that the method has a good tolerance toward matrix interferences.

#### 3.2.2.3. Regeneration of the used sorbent

In the evaluation of the performance of the sorbents, regeneration is an important factor to make an economic process. Moreover, in this work, NaOH was chosen as the stripping reagent for the recovery of sulfate ions from the adsorbents. The concentration of the NaOH solution was optimized, and the results indicated that the highest recovery was obtained by using NaOH 0.1 M solution (Fig. 11).

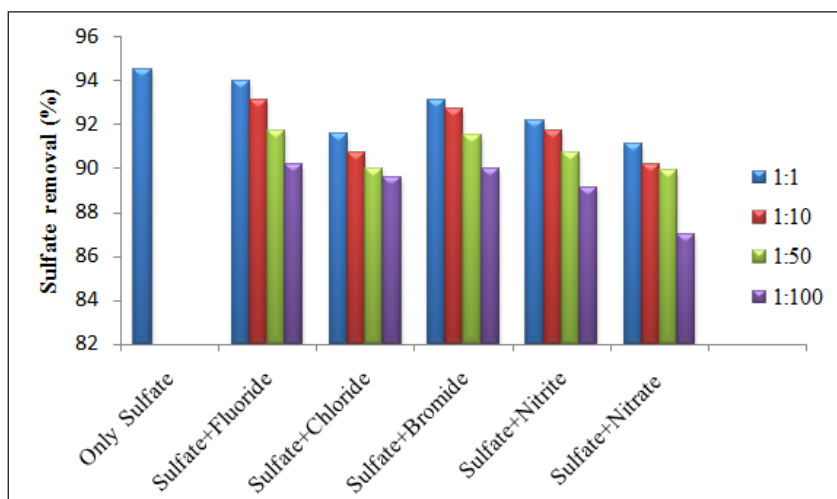


Fig. 10. Effect of co-existing anions on removal efficiency of a 50 mg L<sup>-1</sup> sulfate ion.

Regeneration performance of Fe<sub>3</sub>O<sub>4</sub>/APTES/ZnTCPP was tested for repeatedly use in practice applications. The spent Fe<sub>3</sub>O<sub>4</sub>/APTES/ZnTCPP was immersed in 10 ml 0.1 M NaOH solution and shaken for 30 min to desorb the loaded sulphate ions. Then the exchanger was separated from the NaOH solution with aid of magnet and washed with deionized water until the eluent was up to a neutral pH.

#### 3.2.2.4. Reusability of the recycled sorbent

After the first regeneration, nanosorbent was used in the followed adsorption test to record its sulphate adsorption efficiency again. This adsorption and desorption cycle was repeated five times. As seen

in Figure 12, after four sorption–desorption cycles, the efficiency of nanosorbent for the sulfate removal was not significantly reduced (not more than 5%), but at fifth run, an 8% decrease in its performance was observed; therefore, the desorption limit for sulfate was four cycles. It could be concluded that the chemical bonding between Zn porphyrin group and magnetite plays the major role in retaining the capacity of the Fe<sub>3</sub>O<sub>4</sub>/APTES/Zn (TCPP) nanosorbents.

#### 3.2.2.5. Removal of sulfate from real sample

Considering the practical applicability of proposed nanosorbent for removal of sulfate from real samples, it was also tested with wastewater obtained

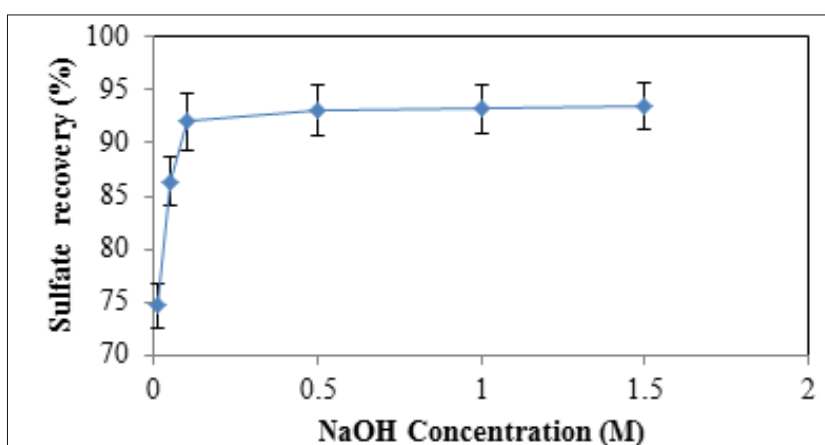


Fig. 11. The effect of NaOH concentration as desorbing eluent on the recovery percentage of sulfate ion.

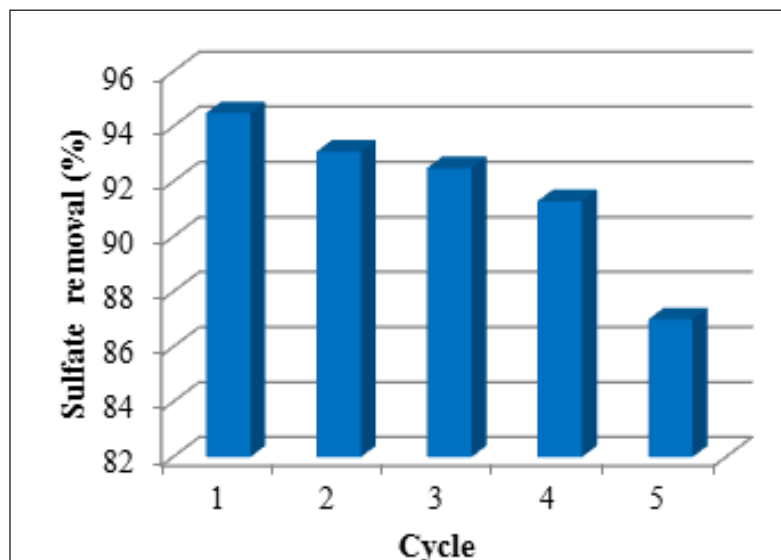


Fig. 12. The removal efficiency after five repetition usage on proposed nanosorbents.

from glass industry (Kaveh glass industry group, Saveh, Iran). The detailed characteristics of the wastewater are presented in Table 1. As can be seen, the untreated wastewater had sulfate concentration of  $108 \pm 15 \text{ mg L}^{-1}$ . Therefore, removal experiments were performed by using 200 mg of nanosorbent at  $\text{pH}=6.5$  and 30 min for contact time. It was found that the sulfate content decreased to  $10 \pm 2 \text{ mg L}^{-1}$  ( $90.7 \pm 2.4\%$  removal efficiency, ( $n=3$ )).

#### 4. Conclusions

In this paper, Zinc (II) metalloporphyrin grafted  $\text{Fe}_3\text{O}_4$  nanoparticle as a new and powerful sorbent for the removal of sulfate ions from aqueous media is introduced. Moreover, the sorbent showed a good efficiency in sulfate extraction and a high selectivity toward the target anion. In addition, the advantage of this product is its ease of separation

by an external magnetic field and possibility of simple recovery after washing with basic aqueous solution. Finally, the recovery of sulfate ion could be achieved, and the reuse of the sorbents is possible.

#### 5. References

- [1] A.J. Silva, M.B. Varesche, E. Foresti, M. Zaiat, Sulphate removal from industrial wastewater using a packed-bed anaerobic reactor, *Process Biochem.*, 37 (2002) 927-935.
- [2] P.N.L. Lens, A. Visser, A.J.H. Janssen, L.W. Hulshoff Pol, G. Lettinga, *Biotechnological Treatment of Sulfate-Rich Wastewaters*, *Crit. Rev. Environ. Sci. Technol.*, 28 (1998) 41-88.
- [3] C. T. Benatti, C. R. Tavares, E. Lenzi, Sulfate removal from waste chemicals by precipitation, *J. Environ. Manag.*, 90 (2009) 504-511.
- [4] R. Ghigliazza, A. Lodi, M. Rovatti, Kinetic and process considerations on biological reduction of soluble and scarcely soluble sulfates, *Resour. Conserv. Recy*, 29 (2000) 181-194.
- [5] World Health Organization (WHO), ISBN 978 92 4 154815 1, *Guidelines for Drinking-water Quality*, 2011.
- [6] F. Register, National Primary and Secondary Drinking Water Regulations; *Synthetic Organic Chemicals and Inorganic Chemical*, *Fed. Reg.*, 55 (1989) 30-37.

**Table 1.** The characteristics of glass industrial wastewater used in this study.

Anions	Value ( $\text{mg L}^{-1}$ )
Chloride	$228 \pm 19$
Fluoride	$35.5 \pm 1.2$
Nitrate	$8.52 \pm 0.6$
Sulphate	$108 \pm 15$
Bromide	$0.06 \pm 0.004$
Nitrite	$0.12 \pm 0.006$

- [7] G. Muyzer, A. J. M. Stams, The ecology and biotechnology of sulphate-reducing bacteria, *Nat. Rev. Microbiol.*, 6 (2008) 441-454.
- [8] S.Y. Chang, N.Y. Zheng, C.S. Chen, C.D. Chen, Y.Y. Chen, C.R.C. Wang, Analysis of peptides and proteins affinity-bound to iron oxide nanoparticles by MALDI MS, *J. Am. Soc. Mass Spectrom.*, 18 (2007) 910-918.
- [9] X. Zhao, Y. Shi, T. Wang, Y. Cai, G. Jiang, Preparation of silica-magnetite nanoparticle mixed hemimicelle sorbents for extraction of several typical phenolic compounds from environmental water samples, *J. Chromatogr. A.*, 1188 (2008) 140-147.
- [10] C. Huang, B. Hu, Speciation of inorganic tellurium from seawater by ICP-MS following magnetic SPE separation and preconcentration, *J. Sep. Sci.*, 31 (2008) 760-767.
- [11] J.S. Suleiman, B. Hu, H. Peng, C. Huang, Separation/preconcentration of trace amounts of Cr, Cu and Pb in environmental samples by magnetic solid-phase extraction with Bismuthiol-II-immobilized magnetic nanoparticles and their determination by ICP-OES, *Talanta*, 77 (2009) 1579-1583.
- [12] B. Zargar, H. Parham, A. Hatamie, Modified iron oxide nanoparticles as solid phase extractor for spectrophotometric determination and separation of basic fuchsin, *Talanta*, 77 (2009) 1328-1331.
- [13] L. Sun, L. Chen, X. Sun, X. Du, Y. Yu, D. He, H. Xu, Q. Zeng, H. Wang, L. Ding, Analysis of sulfonamides in environmental water samples based on magnetic mixed hemimicelles solid-phase extraction coupled with HPLC-UV detection, *Chemosphere*, 77 (2009) 1306-1312.
- [14] H. Parham, N. Rahbar, Solid phase extraction-spectrophotometric determination of salicylic acid using magnetic iron oxide nanoparticles as extractor, *J. Pharm. Biomed. Anal.*, 50 (2009) 58-63.
- [15] L. Sun, C. Zhang, L. Chen, J. Liu, H. Jin, H. Xu, L. Ding, Preparation of alumina-coated magnetite nanoparticle for extraction of trimethoprim from environmental water samples based on mixed hemimicelles solid-phase extraction, *Anal. Chim. Acta*, 638 (2009) 162-168.
- [16] M. Faraji, Y. Yamini, A. Saleh, M. Rezaee, M. Ghambarian, R. Hassani, A nanoparticle-based solid-phase extraction procedure followed by flow injection inductively coupled plasma-optical emission spectrometry to determine some heavy metal ions in water samples, *Anal. Chim. Acta*, 659 (2010) 172-177.
- [17] K. Moeller, J. Kobler, T. Bein, Colloidal Suspensions of Nanometer-Sized Mesoporous Silica, *Adv. Funct. Mater.*, 17 (2007) 605-612.
- [18] K.J. Klabunde, *Nanoscale Material in Chemistry*, Wiley-Interscience, New York, 2001.
- [19] M. Faraji, Y. Yamini, M. Rezaee, Magnetic nanoparticles: Synthesis, stabilization, functionalization, characterization, and applications, *J. Iran. Chem. Soc.*, 7 (2010) 1-37.
- [20] Ch. Huang, B. Hu, Silica-coated magnetic nanoparticles modified with  $\gamma$ -mercaptopropyltrimethoxysilane for fast and selective solid phase extraction of trace amounts of Cd, Cu, Hg, and Pb in environmental and biological samples prior to their determination by inductively coupled plasma mass spectrometry, *Spectrochim. Acta Part B*, 6 (2008) 437-444.
- [21] K. Jainae, K. Sanuwong, J. Nuangjamnong, N. Sukpirom, F. Unob, Extraction and recovery of precious metal ions in wastewater by polystyrene-coated magnetic particles functionalized with 2-(3-(2-aminoethylthio)propylthio)ethanamine, *Chem. Eng. J.*, 160 (2010) 586-593.
- [22] Zh. Yong-Gang, Sh. Hao-Yu, P. Sheng-Dong, H. Mei-Qin, *J. Hazard. Mater.*, 182 (2010) 295.
- [23] X. Wang, L. Wang, X. He, Y. Zhang, L. Chen, A molecularly imprinted polymer-coated nanocomposite of magnetic nanoparticles for estrone recognition, *Talanta*, 7 (2009) 327-332.
- [24] .P.D Beer, .PA. Gale, Anion Recognition and Sensing: The State of the Art and Future Perspectives, *Chem. Int. Edu.*, 40 (2001) 486-516.
- [25] A. Bianchi, K. Bowman-James, E. Garcia-Espan., *Supramolecular Chemistry of Anions*, Wiley/VCH, 1997.
- [26] J.T. Mitchell-Koch, M. Pietrzak, E. Malinowska, M. E. Meyerhoff, Aluminum(III) Porphyrins as Ionophores for Fluoride Selective Polymeric Membrane Electrodes, *Electroanal.*, 18 (2006) 551-557.
- [27] T. Poursaberi, M. Hassanisadi, K. Torkestani, M. Zare, Development of zirconium (IV)-metalloporphyrin grafted  $\text{Fe}_3\text{O}_4$  nanoparticles for efficient fluoride removal, *Chem. Eng. J.*, 189 (2012) 117-125.

- [28] T. Poursaberi, M. Karimi, M. Hassanisadi, H. Sereshti, Magnetic removal of nitrate ions from aqueous solution using amino-silica coated magnetic nanoparticles modified by oxovanadium(IV) porphyrin, *J. Porphyrins Phthalocyanines*, 17 (2013) 359-366.
- [29] J. G. Erdman, V. G. Ramsey, N.W. Kalenda, W. E. Hanson, Synthesis and Properties of Porphyrin Vanadium Complexes, *J. Am. Chem. Soc.*, 78 (1956) 5844-5847.
- [30] X.L. Zhao, Y.L. Shi, Y.Q. Cai, S.F. Mou, Cetyltrimethylammonium Bromide-Coated Magnetic Nanoparticles for the Preconcentration of Phenolic Compounds from Environmental Water Samples, *Environ. Sci. Technol.*, 42 (2008) 1201-1206.
- [31] R.B.S. Merrifield, *J. Am. Chem. Soc.* 2149 (1963) 85.
- [32] V.V. Egorov, E.M. Rakhman'ko, A.A. Rat'ko, Metalloporphyrin-Based Anion-Selective Electrodes with Unusual Selectivity, *J. Anal. Chem.*, 57 (2002) 46-53.
- [33] K. M. Morehouse and P. Neta, *J. Phys. Chem.*, 18 (1984) 88.
- [34] Y. Kang, C. Lutz, S.A. Hong, D. Sung, J.S. Lee, J.H. Shin, H. Nam, G.S. Cha, M.E. Meyerhoff, Development of a Fluoride-Selective Electrode based on Scandium(III) Octaethylporphyrin in a Plasticized Polymeric Membrane, *Bull. Korean Chem. Soc.*, 31 (2010) 17-29.